AD-A164 209 STUDY OF THE EFFECTS OF DISCRETIZING QUANTITATIVE FEEDBACK THEORY ANALOG..(U) AIR FORCE INST OF TECH WRIGHT-PATTERSON AFB OH SCHOOL OF ENGI.. J S COUCOULES 1/3

UNCLASSIFIED DEC 85 AFIT/GE/ENG/85D-10 F/G 1/3 NL

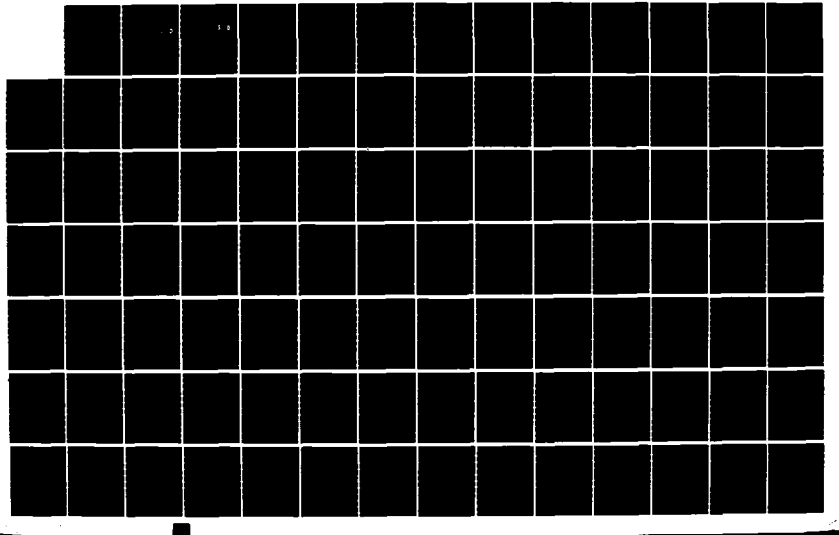

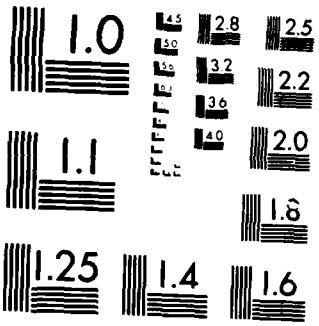

STUDY OF THE EFFECTS OF DISCRETIZING QUANTITATIVE FEEDBACK THEORY ANALOG CONTROL SYSTEM DESIGNS

THESIS

JOHN S. COUCOULES
Capt, USAF

AFIT/GE/ENG/85D-10

DEPARTMENT OF THE AIR FORCE
AIR UNIVERSITY
AIR FORCE INSTITUTE OF TECHNOLOGY

Wright-Patterson Air Force Base, Ohio

AFIT/GE/ENG/85D-10

STUDY OF THE EFFECTS OF DISCRETIZING QUANTITATIVE FEEDBACK THEORY ANALOG CONTROL SYSTEM DESIGNS

THESIS

JOHN S. COUCOULES
Capt, USAF

AFIT/GE/ENG/85D-10

AFIT/GE/ENG/85D-10

STUDY OF THE EFFECTS OF DISCRETIZING QUANTITATIVE FEEDBACK THEORY ANALOG CONTROL SYSTEM DESIGNS

THESIS

Presented to the Faculty of the School of Engineering
of the Air Force Institute of Technology
Air University
In Partial Fulfillment of the
Requirements for the Degree of
Master of Science in Electrical Engineering

John S. Coucoules, B.S.
Captain, USAF

December 1985

Preface

This thesis examined the feasibility and a method of extending continuous domain Quantitative Feedback Theory (QFT) flight control system designs to the discrete domain. Analog QFT control system designs for two diverse aircraft, the AFTI/F-16 and KC-135, were the focus of this study.

I would like to extend my sincere thanks to my thesis advisors, Professors Constantine H. Houpis and Gary B. Lamont, for all their guidance and support throughout this effort. A special thanks to Professor Isaac Horowitz for his tremendous insight and extreme patience.

This preface would not be complete without acknowledging the stimulating and enlightening discussions with my peers and friends, namely Kevin Sheehan, Scott Eckert, Bruce Clough, and Bruce Acker.

And last, but certainly not least, I would like to thank my wife, Catherine, for putting up with me and providing loving support these last 18 months.

Table of Contents

List of Figures

List of Tables

List of Symbols

$\underline{A}$	Plant matrix, state space form
a_{ij}	Model response bound--lower
a_k	Difference equation coefficients (numerator)
$\underline{B}$	Control matrix, state space form
b_{ij}	Model response bound--upper
b_k	Difference equation coefficients (denominator)
db	Decibels
Deg	Degree
d_{ij}	Effective disturbance
$\underline{\delta}$	Plant input vector
δ_r	Rudder deflection
δ_w	Control wheel deflection
δ_e	Elevator deflection
δ_{sb}	Speed brake deflection
δ_T	Percent engine thrust, change from trim
E*(s)	Output of ideal sampler
e	Exponential operator
F	Pre-filter in single loop design
$\underline{F}$	Pre-filter matrix
f_{ij}	Element of $\underline{F}$
f_s	Sample rate (Hertz)
ft	Feet
G	Primary compensator element in single loop design
$\underline{G}$	Compensator matrix
$G_{pa}(s)$	Pade' approximation of ZOH transfer function
$G_{zo}(s)$	ZOH transfer function

g_i	Element of diagonal $\underline{G}$
h	Altitude
Hz	Hertz
L	Control loop transmission (L = GP)
L_o	Nominal loop transmission
$\underline{M}$	Output matrix
M_p	Peak value
$\underline{N}$	Input matrix
P	Plant transfer function
P_o	Nominal plant transfer function
$\underline{P}$	Plant matrix of system transfer function
P_{ij}	Element of $\underline{P}$
p	Roll rate
$\underline{Q}'$	Inverse of plant matrix $(P)^{-1}$
q'_{ij}	Element of $\underline{Q}'$
q_{ij}	$(1/q'_{ij})$
q_{ij_o}	Nominal q_{ij}
q	Pitch rate
rad	Radians
r_j	MIMO system input
s,S	Laplace operator ($s=j\omega$)
sec	Seconds
T	Compensated system transfer function
T	Sample Period
T_R	Command response transfer function
T_D	Disturbance response transfer function
t_p	Peak time

t_r	Rise time
t_s	Settling time
u	Perturbation velocity along x-axis
$\underline{x}$	State vector
$\underline{Y}$	Output vector
Y_i	MIMO system output
z,Z	Discrete domain operator, Z-plane ($z=e^{Ts}$)
ZOH	Zero order hold
δ_1	Elevator input
δ_2	Flaperon input
θ	Pitch Angle
ϕ	Roll Angle
γ	Ratio of effective plant transfer functions
μ_{ij}	Control surface constants
ω	Unit of frequency (rad/sec)
ω_s	Sample rate (rad/sec)

Abstract

This ~~investigation~~ examines the feasibility and a method of extending continuous domain Quantitative Feedback Theory (QFT) flight control system designs to the discrete domain. The results of two previous QFT analog design efforts are modified for a digital implementation. The first design effort is for the KC-135 transport aircraft. Robust analog fixed compensators are designed for three different flight conditions. The second design effort is for the AFTI/F-16 aircraft. In this design, parameter variation is due to both varying flight conditions and different aircraft configurations caused by failed surfaces.

This study is accomplished in two phases. In the first phase only the effects of sampling are included. The compensators are discretized using two transformation techniques after they are modified to counteract the effects of the sampler and zero order hold (ZOH). Simulation results show that the Tustin transformation using a sampling rate of 40 Hz provides good results, as compared to the analog design, for the KC-135 aircraft. For the AFTI/F-16, acceptable results are obtained using the Tustin transformation and a sampling rate of 60 HZ, but only for two out of four flight conditions.

In the second phase both sampling and finite wordlength

effects are considered. A computer program is developed to simulate the effects of finite wordlength. It is sufficiently general to allow the specification of rounding or truncation, the controller wordlength and the number of desired binary digits to the right of the radix point. Simulations are conducted using various wordlengths and numbers of digits to the right of the radix point as well as appropriately quantized controller coefficients.

The conclusion drawn from this study is that the Tustin transformation provides good discrete system performance as compared to the continuous QFT design, if the compensator real zeros and poles are located at $S \geq -T/2$. To ensure the same system performance guarantees as provided by QFT in the continuous domain, it is recommended that the QFT design be performed directly in the discrete domain, as opposed to extending analog QFT designs.

STUDY OF THE EFFECTS OF DISCRETIZING QUANTITATIVE FEEDBACK THEORY ANALOG CONTROL SYSTEM DESIGNS

I. Introduction

Quantitative Feedback Theory developed by Dr. Isaac Horowitz has been used successfully to design "robust" control systems (1; 2; 3). A robust control system is generally considered to be one which has reduced sensitivity to plant parameter variations and disturbances, i.e. less than in an open loop system. These parameter variations result from uncertain plant parameters or uncertain external disturbances. Plant parameter variations occur when an aircraft is operated at a flight condition other than the flight condition used to generate the linear plant model incorporated in the basic control system design. Loss or failure of a flight control surface can also cause large plant parameter variations.

There are many advantages to implementing control compensators using a digital controller. Digital controllers have improved reliability and maintainability over analog compensators. A great degree of flexibility can also be realized with a digital controller implementation. A completely new control law can be implemented simply by making a software change instead of a hardware change. Several control laws can be stored simultaneously. Depending

on mission requirements, a particular control law can be "switched on" by use of a software algorithm.
Previous applications of Quantitative Feedback Theory (QFT) have been limited to the design of control systems in the continuous domain. In order to realize the inherent advantages of a digital controller, such as those cited above, either QFT or QFT designs must be extended to the discrete domain. A digital implementaion of a QFT analog design was done for the lateral mode of the YF-16 CCV aircraft (4:174), but finite wordlength effects were not considered.

In this thesis investigation, the results of two previous QFT design efforts (1; 2) are extended to the discrete domain. An analysis of these discrete designs are made to determine if they meet the performance objectives of the original designs.

This chapter presents the pertinent background information, statement and scope of the problem, assumptions, the approach and the sequence of thesis presentation.

I-1 Background

Several difficult control problems involving highly uncertain parameters have been solved by Dr. Isaac Horowitz using the QFT technique (5:287-309; 6:81-106). In addition to Dr. Horowitz's work, several AFIT Master's theses have applied the QFT technique to flight control problems involving uncertain parameters, two of which are used to provide the starting point for this thesis effort (1; 2). These two theses are discussed next:

The objective of the first thesis effort, by Captain Russell, was to design two robust controllers for the KC-135 transport aircraft (1:2). The first design involved two inputs and two outputs, and controlled the lateral mode of the aircraft during two separate maneuvers. The second design involved three inputs and three outputs, and controlled the longitudinal mode during one maneuver. In Russell's thesis, the linearized lateral and longitudinal equations of motion are (assumed) decoupled and treated separately throughout (see Chapter II). Both controllers were designed to operate over the entire flight envelope of the aircraft. All performance specifications were met for all three flight conditions in both the lateral and longitudinal designs using only fixed compensation (1:99).

The objective of the second thesis, by Major Arnold, was to investigate QFT "inherent reconfiguration" design for the AFTI/F-16 aircraft (2:2). In this context, inherent reconfiguration means the ability of the control system to maintain aircraft control even under one or more simultaneous losses or failures of control surfaces. Inherent reconfiguration is accomplished by a fixed controller using individual control of all (including redundant) flight control surfaces of the AFTI/F-16 aircraft. Thus in the above work, the two flaperons and the two horizontal tails were individually controlled. The plant model explicity displayed the effect of each control surface on the two chosen output variables, pitch rate (q) and roll rate (p) (see Chapter II). Two command input sources

q_c and p_c were assumed, and quantitative basically noninteracting performance was specified. Not only was the controller designed to operate over the entire flight envelope, as in Russell's thesis, but it was also designed to operate over 6 different failure combinations. Not all performance specifications were met in Arnold's design as the settling time tolerance was exceeded for several aircraft configuration/ flight condition combinations (2:58). QFT guarantees that the original performance tolerances are satisfied despite uncertainty (5). No exact reason is given for this inconsistency, but Arnold does speculate that one possible reason is that approximations were made for the compensators g_1 and g_2 so their order could be reduced (2:60). The order reduction was required due to limitations of the simulation program utilized.

The number of compensators for each of the designs discussed above is determined by the dimensionality of the system and the number of "non-zero" inputs. For instance, for a three input-three output system (3 loops or channels), as in Russell's longitudinal design, three feedforward path (inner loop) compensators and one prefilter are required to complete the control design. In Russell's longitudinal design the only non-zero input was pitch angle. Note that in Russell's design, the term "robust" refers to the plant parameter variation due only to different flight conditions. In Arnold's design, "robust" means parameter variation due to both varying flight conditions and the

different configurations of the aircraft caused by failed surfaces.

I-2 Problem

The main purpose of this effort is to investigate the suitability of continuous domain QFT control system designs for digital implementation. This general problem is separated into several smaller but related problems. The results of Russell's and Arnold's designs are extended to the discrete domain. This is accomplished by discretizing the compensators using various transformation techniques. The performance of the digital controllers are examined by use of a very large wordlength digital computer simulation program (7). Performance is judged via comparisons to the original time domain specifications and performance achieved in references 1 and 2. Implementation issues, such as the effects of finite word length and sample time, are discussed.

Recommendations are made, based upon the above analysis, to aid the design of s-domain compensators using QFT so that performance objectives are met when the designs are implemented digitally.

I-3 Scope

This study extends continuous domain QFT flight control designs (1; 2) to the digital domain. The digital design starting points are the continuous designs of Captain Russell (KC-135) and Major Arnold (AFTI/F-16). Only the rigid body aircraft is considered for the AFTI/F-16. For the KC-135, the

first two body bending modes are also included. This study involves only constant rate sampling. The following information is provided concerning the above two design efforts.

For the KC-135, the digital designs are done for the decoupled longitudinal and lateral modes. The performance of the lateral digital control design is examined using two maneuvers: a coordinated turn and a sideslip. The longitudinal digital control design involves a pitch pointing maneuver. The KC-135 designs are for the following flight conditions (F.C.) (1:3):

F.C. #1: High altitude cruise (45,000 ft at mach 0.77).

F.C. #2: Medium altitude cruise (28,500 ft at mach 0.77).

F.C. #3: Approach (sea level at mach 0.21).

The AFTI/F-16 design is for the following four F.C.s (2:97):

F.C. #1: Approach (30 ft at mach 0.2).

F.C. #2: High altitude/medium speed cruise (30,000 ft at mach 0.6).

F.C. #3: Medium altitude/medium speed cruise (20,000 ft at mach 0.9).

F.C. #4: High altitude/high speed cruise (30,000 ft at mach 1.6).

To incorporate the reconfiguration aspect into the design, the following control surface configuration (CSC) modes are utilized (2:4):

Mode 1 - All four surfaces are operating normally.

Mode 2 - One horizontal tail is failed

Mode 3 - One flaperon is failed.

Mode 4 - One horizontal tail and one flaperon are failed (same side).

Mode 5 - One horizontal tail and one flaperon are failed (opposite sides).

Mode 6 - Both flaperons are failed.

A failed surface is defined to be in the neutral reference position.

Although a detailed discussion of the QFT design technique is not a purpose of this investigation, two appendices are included which do present this material. They are included as a convenience to the reader and because of the relatively small amount of literature available on Quantitative Feedback Theory. The single input-single output (SISO) system design philosophy is presented in detail in Appendix A and the multiple input-multiple output (MIMO) design technique is presented in Appendix B. The emphasis in Appendix B is on the (2x2) and (3x3) MIMO system design.

I-4 Assumptions

Several assumptions are made in the course of this investigation. Seven of these assumptions are the same as those made by Russell and Arnold (1:3; 2:4). They generally cover various aspects of generating the linear, time-invariant, decoupled aircraft equations of motion. Russell and Arnold also assume that "continuous time" performance simulations executed on a large wordlength digital computer provide realistic responses of the aircraft motion. It is assumed that the design work done by Russell and Arnold in their respective QFT design efforts is correct as presented,

although some cursory checks of their work are made.

This study involves various computer-aided-design (CAD) and computer-aided simulation tools to examine the performance of the digital control system designs. These simulations are carried out on large wordlength digital computers. It is assumed that these simulations provide realistic responses when an appropriate time relationship has been established between the digital controller and the "analog plant."

It is assumed that the reader of this thesis is at least familiar with the work done by Russell and Arnold in references 1 and 2, respectively. This is important, since the digital controller performance is compared directly to their specifications and results. In addition, a general understanding of the QFT design technique is assumed on the part of the reader.

I-5 Approach

This digital design study involves two general phases. Phase 1 discusses the theoretical aspects of the digital design and examines the performance of the theoretical design. In this context, "theoretical" means that finite wordlength effects are not considered. Phase 2 discusses various implementation issues associated with a finite word length digital controller. A performance simulation is done which takes into account the effects of finite word length. With the above design phases in mind, the digital design approach incorporates the following steps:

The first step of the theoretical phase developes a suitable system model in the form of a system block diagram including samplers and zero order holds (ZOH). The second step developes a means to counteract the lag effects of the ZOH. Next, the sample rate is determined from a theoretical standpoint and this sample rate is then compared to sample rates that can be practically realized. The fourth step is to transform the modified compensators to the discrete domain using the Tustin and standard Z-transforms. The effects of "folding" and "warping" of poles and zeros are then discussed. The last step of the theoretical phase involves a simulation of the theoretical digital design, using various sample rates, as necessary, to determine the theoretical performance. The results are then compared to the specifications and continuous domain performance.

The first step of the implementation phase developes a "hybrid" simulation program using existing simulation tools. The second step performs a hybrid simulation using various wordlengths. The results of this simulation are then compared to the original specifications and continuous domain performance results.

Throughout both the theoretical and implementation phases, discussion is included with suggestions for additions or changes to the QFT design technique, to improve the results obtained in an eventual digital implementation. These guidelines are summarized at the end of this thesis.

I-6 Presentation

This thesis consists of seven chapters. Chapter II contains a detailed discussion of the system models to be used. Chapter III presents the detailed theoretical digital design. The theoretical simulation ("infinite wordlength") of the digital controllers is contained in Chapter IV. Chapter V discusses the hybrid simulation program and digital implementation issues. The results of the hybrid simulation are presented in Chapter VI. Chapter VII contains the conclusions and recommendations for both the digital implementation of the QFT design technique and future study in this area.

II. System Models

II-1 Introduction

In this chapter the various models used in this thesis are presented. First a generic pseudo-continuous-time (PCT) single input-single output (SISO) system model is developed from a continuous time model. The development of the 2x2 (lateral) KC-135 PCT model is shown next. The form of the aircraft equations given in reference 1 are incompatible with the PCT model configuration developed, therefore the form of the KC-135 equations are changed accordingly. The rigid and elastic body 3x3 (longitudinal) KC-135 PCT model is then developed. As with the lateral aircraft, the longitudinal aircraft equations must be massaged into the proper form. Finally the F-16 continuous time model is discussed and extended to a PCT model. The F-16 plant equations, already in transfer function form, are outlined. Finally, the response models for both the KC-135 and the F-16 are discussed.

II-2 Generic SISO Model

A general continuous time SISO system is shown in Figure 2-1 where P represents the plant, D is a disturbance to the plant, G is the fixed compensator and F is a prefilter to the system. Since it is desired to implement G as a digital controller, the continuous signal E(s) must be sampled to generate a suitable digital signal to present to the controller. The output of a digital controller is a discrete signal and therefore must be transformed into a continuous

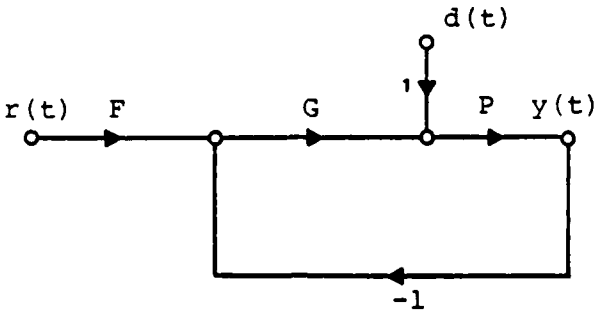

Fig. 2-1. Continuous Time System Model

signal to drive the plant P. This is because in general, it is undesirable to apply a signal in sampled form to a plant, because of the high frequency components inherently present in the sampled signal (9:103). This process is performed by a hold device. The simplest data hold device (requires no memory) and by far the most common, is the zero-order hold (ZOH). This type of hold device is assumed throughout this thesis investigation. Figure 2-2 shows a representation of the sampling and data hold operations where the ZOH transfer function is defined by

$$G_{zo}(s) = \frac{1 - e^{-Ts}}{s} \qquad (2\text{-}1)$$

It should be noted that individually the sampler in Figure 2-2 does not model a physical sampler nor does the block model a physical hold device. However, it can be shown mathematically (8:71) that the combination does accurately model a physical sampler/data-hold device.

The sampler and ZOH are included in the block diagram shown in Figure 2-3 to generate the sampled-data system model.

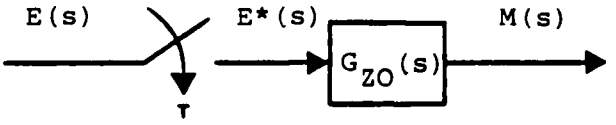

Fig. 2-2 Sampler and Data Hold Representation

Note that now a digital controller, G(z), is used as the compensator. The output of the digital controller block G(z) is a discrete signal. This is emphasized in some digital control system texts by "inserting" a fictitious sampler after the digital controller. This fictitious sampler is not shown in the diagrams contained in this study. The prefilter F is implemented as an analog compensator. The reason for this is that generally, QFT design technique generates a very simple prefilter. The prefilter is usually either a first or second order compensator. There is also a distinct advantage

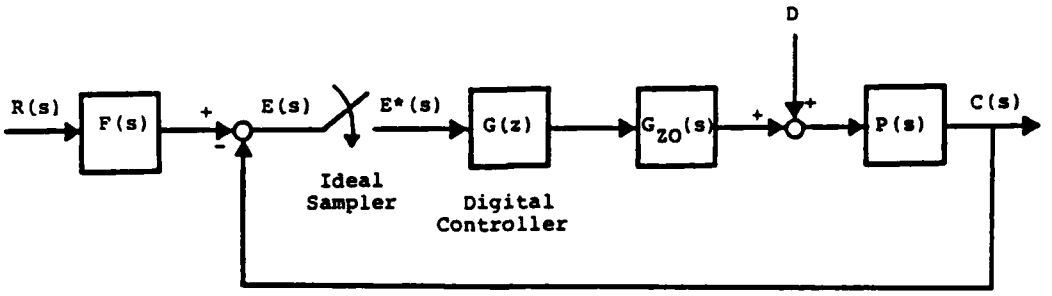

Fig. 2-3. Sampled-Data System Model

to implementing the prefilter with an analog circuit. The prefilters are essentially low pass devices and serve effectively as an antialiasing device where input noise above the prefilter breakpoint is attenuated. The prefilters for both

aircraft are shown in Appendix E.

An approximation to the sampled-data system of Figure 2-3 can be made using the PCT model (9:248-251). In the PCT system model the ideal sampler of Figure 2-3 is approximated by the first block of Figure 2-4. This approximation is appropriate because the sampling process modifies the fundamental frequency and all its harmonics by a factor of T^{-1} (9:84).

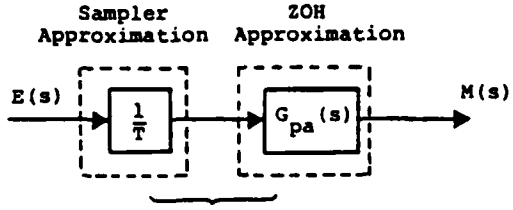

Fig. 2-4. Sampler and ZOH Approximations

The ZOH is approximated by the first-order Pade' approximation as follows:

$$G_{zo}(s) = \frac{1 - e^{-Ts}}{s} \approx \frac{2T}{Ts + 2} = G_{pa}(s) \qquad (2\text{-}2)$$

The Pade' approximation is satisfactory only for small values of T (9:251). Specifically, the approximation is good for $\omega_c \leq \omega_s/10$. The PCT system model is shown in Figure 2-5 with the sampler and ZOH approximations included. Therefore the sampler and ZOH devices contained in the sampled data system are approximated in the PCT system by the transfer function

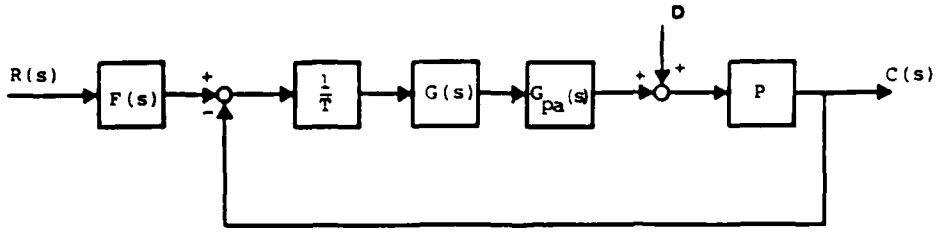

Fig. 2-5. PCT System Model

$$G_A(s) = \frac{1}{T} G_{pa}(s) = \frac{2}{Ts + 2} \qquad (2\text{-}3)$$

The usefulness of the PCT system model and Equation (2-3) are discussed in Chapter 3.

II-3 KC-135 Lateral Mode Models

The lateral mode equations of the KC-135 aircraft are reduced in reference 1 to a linear two input-two output model. Those equations were used to design the compensator for the lateral aircraft. A general block diagram corresponding to the lateral aircraft is shown in Figure 2-6 where $\underline{F}$, $\underline{G}$, and $\underline{P}$ are the prefilter, fixed compensator and plant matrices, respectively.

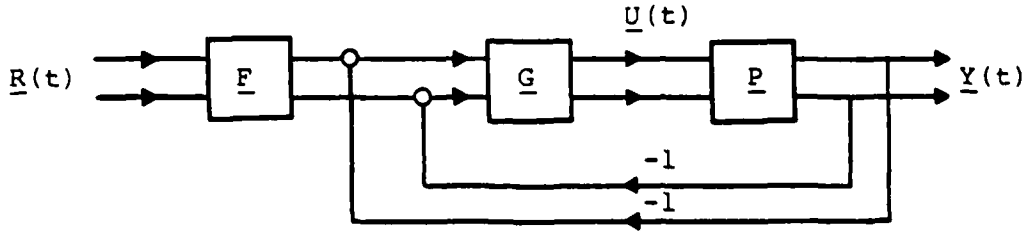

Fig. 2-6. KC-135 General Lateral Mode System Model

A more detailed continuous time signal flow diagram is shown in Figure 2-7. Note that both the prefilter and fixed compensator matrices are diagonal. QFT is not restricted to diagonal matrices, but the designs in both references 1 and 2 used diagonal $\underline{F}$ and $\underline{G}$. The inputs to the 2x2 model are: r_1 (bank angle command) = 30; r_2 (sideslip angle command) = 5. It is desired that the output y_1 track the input r_1 and that y_2 be ideally zero (with $r_2 = 0$). When r_2 is commanded it is desired that y_2 track r_2 while y_1 should be ideally zero (with $r_1 = 0$).

The sampled-data lateral system model is shown in Figure 2-8. As described in Section II-2, discrete rather than continuous controllers are used. The PCT approximation to the sampled-data model is shown in Figure 2-9.

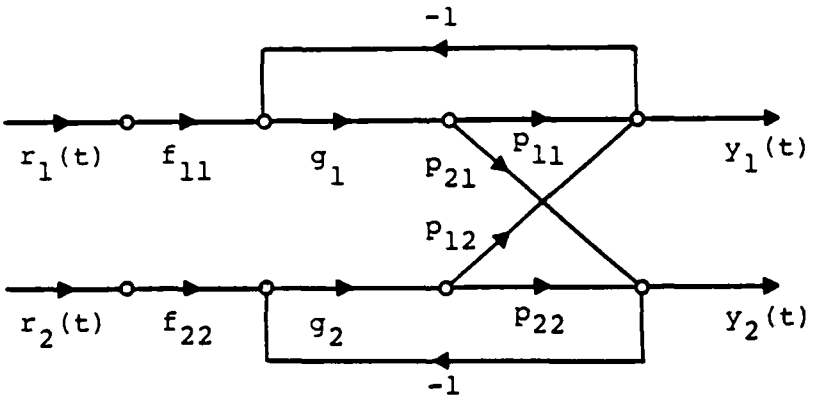

Fig. 2-7. KC-135 Lateral Mode Continuous Time System Model

The lateral aircraft equations given in reference 1 are in input-output matrix form, where an input matrix $\underline{N}$ premultiplies the input vector and an output matrix $\underline{M}$ premultiplies

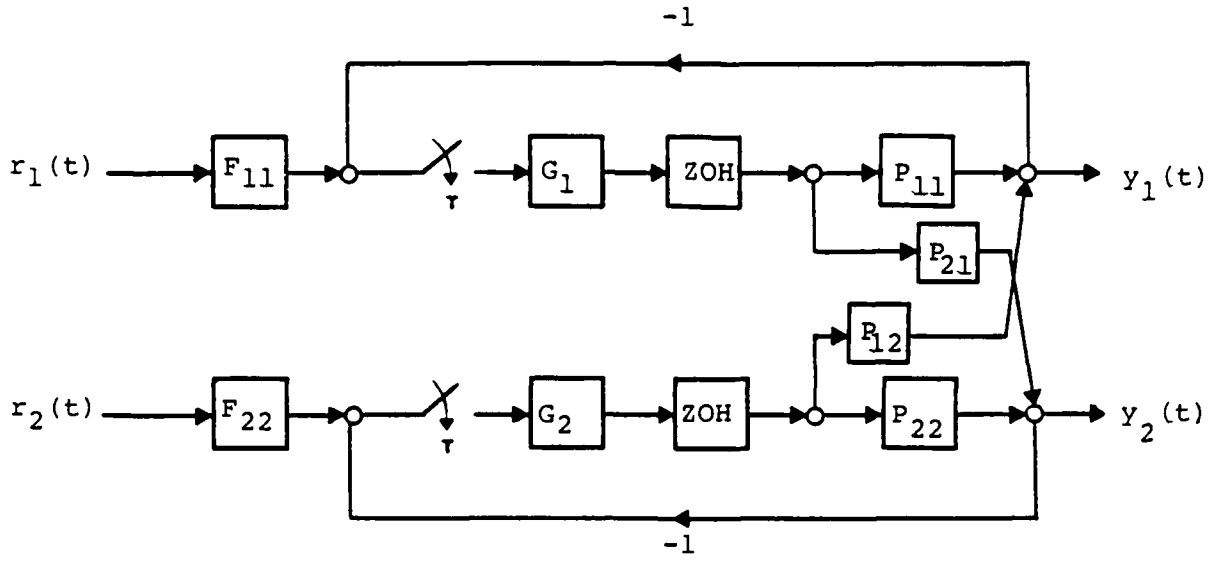

Fig. 2-8. KC-135 Lateral Mode Sampled-Data System Model

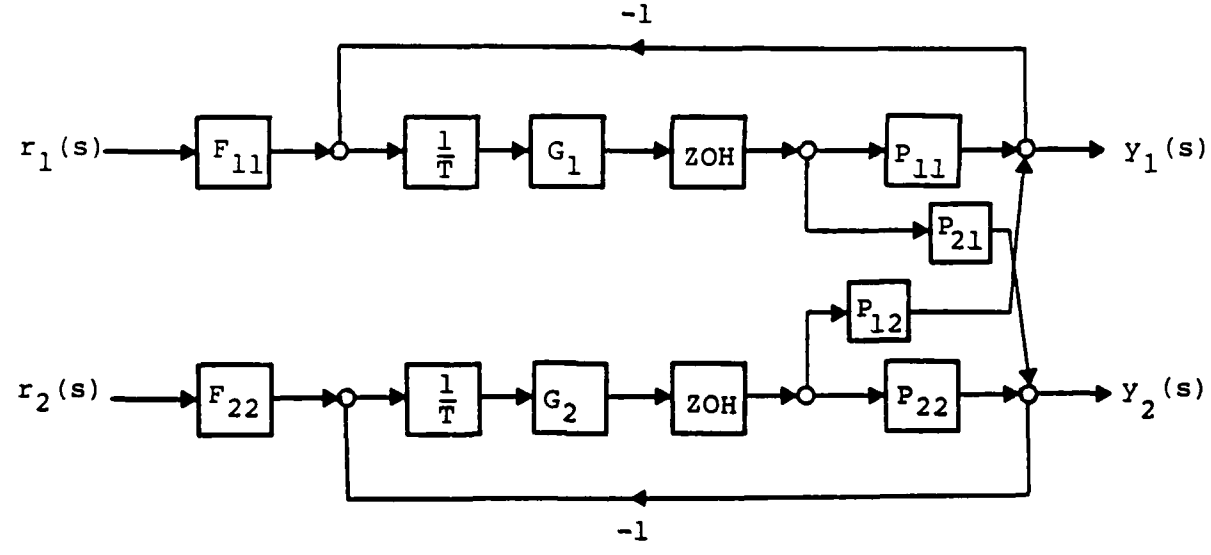

Fig. 2-9. KC-135 Lateral Mode PCT System Model

the output vector. The input and output vectors (1:35) are defined respectively as:

$$\underline{\delta} = \begin{bmatrix} \delta_w \\ \delta_r \end{bmatrix} \qquad \text{and} \qquad \underline{Y} = \begin{bmatrix} \phi \\ \beta \end{bmatrix}$$

The input vector variables are control wheel deflection and rudder deflection respectively. The output vector variables are roll angle and sideslip angle respectively. For flight condition (F.C.) #1 the lateral mode equations in input-output matrix form are (1:36):

$$\begin{bmatrix} (S^2+.74028S-.010714) & (.24789S+4.46897) \\ (.039665S^2+.06142S+.0065) & -(S^2+.227437S+1.43226) \end{bmatrix} \begin{bmatrix} \phi \\ \beta \end{bmatrix}$$

$$= \begin{bmatrix} .364455 & .708183 \\ (.00074615S+.020812) & -(.026647S+1.01677) \end{bmatrix} \begin{bmatrix} \delta_w \\ \delta_r \end{bmatrix} \quad (2\text{-}4)$$

The corresponding input-output matrix equations for F.C.'s #2 and #3 are contained in Appendix C.

As can be seen in Figure 2-8, the individual plant transfer functions, relating specific inputs to outputs, are needed for the model. Equation (2-4) can be written in general terms as:

$$\underline{M}\underline{Y} = \underline{N}\underline{\delta} \quad (2\text{-}5)$$

$$\underline{Y} = \underline{M}^{-1}\underline{N}\underline{\delta} \quad (2\text{-}6)$$

Using Equation (2-6), the plant transfer function matrix can be defined as:

$$\underline{P} = \underline{M}^{-1}\underline{N} \quad (2\text{-}7)$$

The matrix $\underline{P}$ contains the individual transfer functions needed for the system model used in this study. To obtain the plant transfer function matrix, a matrix inverse and

multiplication must be done. Since the individual elements of the input and output matrix are polynomials in S it is apparent that a great deal of effort would be required to obtain the transfer function matrix $\underline{P}$, especially if the order of the plant matrix is greater than 2x2. In addition to being a very tedious task, the large amount of algebraic manipulations involved would invariably result in many errors. The continuous domain design effort for the KC-135 required similar manipulations but instead of obtaining an exact solution, a computer program was utilized to numerically generate the magnitude and phase angle, as a function of frequency, of the individual functions. This method is undesirable since the transfer functions are not known explicitly. Using this method one must interpret the numerical magnitude and phase data. Although not necessary, it is usually convenient to then synthesize an appropriate transfer function. If non-minimum phase terms are present in the plant, it is very easy to misinterpret the data (10:272).

To avoid this problem altogether, a computer program called MACSYMA (11) that performs symbolic mathematical manipulations is used to obtain the transfer function matrices. This program is chosen over other similar programs because the computer it is hosted on (Digital Equipment Corp. PDP-10) has a large amount of core memory (as compared to various microcomputer hosted programs). Since the algebraic manipulations are symbolic rather than numerical, the results are in terms of the variable S and therefore explicit

transfer functions are obtained. Within the program there are functions that allow the inversion and multiplication of matrices whose elements are polynomials. It should also be noted that the symbolic algebraic manipulations are very accurate since intermediate operations are done with rational numbers instead of real numbers. The resulting plant transfer functions corresponding to Equation (2-4), F.C. #1, are:

$$P_{11} = \frac{.364635(S+.125308\pm1.29263)}{(S+.0104168)(S+.802130)(S+.0825017\pm j1.27795)} \quad (2\text{-}8)$$

$$P_{12} = \frac{.701577(S+2.39768)(S-2.09826)}{(S+.0104168)(S+.802130)(S+.0825017\pm j1.27795)} \quad (2\text{-}9)$$

$$P_{21} = \frac{-.00074615(S+.290305)(S+10.1471)(S-1.17926)}{(S+.0104168)(S+.802130)(S+.0825017\pm j1.27795)} \quad (2\text{-}10)$$

$$P_{22} = \frac{.026647(S+.770138)(S+39.189122)(S-.00782111)}{(S+.0104168)(S+.802130)(S+.0825017\pm j1.27795)} \quad (2\text{-}11)$$

The plant transfer functions for F.C.'s #2 and #3 are contained in Appendix C.

II-4 KC-135 Longitudinal Mode Models

Rigid Body

The longitudinal mode equations were developed in reference 1 as a three input-three output model. Only one maneuver is done in the longitudinal direction and it is a four degree pitch pointing maneuver. The pitch angle output, y_2 should track the pitch angle command input, r_2. The pitch pointing maneuver is to be done with minimum response in

altitude (y_1 = h) and horizontal velocity (y_3 = u). Ideally, the altitude and horizontal velocity outputs are zero. A general block diagram of the 3x3 longitudinal system is shown in Figure 2-10. A detailed continuous domain signal flow graph is shown in Figure 2-11 where it should be noted that as in the lateral model, $\underline{G}$ is diagonal. Since there is only one

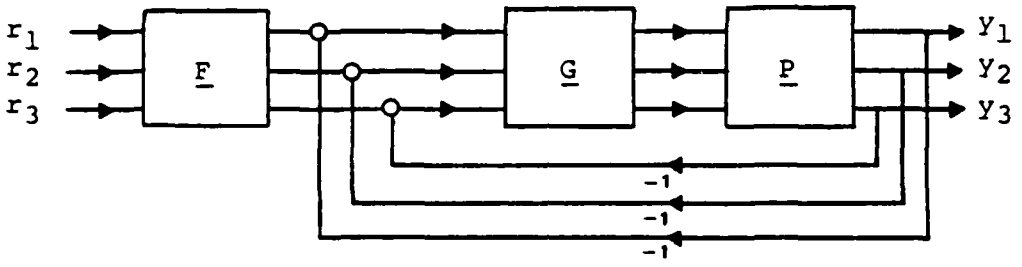

Fig. 2-10. KC-135 General Longitudinal Mode System Model

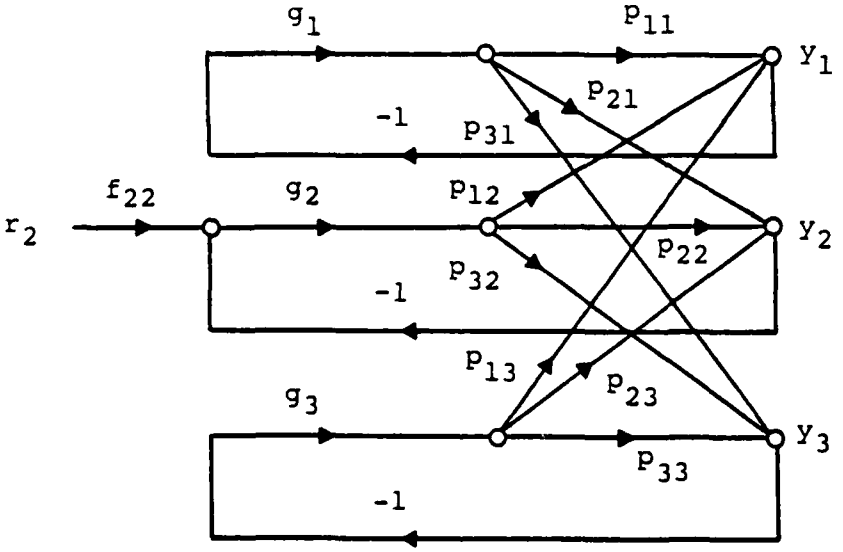

Fig. 2-11. KC-135 Longitudinal Mode Continuous Time System Model

commanded maneuver for the longitudinal mode, $\underline{F}$ has only one element, f_{22}. This implies that the inputs to loop one and three are zero.

The sampled-data longitudinal system model is shown in Figure 2-12 in block diagram form. Again, as in the lateral sampled-data model, the compensation is performed by digital controllers driven by sampled-signals. The ZOH's provide a piecewise continuous signal to the plants, p_{ij}. The diagram of the PCT approximation to the sampled-data system is the same as Figure 2-12 except that the sampler and ZOH are replaced by their continuous domain approximations, as discussed in Section II-2, and the continuous domain compensator transfer function is used in the PCT model.

The longitudinal mode aircraft equations given in reference 1 are in input-output matrix form, as shown in Equation (2-5). The input and output vectors are respectively:

$$\underline{\delta} = \begin{bmatrix} \delta_e \\ \delta_{sb} \\ \delta_T \end{bmatrix} \qquad \underline{Y} = \begin{bmatrix} h \\ \theta \\ u \end{bmatrix}$$

The input variables are defined respectively as elevator deflection, speed brake deflection and percent engine thrust (change from trim). The input-output matrices for F.C. #1 are shown in Equation (2-12) (1:69).

$$\begin{bmatrix} .0411S & (.53477S-1.096) & (S+.003) \\ (-.0769S^2-.0417S) & (.007S+.5441) & .0049 \\ -.2151S & (S^2+.7537S+2.797) & -.0105 \end{bmatrix} \begin{bmatrix} h \\ \theta \\ u \end{bmatrix}$$

$$= \begin{bmatrix} .011619 & -.0827 & .0495 \\ -.021319 & .032 & 0 \\ -1.649 & .1733 & 0 \end{bmatrix} \begin{bmatrix} \delta_e \\ \delta_{sb} \\ \delta_T \end{bmatrix} \qquad (2\text{-}12)$$

The input-output matrices for F.C.'s 2 and 3 are given in Appendix C.

The symbolic mathematical manipulation program was again used to perform the inversion and multiplication operations indicated in Equation (2-7) to yield the transfer function matrix $\underline{P}$. The individual transfer functions P_{ij} for all three F.C.'s are listed in Appendix C.

Elastic Body

A continuous domain controller design was also done for a non-rigid KC-135 model where the first and second body bending modes were included (1:89). Due the small magnitudes of these two modes, the continuous domain QFT design process generated the same compensators as for the rigid body (1:97). To enable hybrid simulations to be performed on the elastic body, the elastic body transfer functions must be obtained. The following discussion explains this process.

The form of the rigid aircraft equation is

$$\underline{M}_R\underline{Y} = \underline{N}_R\underline{\delta} \qquad (2\text{-}13)$$

where $\underline{M}_R$ and $\underline{N}_R$ are defined as the rigid aircraft input and output matrices respectively. The form of the elastic aircraft equation is

$$\underline{M}_e\underline{Y} = \underline{N}_e\underline{\delta} \qquad (2\text{-}14)$$

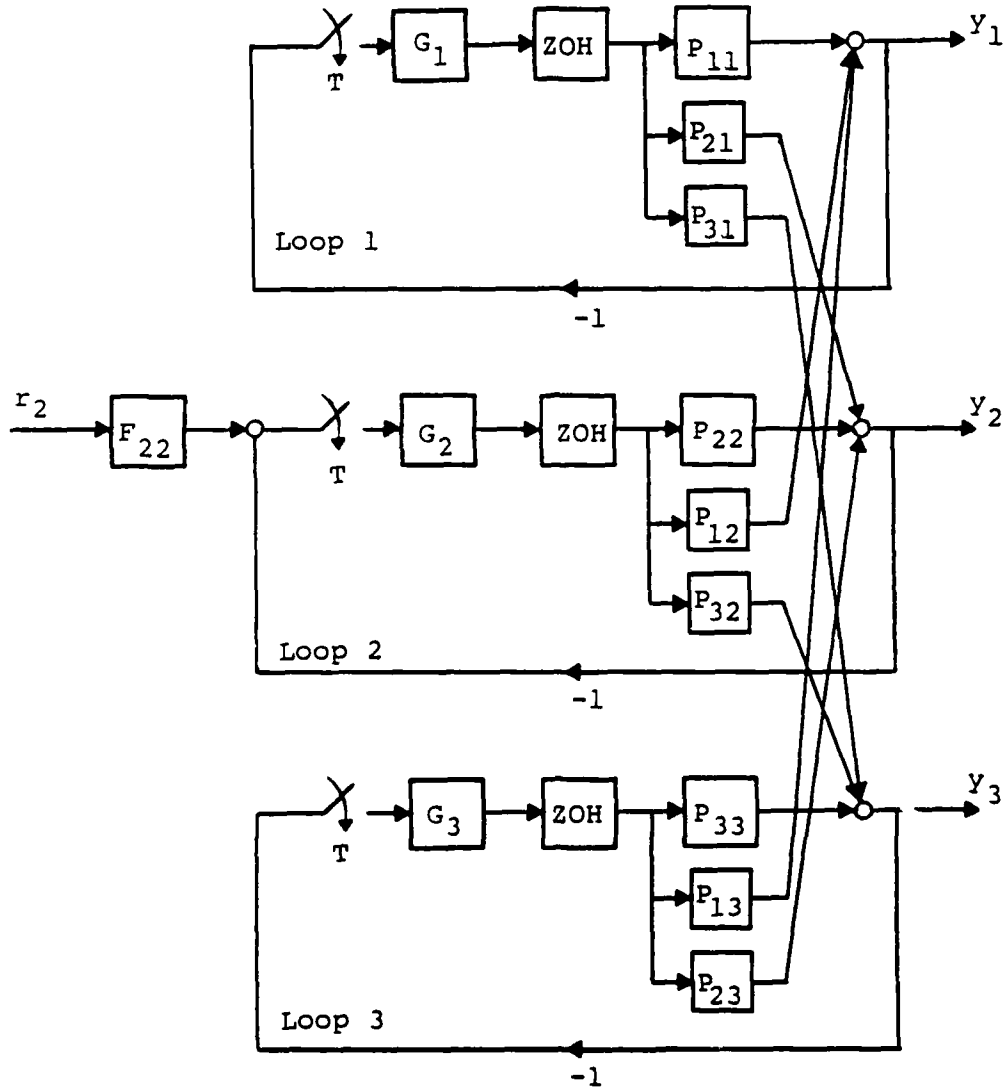

Fig. 2-12. KC-135 Longitudinal Mode Sampled-Data System Model

where $\underline{M}_e$ and $\underline{N}_e$ are defined as the elastic body input and output matrices respectively. The elastic body input-output matrices are included in Appendix C. Equations (2-13) and (2-14) can be written in the following form

$$\underline{Y} = \underline{M}_R^{-1}\underline{N}_R\underline{\delta} \qquad (2\text{-}15)$$

and

$$\underline{Y} = \underline{M}_e^{-1}\underline{N}_e\underline{\delta} \qquad (2\text{-}16)$$

where the input and output vectors are defined as indicated for the rigid body case above. Combining the rigid and bending mode equations yields

$$\underline{Y} = \left[\underline{M}_R^{-1}\underline{N}_R + \underline{M}_e^{-1}\underline{N}_e\right]\underline{\delta}$$

Therefore

$$\underline{P}_c = \underline{M}_R^{-1}\underline{N}_R + \underline{M}_e^{-1}\underline{N}_e = \underline{P}_R + \underline{P}_e \qquad (2\text{-}17)$$

As before, the manipulation needed in Equation (2-16) is performed using the symbolic math program. The results of this manipulation showed that all elements of $\underline{P}_e$ are zero except for P_{e11} and P_{e21}. Therefore the only difference between $\underline{P}_c$ and $\underline{P}_R$ are the elemental transfer functions P_{c11} and P_{c21}. These two elemental transfer functions are obtained using Equation (2-17). The transfer functions P_{c11}, P_{c21}, P_{e11} and P_{e21} are shown in Appendix C.

The elastic system model diagrams are the same as those for the longitudinal rigid body except the appropriate transfer functions are substituted as discussed above.

II-5 F-16 Models

The F-16 model is significantly more complicated

than the KC-135 models due to the reconfiguration nature of the original design. The need to maintain stability and control of the aircraft in the event of single or simultaneous control surface failures requires cross coupling of the compensation signals. Because of the added complexity, a more detailed discussion of the model is included for the F-16. The following two paragraphs are taken from reference 2 with some minor modifications.

The structure for the continuous time domain system model for the F-16 is shown in Figure 2-13 (2:16) in signal flow graph form. A two-elevator, two-flaperon system is represented with each individual surface separately controllable. The elevators and flaperons are capable of moving individually, and symmetrically or differentially in pairs. The right and left elevators are designated by δ_1^a and δ_1^b, respectively and the flaperons are designated similarly by δ_2^a and δ_2^b. The longitudinally controlled output variable is pitch rate, q, while the laterally controlled output variable is roll rate, p. The plant transfer function designator, P_{ij}, relates the i^{th} output to the j^{th} input (control variable). A superscript "a" or "b" denotes the right or left control. For example, P_{21}^a denotes the effect of the right elevator (δ_1^a) on roll rate (output y_2). For a normally operating system, $P_{ij}^a = P_{ij}^b$. Minus signs are associated with P_{21} and P_{22} so that the two pairs of surfaces move differentially to generate roll rate. In the no fail case, surfaces move an equal amount in either direction to generate the commanded rates.

No interaction is desired between the longitudinal and lateral modes under normal operating conditions.

Normally, the elevators move together in the same direction to excite only the longitudinal mode, and the flaperons move opposite each other to excite only the lateral mode. Separate control of the surfaces increased the flexibility of a system by exciting both aerodynamic modes when a single surface is actuated. For instance, using the structure of Figure 2-13, the surfaces continue to act in pairs under normal operation, but act separately, as necessary, to offset

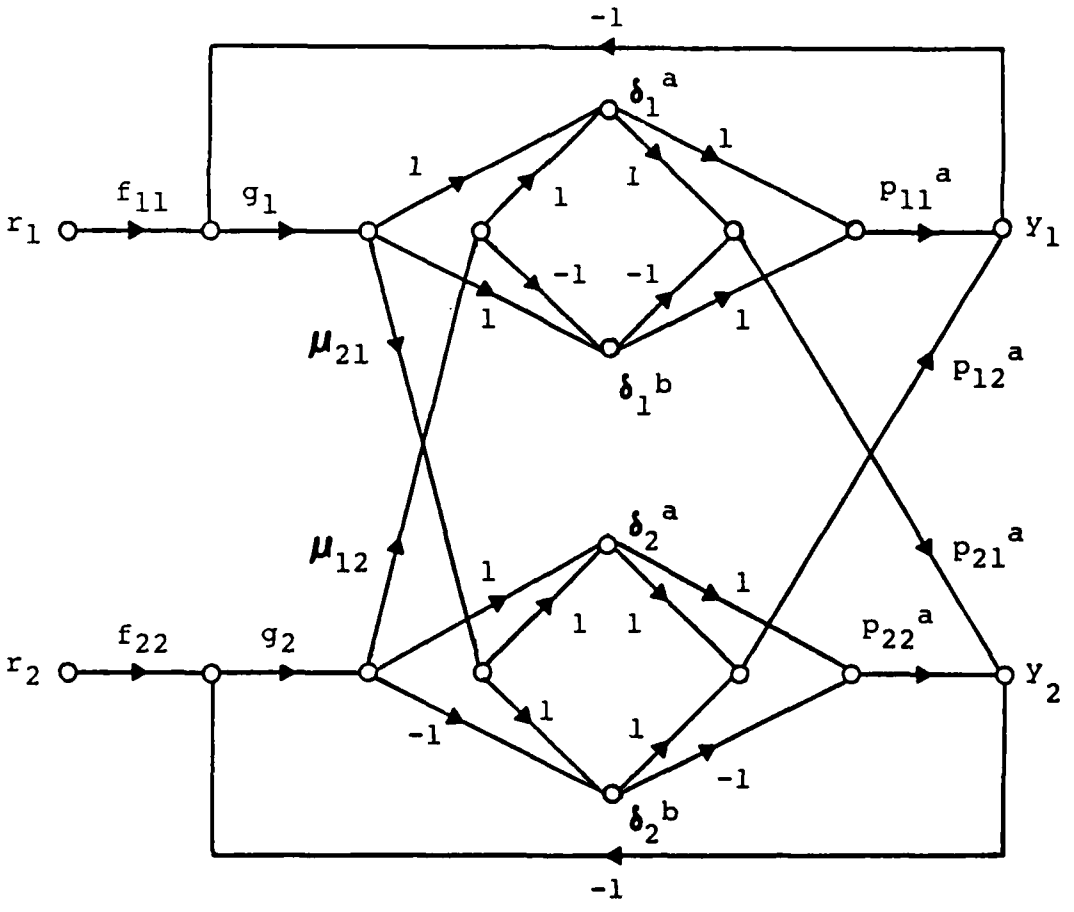

Fig. 2-13. F-16 Continuous Time System Model

parameter changes resulting from single or multiple control system component failure. In Figure 2-13, μ_{12} and μ_{21} are constants which determine the division of control effort between the flaperons and elevators. In the preliminary reconfiguration study done in reference 2, optimization of these constants was not addressed, and both μ's were set equal to 0.25. Henceforth, the subscripts are dropped on these two constants.

Figure 2-14 shows the sampled-data system model for the F-16 in block diagram form. As for the KC-135, the sampled-

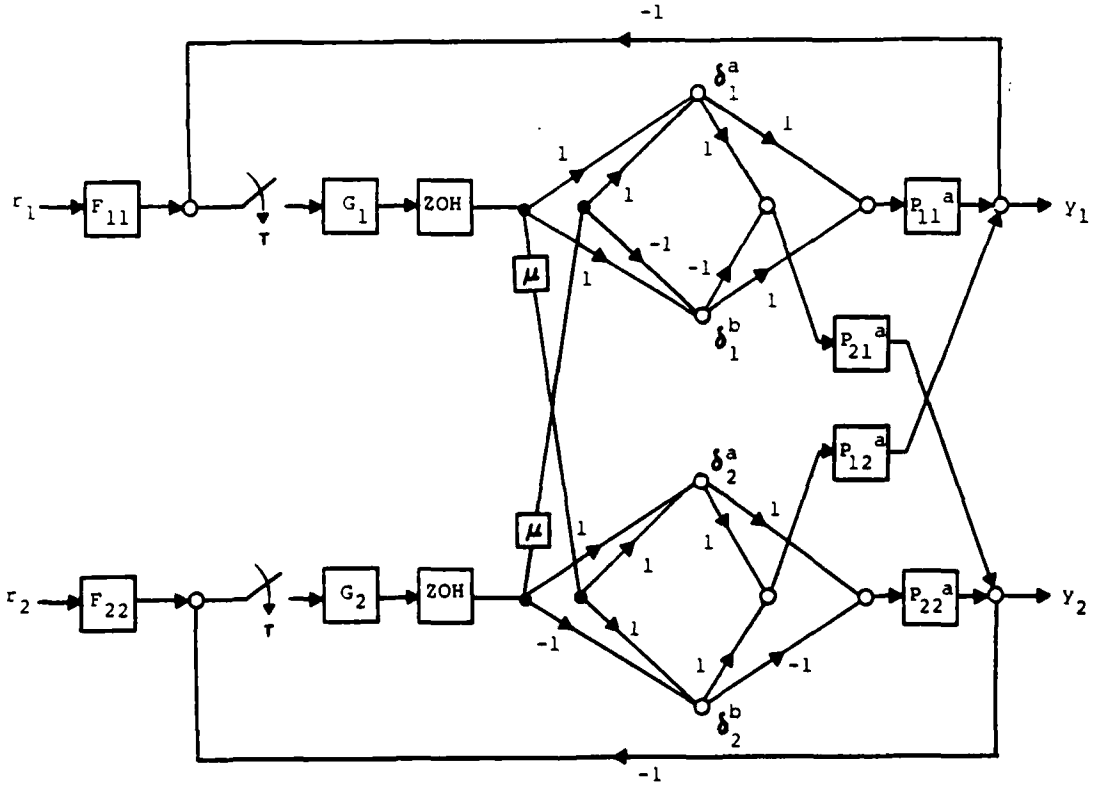

Fig. 2-14. F-16 Sampled-Data System Model

data system model is generated by replacing the continuous domain compensator with the sampler/digital controller/ZOH combination. The PCT system diagram is the same as Figure 2-14 except that the sampler and ZOH are replaced by their continuous time domain approximations, as discussed in Section II-2, and the continuous domain compensator is used in place of the digital controller.

A set of equivalent plant transfer functions were developed in reference 2 to populate the 2x2 multiple input-multiple output (MIMO) system model discussed above for four different F.C.'s. Each set of transfer functions model the healthy (no failures) aircraft. The P_{ij}'s for all four F.C.'s are given in Appendix C (2:13).

II-6 Response Models

As discussed in Appendix A, the QFT design technique involves quantifying the range of desired responses for a given command input. The response range for tracking is expressed as an upper and lower limit while the disturbance rejection response often is just an upper bound. The desired responses are usually given as time domain specifications, such as the figures of merit M_p, t_s, t_p, and K_m and are based on a step or ramped step input. These desired responses are used to determine bounded regions in the frequency domain as part of the design process and to check the system performance. The figures of merit for the KC-135 and the F-16 QFT designs were established as part of the continuous domain design process of reference 1 and 2. The performance obtained

by the sampled-data system designed in this thesis is compared against the performance of the continuous system and its associated response models. The response models for both aircraft are contained in Appendix D (1:211; 2:152). Only the figures of merit are given. The response model transfer functions can be found in reference 1 and 2. A detailed description of how the response models are specified and used is contained in Appendix A.

II-7 Summary

The system models for the KC-135 lateral and longitudinal modes and the F-16 are presented in this chapter. The relationship between the continuous domain, sampled-data and PCT systems models are discussed. Plant transfer functions for both aircraft are given. Response models for the KC-135 and F-16 are presented.

III. Theoretical Digital Design

III-1 Introduction

This chapter is devoted to the design of robust discrete controllers for the KC-135 and F-16 aircraft. Since the intent of this thesis investigation is to determine the feasibility of extending continuous domain QFT designs to discrete designs while still maintaining acceptable performance and robustness, the original continuous domain designs provide the starting point for this study. The first aspect of the digital design is to examine a technique for compensating for one of the sources of lag in a sample-data system. Sampling rates for both aircraft are discussed and selected. Once the sampling rates (i.e. frequency) have been established, various transformations are performed on the modified continuous domain QFT controllers to generate the discrete controllers. Both the standard Z and Tustin transformations are examined. The last portion of this chapter discusses the problems encountered in extending the F-16 continuous domain design to the discrete domain.

III-2 Counteracting ZOH Lag

QFT design technique is usually applied in the continuous frequency domain (although QFT can be applied in the discrete frequency domain). As discussed in Appendices A and B, desired response models are used to develop bounds in the continuous frequency domain which are constraints on the loop transmission function, L, for each channel. These bounds are

usually placed on a Nichols chart to show by graphical means the constraints or requirements on the loop transmission. Figure 3-1 shows an example of a loop transmission shaped to meet bounds at various frequencies. In fact this is the continuous domain nominal loop transmission designed for loop two (tracking loop) of the KC-135 longitudinal mode (1:81). In QFT, an "optimum" loop transmission design is one for which $\underline{L}_o(j\omega_i)$ lies just on the boundary $\underline{B}(j\omega_i)$. In this case, optimum means that the desired performance and robustness are guaranteed while obtaining the smallest bandwidth possible. As can be seen from Figure 3-1, the loop transmission tracks down the universal high frequency boundary (UHFB) with only a few degrees of separation over a frequency range of about 75 rad/sec. Remembering that

$$L = PG \tag{3-1}$$

it is apparent that any change in the compensation, G, which results in additional lag could take the loop transmission into the UHFB. If this occurs, and depending on the severity of the additional lag, some plants in the parameter space can exhibit less than desired performance or they can be unstable (5:291).

As discussed in Section II-2, a ZOH is included in the sampled-data system models to construct a piecewise continuous signal from the discrete output of the digital controllers. Figure 3-2 shows the frequency response characteristics of the

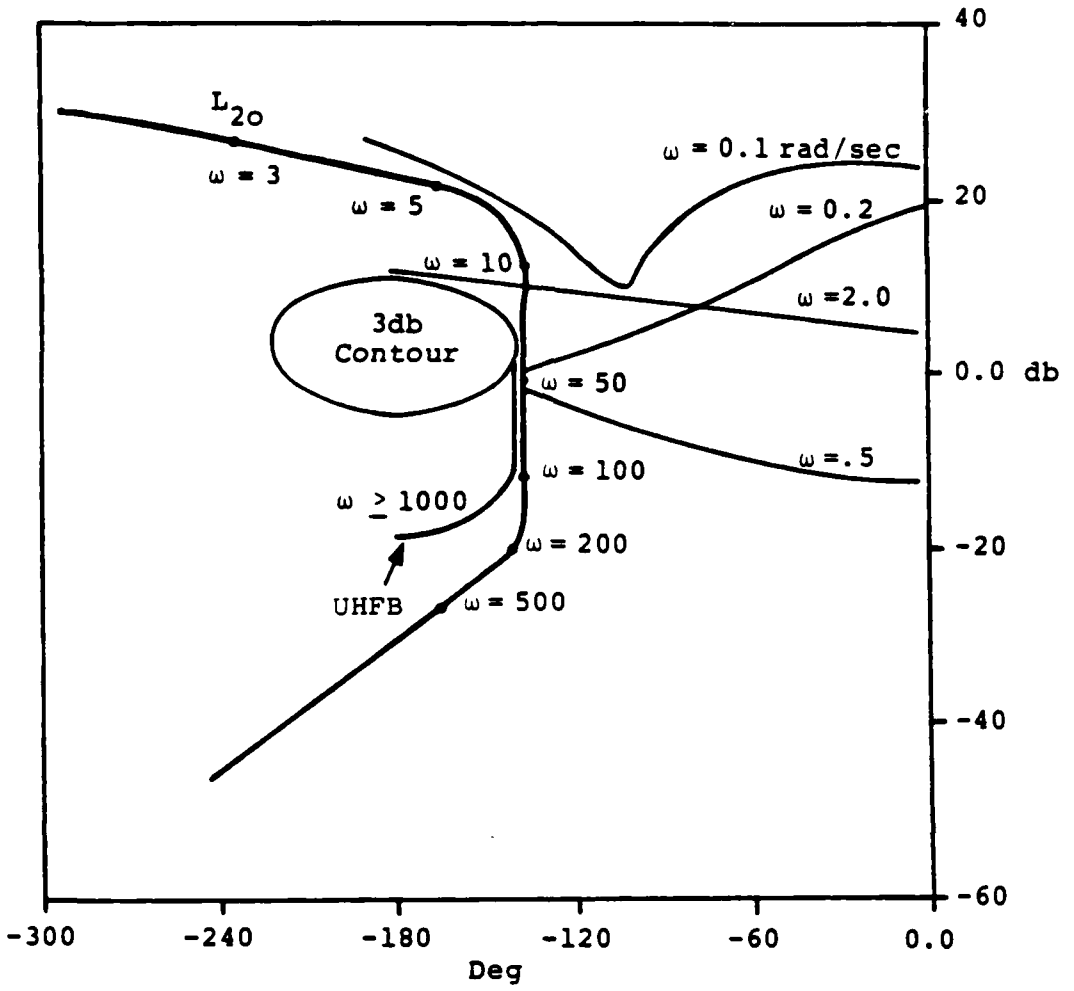

Fig. 3-1. Example of Bounds and Nominal Loop Transmission

ZOH where the ZOH transfer function is shown in Equation (2-1). It is clear from the magnitude curve of Figure 3-2 that the ZOH approximates the behavior of a low-pass filter. This is desirable, as previously mentioned, because the low-pass characteristic tends to smooth the high frequency noise in the system. The phase curve of Figure 3-2 shows that the ZOH has a considerable lag characteristic. Since the intent in the sampled-data system is to maintain the frequency

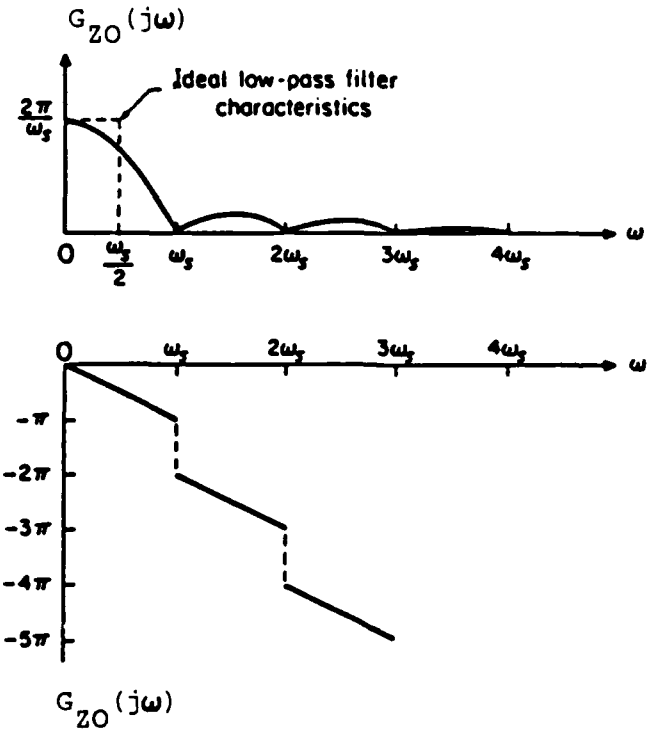

Fig. 3-2. Gain and Phase Characteristics of a ZOH

response characteristics of the original continuous domain loop transmission (and therefore compensators), it is clear then that the ZOH by itself can have an undesirable effect. Also, by comparing the frequency spectra of a continuous signal, $E(j\omega)$, and the associated output of an ideal sampler, $E^*(j\omega)$, it can be seen that the output magnitude has been changed by a factor of T^{-1} (9:85).

Thus it is desirable to modify the original compensators in a fairly straightforward manner whereby the undesirable effects of the sample and hold processes are diminished. In Section II-2, the PCT system model is developed as a means of approximating the effects, in the S domain, of the sample and hold processes. Equation (2-3) shows the transfer

function, $G_A(s)$, which approximates these two processes. The original S domain QFT compensators, $G'(s)$, can be modified by $[G_A(s)]^{-1}$ to obtain

$$G(s) = [G_A(s)]^{-1}G'(s) \qquad (3\text{-}2)$$

The net affect is that the gain is modified by a factor of T and phase lead is added to the compensation. The overall effect on the loop transmission can be shown mathematically in the following way. Assuming the PCT approximation to the sampled-data system model, the loop transmission can be written as

$$L = \left[G_A(s)\right]^{-1}G'(s)P(s) \qquad (3\text{-}3)$$

If the original S domain compensators $G'(s)$ are replaced by the modified compensators G(s) using Equation (3-2) it can be seen that the original loop transmission of Equation (3-1) results. All of the S domain QFT compensators are modified as shown in Equation (3-2) before being transformed to their discrete form. The transformations are discussed in Section III-4.

III-3 Sample Rate Selection

There are a multitude of techniques used to select the sample rate of a sampled-data system, many of which often depend on the original design technique used. A review of the literature (12:975) shows that in general, control system designs done first in continuous domain and then extended to the discrete domain, tend to require a higher sample rate than

those systems designed originally in the discrete domain (direct method). The major considerations which influence the selection of sample rate can be divided into three broad categories: closed-loop bandwidth or time response requirements, rejection of unwanted disturbances and sensitivity to parameter variations (12:975). These categories tend to provide bounds only on the lower limit of the sample rate. Generally, for an aircraft digital controller, the selection of a sample rate represents a trade off between cost/accuracy and desirable characteristics in one of the three areas listed above. By lowering the sampling frequency, ω_s, the A/D and D/A equipment cost is reduced directly. Also, the increased accuracy obtained by slower sampling (increased T) is well documented (12:975) and can be reflected into reduced costs by decreasing the microprocessor and A/D wordlength. Since cost is not a direct concern of this study, an upper bound on the sampling rate is established by what sample rates are currently considered practical and realizable in avionics systems. Sample rates of 40 to 60 Hz are used as a realistic upper bound. Only the first category of the three mentioned above is considered in the selection of the value of T in this thesis since the last two categories are explicitly included in the QFT design process. These two categories are usually reflected in the bandwidth of the system anyway (QFT designs).

An absolute lower bound on the sample rate is established by a desire to track a specified command input signal. This bound derives its theoretical basis from Shannon's

Sampling Theorem. The theorem states that in order to reconstruct a band-limited continuous signal from samples of that signal, one must use a sample rate which is at least twice as high as the highest frequency contained in the signal. It should be added that only signals of "significant amplitudes" need be considered (8:79). The implication here is that the signals are from the closed-loop system. This theorem, however, only provides a fundamental lower limit and in practice it tends to be significantly higher. Franklin and Powell provide a "rule of thumb" that the sample rate must be about 4 to 20 times the closed loop bandwidth of the system to obtain the desired transient characteristics (13:276). This rule is used as a "guide-post".

The closed-loop bandwidth of both aircraft can be estimated from the Nichols charts used in the designs of references 1 and 2. For the KC-135, the largest closed-loop bandwidth was approximately 55 rad/sec which was associated with the longitudinal mode tracking channel (loop 2). This bandwidth is quite high. The other loops were generally well below 30 rad/sec. The design of the loop transmission corresponding to this maximum bandwidth (1:86) shows that there is some overdesign, which translates into a higher than necessary bandwidth. Since the initial selection of sample rate is based upon bandwidth it is important to stress that the designer of QFT continuous domain compensators insure that the bandwidth be as small as possible. As a first trial for both the lateral and longitudinal modes of the KC-

135, a sample rate of 40 Hz is used which is about five times the maximum closed-loop bandwidth. As is discussed in the next chapter, this sample rate proves to be quite satisfactory.

The maximum closed-loop bandwidth for the F-16 continuous domain design was 34 rad/sec (2:37). A sampling rate of 40 Hz, which represents a multiplier of about 7, is also chosen for the F-16. Intuitively, one can expect the F-16 to require a higher sampling rate due to the naturally faster response of the aircraft, its relative size, and the reconfiguration requirements on the QFT design. In part, this can be explained by the fact that the designs were done by two different designers who attained different levels of proficiency in the QFT design technique. Although not accomplished in this study, it is quite possible that a sampling rate of less than 40 Hz would have provided good performance for the KC-135.

The F-16 proved to be unstable for all four F.C.'s at the 40 Hz sample rate initially chosen. The sample rate was then increased to 60 Hz which generated satisfactory performance for one of four F.C.'s (#1). Some modifications to the Z domain compensators were made which provided some additional improvement in performance. The modifications made to the controllers and explanation of the poor performance are discussed in the last section of this chapter.

The continuous domain QFT compensators for the lateral mode of the KC-135 are shown in Equations (3-5) and (3-6)

after having been modified as discussed in Section III-2. The unmodified compensators can be found in reference 1. As discussed previously, the sample rate chosen was 40 Hz.

$$G_1(s) = \frac{1081075(S+4)(S+4)(S+17)(S+50)(S+80)}{(S+10)(S+10)(S+83)(S+100)(S+60\pm j80)} \qquad (3\text{-}5)$$

$$G_2(s) = \frac{295125(S+7)(S+80)}{(S+50)(S+96\pm j128)} \qquad (3\text{-}6)$$

At the beginning of this thesis effort a gross overdesign was discovered in the loop transmission (loop 1) of the KC-135 lateral mode. This was due to an error in plotting the UHFB on the Nichols chart. After reference 1 was finished, the author (Capt Russell) removed some of the overdesign by adjusting the location of the complex pole pair of $G_1(s)$. The previous location was at $s = -900\pm j1200$. As can be seen, this was a significant modification and explains the difference between Equation (3-5) and $G_1(s)$ in reference 1. The modified S domain QFT compensators for the KC-135 longitudinal mode and the F-16 are given in Appendix E.

III-4 Transformation of Compensators

There are several ways of obtaining G(z) from G(s), but only two are considered in this thesis. As mentioned previously, these two methods are the standard Z transform and the Tustin transformation (also called the bilinear transformation or trapezoidal integration). Some of the other methods are forward rectangular integration (forward difference), backward rectangular integration (backward difference),

matched Z transform (pole-zero mapping) (8:338; 13:61) and hold equivalence (13:62). Of the other methods, the matched Z transform and the hold equivalence seem to provide the best results while the rectangular integration methods generally give poor results (13:66).

III-4-1 Standard Z Transform. The standard Z transform is chosen primarily because it encompasses the definition of the Z transform. The Z transform can be stated in its most simple form as a mapping from the Laplace domain to the Z domain:

$$z = e^{Ts} \tag{3-6}$$

To transform G(s) to G(z) using the standard Z transform in a closed form one must first obtain a partial fraction expansion of G(s). Generally, the poles of each term in the resulting summation are then mapped using Equation (3-6) and the residues of each term are calculated (9:113). The standard Z transform is best applied using a computer-aided design program such as TOTAL (14), especially if G(s) is of higher order than two and/or has repeated poles. The CAD package of reference 14 is used to obtain G(z) from G(s) using the standard Z transform. Simulations using these compensators showed that the system is unstable. Closer examination of the discrete compensators revealed that the transformation generated the proper poles but had mapped the zeros to the same location as the poles. Graphically this can be seen by comparing Figures 3-3 and 3-4. Figure 3-3 is the

continuous frequency response of Equation (3-4), which is $G_1(s)$ for the lateral mode of the KC-135. The discrete frequency response of $G_1(z)$ is shown in Figure 3-4. As can be seen, the frequency response is essentially flat in the frequency range defined by the primary strip, $\omega_s/2$. The Z transform of Equation (3-5) is given by Equation (3-7). Similar results are obtained on all the other compensators transformed using the CAD package (14) and the standard Z transform. The desirable gain and phase characteristics of the compensators have therefore been lost in the transformation.

$$G_1(z) = \frac{1081075Z(Z-.1306)(Z-.7798\pm j.01498)}{(Z-.08208)(Z-.1256)(Z-.7788)^2} \qquad \frac{(Z-.04187\pm j.2072)}{(Z-.09285\pm j.2029)} \qquad (3\text{-}7)$$

Another discrepancy in the CAD package arose using the standard Z transform. Equation (3-8) shows $G_1(z)$ for the longitudinal mode of the KC-135 resulting from the CAD program.

$$G_1(z) = \frac{-654.75Z(Z-1.115)}{(Z-.3824\pm j.3937)} \qquad (3\text{-}8)$$

The corresponding continuous domain compensator is shown in Appendix E. The significant point here is that the CAD package generated a compensator with a zero outside the unit circle from one that contained only left half plane poles and zeros. Performing the standard Z transform by hand produced

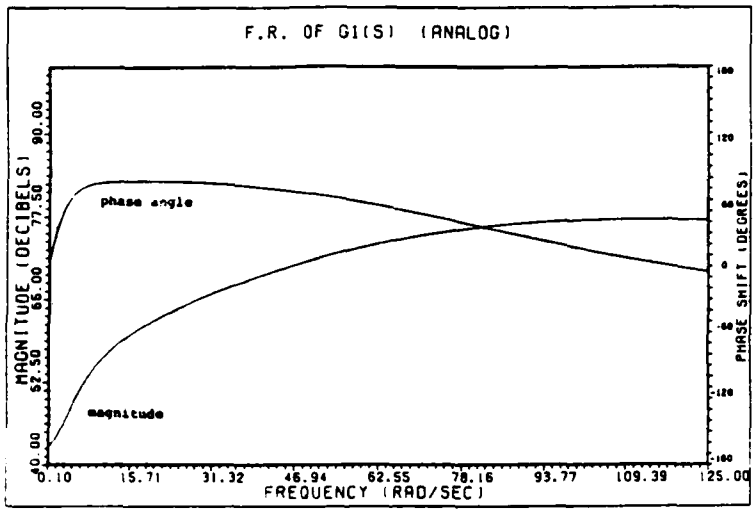

Fig. 3-3. Continuous Frequency Response of $G_1(s)$, KC-135 Lateral Mode

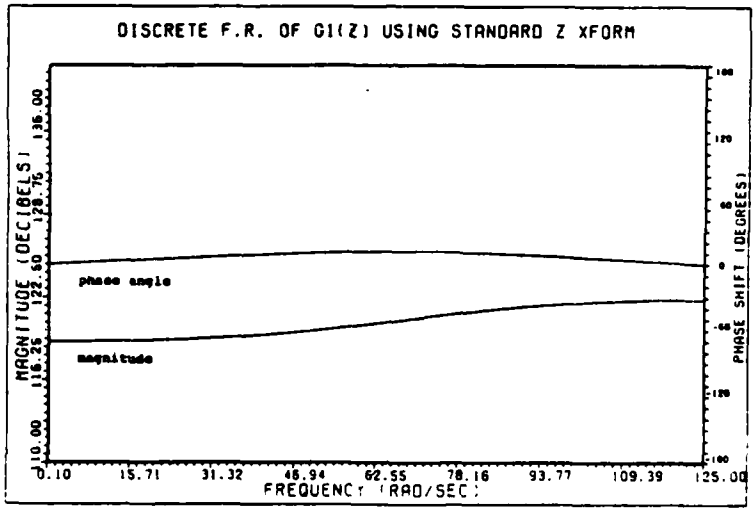

Fig. 3-4. Discrete Frequency Response of $G_1(z)$, KC-135 Lateral Mode

the following compensator:

$$G_1(z) = \frac{-672.94(z-.0220)(z-.3708)}{(z-.3824 \pm j.3937)} \qquad (3\text{-}9)$$

Thus it is apparent that the CAD package is not producing the correct results. In addition, examination of the discrete frequency response of Equation (3-9) exhibited the same loss of desirable magnitude and phase characteristics as compared with the analog frequency response. In light of the above discussion, the standard Z transform is not a useful tool in extending the continuous domain compensators to discrete domain and is not discussed further in this study.

III-4-2 Tustin Transformation. The Tustin transformation is an approximation to the standard Z transform (8:194; 9:237; 13:56). For a properly chosen sample period, T, the Tustin transformation has shown to provide good correspondence between the continuous and discrete domain frequency responses and thus is quite popular as a design tool. The definition of the Tustin transformation is

$$s = \frac{2}{T}\frac{z - 1}{z + 1} \qquad (3\text{-}10)$$

The transformation is applied by substituting the above relation into the S domain compensator transfer functions with a specified sample period. In some cases, if good discrete response characteristics are not achieved, it is necessary to "prewarp" the S domain frequencies prior to using Equation (3-10) (9:246). The Tustin transformation is applied, at least initially, without prewarping.

As mentioned previously, the accuracy of the mapping of the Tustin transformation is dependent on the relationship

between the sample period and the location of the S plane poles and zeros. Figure 3-5 shows the regions in the S plane, as a function of T, where the Tustin approximation produces good results (9:247). The warping of poles and zeros located within the cross-hatched area is negligible. Poles and zeros located within the enclosed uncross-hatched area are warped to some extent but real poles and zeros in this region still remain on the real-axis in the right-half of the Z plane unit circle. This is an important point and is discussed further in the next section.

The allowable regions for the KC-135 and F-16 are shown in Figures 3-6 and 3-7, respectively. A comparison of these two figures and the original S domain QFT compensators shows

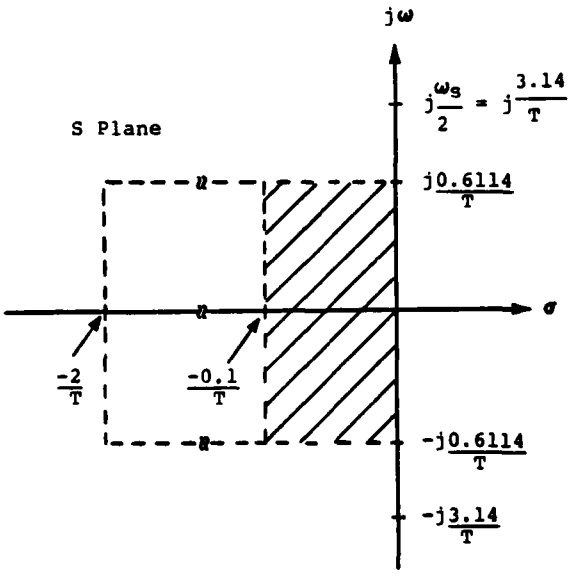

Fig. 3-5. S-Plane Regions for Good Tustin Approximation

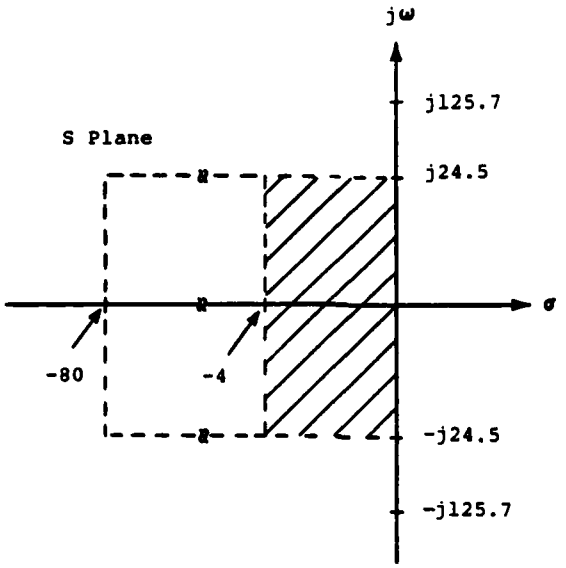

Fig. 3-6. KC-135 Tustin Mapping Regions, f_s = 40 Hz

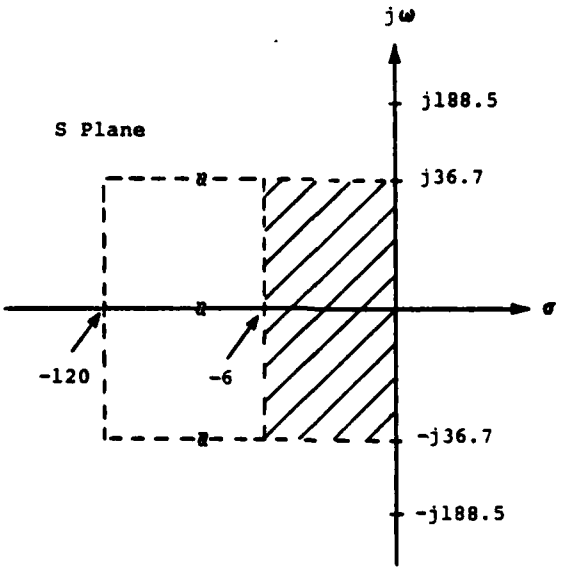

Fig. 3-7. F-16 Tustin Mapping Regions, f_s = 60 Hz

that good mapping characteristics can be expected for the majority of the poles and zeros. There are, however, some

exceptions. Each S domain QFT compensator has a high frequency complex pole pair for the purpose of noise rejection. All of the pole pairs (both aircraft) except for $G_1(s)$ and $G_3(s)$ of the KC-135 longitudinal mode are warped significantly. This warping has no real effect since these poles were generally at or well above the sampling frequency. $G_1(s)$ for the KC-135 lateral mode had several real poles that were warped onto the left-half Z plane real axis within the unit circle thereby severally limiting there intended lag effect (on the loop transmission). As is shown in the next chapter, this warping had no effect on the robustness or performance because all the bounds are still met. In other words, the loop transmission moved to the right due to the loss of the lag effect but still met all the bounds. The F-16 compensators each had a zero that is warped significantly and the effect of the warping is discussed in the next section.

The result of performing the Tustin transformation on the KC-135 lateral mode compensators is shown in Equations (3-11) and (3-12).

$$G_1(z) = \frac{2490.75z(z+1)(z-.904762)^2(z-.649485)}{(z-.777778)^2(z+.018405)(z+.111111)} \cdot \frac{(z-.230769)}{(z+.138462\pm j.492308)} \qquad (3\text{-}11)$$

$$G_2(z) = \frac{667.252z(z+1)(z-.839080)}{(z-.230769)(z+.405405\pm j.432432)} \qquad (3\text{-}12)$$

An example of the good mapping characteristics achieved by

the Tustin transformation can be seen in Figure 3-8 where both the discrete frequency response for the KC-135 lateral mode $G_1(z)$ and the corresponding continuous frequency response are plotted. The Tustin transformed discrete controllers for the KC-135 longitudinal mode and the F-16 are shown in Appendix E.

It should be noted that the Tustin transformation algorithm in the CAD program (14) performed the transformation correctly for the relatively low order compensators associated with the KC-135. The CAD program was inaccurate for the high order F-16 compensators. The algorithm produced poles outside the unit circle from transfer functions that contained all left-half S plane poles and also generated complex pole pairs from real S plane poles. It is assumed that these inaccuracies are the result of numerical problems within the compu-

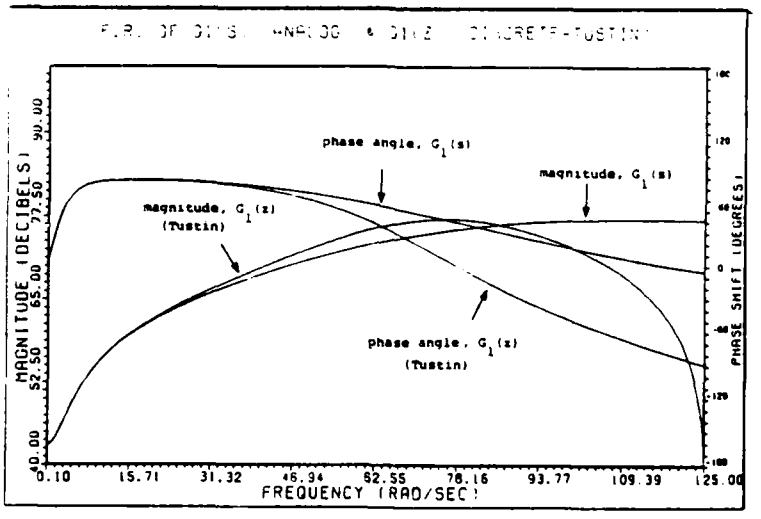

Fig. 3-8. Frequency Response for $G_1(z)$ and $G_1(s)$, KC-135 Lateral Mode

ter. Due to this numerical problem, the Tustin transformation for the F-16 compensators were obtained by hand calculations.

III-5 F-16 Pole-Zero Mapping Problems

Simulations for the F-16 sampled-data system showed that for F.C.'s 2, 3, and 4, the system is unstable when using the discrete compensators transformed via Tustin. Simulations involving F.C. 1 (all CSC modes) are stable and met all specifications. As mentioned in the previous section, one real zero in each of the F-16 compensators is warped onto the left-half real axis within the unit circle at sampling frequencies of 40 and 50 Hz. With f_s = 60 Hz the zero associated with $G_2(z)$ is mapped into the origin of the Z plane while the zero associated with $G_1(z)$ is mapped into the left-half Z plane real axis within the unit circle. Table 3-1 shows the migration of the poles and zeros of $G_1(z)$ as the sampling frequency is increased from 40 Hz to 200 Hz. Table 3-2 presents similar data for $G_2(z)$. Zeros number 8 and 7 are the zeros in question for $G_1(z)$ and $G_2(z)$, respectively.

The instability is produced by a net increase in phase lag introduced by the Tustin transformation. In order to alleviate this problem, some phase lead is added to $G_2(z)$ directly in the form of pole-zero pair. Simulations are performed on F.C. 2 with several pole-zero combinations. With a pole-zero combination of

$$\frac{Z - .5}{Z - .7}$$

added to $G_2(z)$ and the overall compensator gain set equal to -2.0, a stable system is achieved which met specifications for F.C.'s 1 and 2 although F.C.'s 3 and 4 are still unstable.

Poles or zeros located on the negative real axis within the Z plane unit circle have only a small effect on the system response (13:36). Inspection of Table 3-2 reveals that even for very high sample rates (200 Hz), zero number 8 of $G_1(z)$ remains in the left-half Z plane. Essentially, the phase lead associated with this zero in the S plane (S=-430) has been lost through the transformation and the UHFB has been crossed. Even though this zero is located far out in the left-half S plane, it contributes a phase lead of six degrees one decade before the corner frequency and increases from there. Due to the method of presentation of the template data in reference 2, it is not possible to determine which point on the templates is generating the instabilities for F.C.'s 3 and 4.

It is hypothesized that the addition of phase lead to $G_1(z)$ in the form of a pole-zero combination will produce a stable system and satisfy the specifications. A satisfactory pole-zero combination will of course require some amount of "cut and try" and may produce stable systems for F.C.'s 3 and 4 but at the same time make F.C.'s 1 and/or 2 unstable. Instead of adding phase lead to the discrete compensators, better results from the Tustin transformation might be obtained by first prewarping the poles and zeros. Of course only the poles and zeros which show significant warping

need be prewarped. Another possible way to obtain better mapping characteristics is to use the matched Z transform where both the poles and zeros are mapped to the Z plane using Equation (3-6). This transform never maps stable real poles or zeros to the negative Z axis as occurs with the Tustin transformation. The application of the systematic approach of QFT design technique is not possible in the Z domain without mapping the plant templates and bounds into the Z plane (or equivalent). Due to time limitations and the above considerations, only the KC-135 aircraft is discussed in the Implementation Phase of this thesis. The time responses for the KC-135 and F-16 continuous and sampled-data systems are presented in Chapter IV.

Table 3-1

F-16 $G_1(z)$ Pole-Zero Migration

Zeros

f_s	1	2	3	4	5	6	7	8	9 & 10
40	0	-1	.9925280	.9728730	.9712445	.9505535	.6000000	-.6862745	.9998363±j.0019504
50	0	-1	.9940179	.9782394	.9769292	.9602462	.6666667	-.6226415	.9998694±j.0015604
60	0	-1	.9950125	.9818332	.9807373	.9667617	.7142857	-.5636364	.9998913±j.0013005
100	0	-1	.9970045	.9890602	.9883977	.9799236	.8181818	-.3650794	.9999350±j.0007803
200	0	-1	.9985011	.9945151	.9941820	.9892843	.9047619	-.0361446	.9999676±j.0003897

Poles

f_s	1	2	3	4	5	6	7	8	9 & 10
40	1	1	.9997325	.9879604	.9875776	.9875776	.3913043	-.0419162	-.9069949±j.1101513
50	1	1	.9997860	.9903567	.9900498	.9900498	.4814815	.0695187	-.8832487±j.1345178
60	1	1	.9998217	.9919575	.9917012	.9917012	.5483871	.1594203	-.8594186±j.1576892
100	1	1	.9998930	.9951667	.9950125	.9950125	.7021277	.3937282	-.8348228±j.0594402
200	1	1	.9999465	.9975804	.9975031	.9975031	.8390805	.6427105	-.5376032±j.3784869

Table 3-2

F-16 $G_2(z)$ Pole-Zero Migration

Zeros

f_s	1	2	3	4	5	6	7	8 & 9
40	0	-1	.9991384	.9925280	.9471590	.7222820	-.2000000	.9845892±j.0771396
50	0	-1	.9993106	.9940179	.9575026	.7714792	-.0909091	.9881305±j.0618986
60	0	-1	.9994255	.9950125	.9644597	.8058691	0	.9903658±j.0516830
100	0	-1	.9996553	.9970045	.9785231	.8788163	.2500000	.9945307±j.0311263
200	0	-1	.9998276	.9985011	.9892036	.9375151	.5384615	.9973832±j.0156049

Poles

f_s	1	2	3	4	5	6 & 7	8 & 9
40	1	1	.9950125	.9170860	.2500000	.9734108±j.1487235	-.8676861±j.1497894
50	1	1	.9960080	.9331142	.3513514	.9804553±j.1195875	-.8339623±j.1811321
60	1	1	.9966722	.9439495	.4285714	.9846840±j.0999717	-.8002628±j.2102497
100	1	1	.9980020	.9659884	.6129032	.9919921±j.0603279	-.6677316±j.3067093
200	1	1	.9990005	.9828484	.7857143	.9964456±j.0302782	-.3718245±j.4434180

III-6 Summary

This chapter discusses a method for reducing the lag effect of the ZOH in the discrete system. This method is based on the PCT approximate model for the sampled-data system. Considerations in the selection of a sample rate are outlined and the sample rates for the two aircraft are chosen. The standard Z and Tustin transformations are discussed as they apply to the continuous QFT designs. It is found that the standard Z transform is not a practical tool for discretizing the QFT analog compensators. The results of the Tustin transformation are presented. The mapping characteristics of the Tustin transformation, in relation to the QFT continuous domain designs are also discussed. Finally, a possible explanation for the poor performance of the F-16 sampled-data system is presented.

IV. Theoretical Phase Simulation Results

IV-1 Introduction

This chapter contains the KC-135 and F-16 simulated responses obtained in the "theoretical phase" of this study. The general simulation methodology is discussed in the first section. The KC-135 lateral mode responses are then presented. The KC-135 longitudinal mode simulation results for the rigid and elastic aircraft are presented together in the third section. Finally, the simulation results for the F-16 are discussed.

IV-2 Simulation Methodology

As discussed previously, the theoretical phase of this thesis considers only the discrete time or sampling aspects of the digital system. Therefore, the simulations of this chapter are performed using the same computational precision for both the controllers and the plants. The simulations are performed on a Digital Equipment Corporation VAX 11/780 digital computer using double precision floating point (DPFP) arithmetic. For the purposes of this study, DPFP constitutes a very large or "infinite" wordlength. Chapters V and VI examines the finite word length case.

The original continuous domain designs of references 1 and 2 are simulated first. This is intended to be an empirical validation/verification step and is done for several reasons. First, a considerable amount of manipulation is performed on the KC-135 plants, as discussed in Chapter II, to

obtain the form used in this thesis. A good comparison between the continuous domain results is considered an implicit validation of the equivalent plants. The setup of the simulations in this thesis is essentially along the lines of the system block diagrams shown in Chapter II and is slightly different than the simulation structures used in references 1 and 2 (1:262; 2:163). Also, various discrepancies are reported in reference 2 with respect to simulation results (2:58,60,73). They are attributed to either the use of compensator approximations or the need for an adjustment in the prefilters. Due to a state limitation in the computer program used in reference 2 (F-16), the orders of $G_1(s)$ and $G_2(s)$ were reduced from 10th to 5th and from 9th to 5th, respectively. The simulation program used for this thesis has no state limitations, therefore the full order compensators are used in the simulations. Several of the discrepancies referred to above did not appear in the simulations involving the full order compensators, as can be seen in Appendix F.

A computer program called $MATRIX_X$ (7) is used in this study to perform the continuous and "hybrid" simulations. This program has a wide variety of MIMO system modeling and simulation capabilities. The actual simulations are performed using a subset set of the $MATRIX_X$ software called System Build. The System Build capability in $MATRIX_X$ provides an interactive, menu-driven graphical environment for building, modifying, and editing computer simulation models. Any combination of linear, non-linear, continuous-time, discrete-

time, or multi-rate models that describe a system can be constructed from a library of basic building blocks (7:SB P-1). This capability replaces the FORTRAN programing and batch operation that was used in references 1 and 2.

Both the continuous and sampled-data simulations are performed using the system block diagram structures of Chapter II. For the continuous time simulations, refer to Figures 2-7, 2-11, and 2-13, respectively, for the KC-135 lateral mode, KC-135 longitudinal mode and the F-16. Similarly, refer to Figures 2-8, 2-12 and 2-14 for the sampled-data simulations. Note that each simulation plot in this thesis contains all three F.C.'s for the KC-135 or all four F.C.'s and all six CSC modes for the F-16 except where stated otherwise. This form of presentation is chosen because it effectively illustrates the robust characteristics of the QFT design technique.

Computational time delay is not included in the simulations of this thesis in order to simplify somewhat the system model. Although at first this seems to be a gross simplification, it must be remembered that in the limited scope of a thesis study, inclusion of delay usually addresses the delay associated with the computation of the difference equation only. This does not include the delay attributed to the "overhead" tasks of executing extensive software algorithms for system error checking or utility functions. In addition, it is reasonable to expect a decrease in computational time for these overhead tasks anyway, since robust QFT controllers might relieve the need for gain and/or controller

scheduling. As microprocessors (digital avionics computers) continually improve in speed and computational efficiency, the computational delay associated only with the calculation of the difference equations becomes less significant.

As an example, consider a recent study done (15:75) using the Texas Instruments TMS32010 general digital controller/digital signal processing computer (available since 1983). The TMS32010 can execute an add or multiply in 200 nanoseconds and can perform a combination add, multiply, and shift in 400 nanoseconds. These are the basic operations required to solve the difference equation. It was shown that, using a sample frequency of 40 Hz, the calculation of a 1000th order digital filter (difference eqn) would require only 5% of the sample period. Thus the effect would be fairly negligible for a 10th order controller. Another way to see the effect is to consider the definition of transport lag

$$e^{-st'} = e^{-j\omega t'} \qquad (4\text{-}1)$$

where t' is the computational delay time associated with the difference equation. The computational time for a second order filter requires 2.5 microseconds (15:75), therefore for a 10th order filter, t' = 12.5 microseconds. Inserting this t' into Equation (4-1) and considering the frequencies contained in the system with a sampling frequency of 40 Hz, it is clear that the lag effect is quite small.

The standard figures of merit (10:92) are used to assess the performance of the continuous and sample-data

systems. The specifications for each system are shown in Appendix D. Although the responses are plotted for 10 seconds, they are examined beyond that point to verify the onset of steady-state conditions. It should be noted that in some cases for the KC-135, final values are obtained at times beyond 10 seconds, as was done in reference 1.

In the simulation plots shown in this thesis, all F.C. responses due to the same input command are shown on the same plot. In addition, for the longitudinal mode of the KC-135 rigid and elastic body responses are also shown on the same plot. Responses at all F.C.s and for all CSC modes for the F-16 are shown on the same plot. Exceptions to the above statement are specifically noted where applicable. The individual F.C. (and/or CSC mode) responses are not labeled on the plots. The figures of merit data given allow identification of specific responses wherever the responses are significantly different. The figure label for each sampled-data system simulation plot (Chapter IV and V) contains a parenthetical reference to the corresponding continuous system plot for comparison purposes.

IV-3 KC-135 Lateral Mode Responses

The input for the KC-135 lateral mode is a 30 degree bank angle command for the first maneuver and a 5 degree sideslip command for the second maneuver.

Bank Angle Command Response - Continuous System

The bank angle command responses for the continuous

system are shown in Figures 4-1 and 4-2. As can be seen from Figure 4-1, the bank angle responses have very desirable characteristics. Note that there is no visible difference between the responses for the three F.C.s plotted in Figure 4-1, thus showing that robust performance is achieved by the continuous system. The responses start out slowly and then increases more rapidly as time increases. This is desired in a heavy transport since it cannot react to rapid changes as can a fighter aircraft. The sideslip responses to a bank angle command are shown in Figure 4-2. It can be seen that the magnitude of the sideslip responses are quite small, as desired. The characteristics of these responses are given in Table 4-1. Comparison of these responses with those of reference 1 shows that they are identical for all practical purposes. In addition all specifications are met as can be seen by comparing the results shown in Table 4-1 with the specifications given in Appendix D.

Sideslip Command Response - Continuous System

The sideslip command responses for the continuous system are shown in Figures 4-3 and 4-4. The sideslip responses in Figure 4-3 also show the characteristics desired of a large aircraft. The magnitude of the bank angle responses in Figure 4-4 are small as desired. The figures of merit for the continuous system sideslip responses are shown in Table 4-2. Comparison of Table 4-2 with the corresponding specifications given in Appendix D show that the sideslip command response specifications are met. Comparison with the

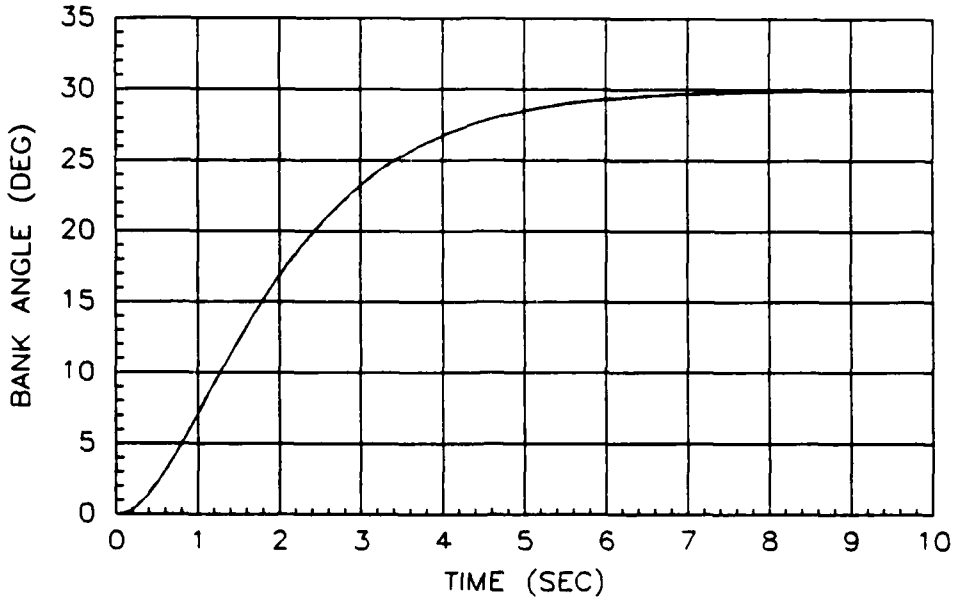

Fig. 4-1. Continuous System Bank Angle Responses

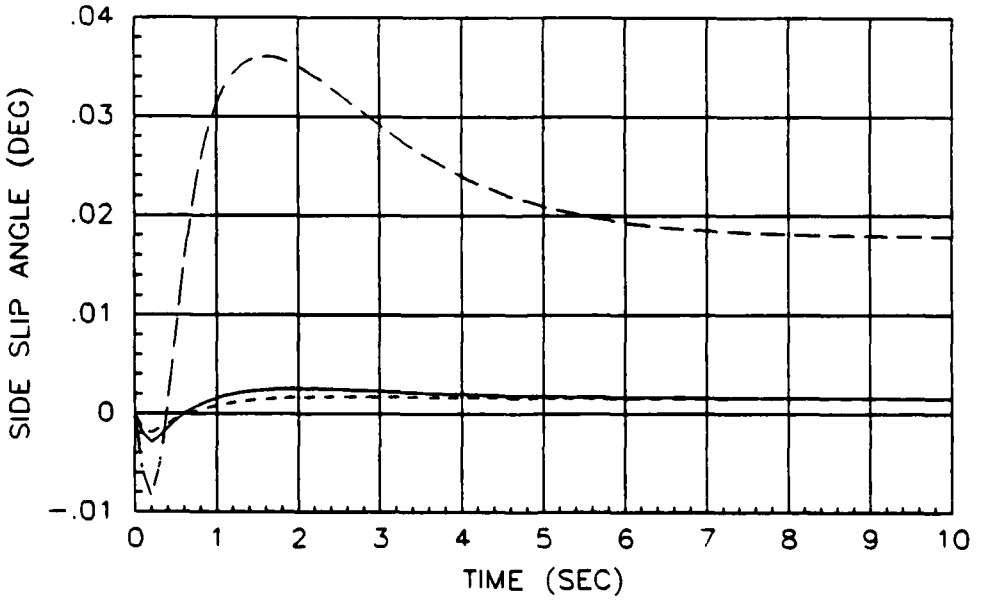

Fig. 4-2. Continuous System Sideslip Responses

Table 4-1

Bank Angle Command - Continuous System

Response	F.C.	Peak Value	Final Value	Rise Time (sec)	Settling Time (sec)
ϕ (deg)	1	30.0	30.0	3.53	6.17
	2	30.0	30.0	3.52	6.17
	3	30.0	30.0	3.51	6.14
β (deg)	1	0.0025	0.0015	--	--
	2	-0.0019	0.0015	--	--
	3	0.0361	0.0178	--	--

responses of reference 1 indicates the systems are equivalent.

Bank Angle Command Response - Hybrid System

The hybrid system responses for a bank angle command are shown in Figures 4-5 and 4-6. The bank angle responses are shown in Figure 4-5. Figure 4-6 shows the sideslip responses for the hybrid system. A comparison of the hybrid system responses with the continuous system shows that essentially equivalent performance has been achieved with the hybrid system. Table 4-3 gives the characteristics of the bank angle responses.

Sideslip Command Response - Hybrid System

The responses for the sideslip command are given in Figures 4-7 and 4-8 for the hybrid system. Figure 4-7 shows the sideslip responses. The bank angle responses are shown in

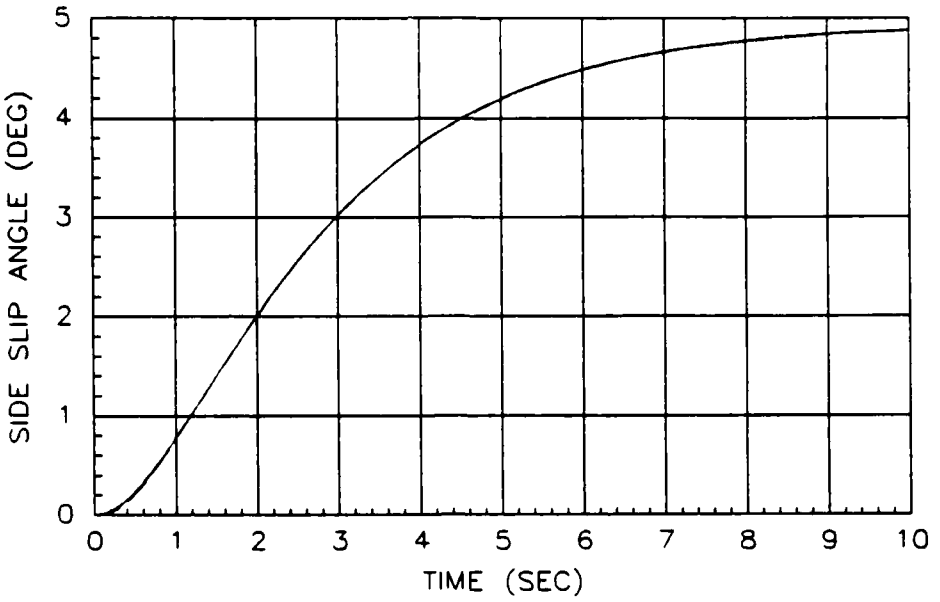

Fig. 4-3. Continuous System Sideslip Responses

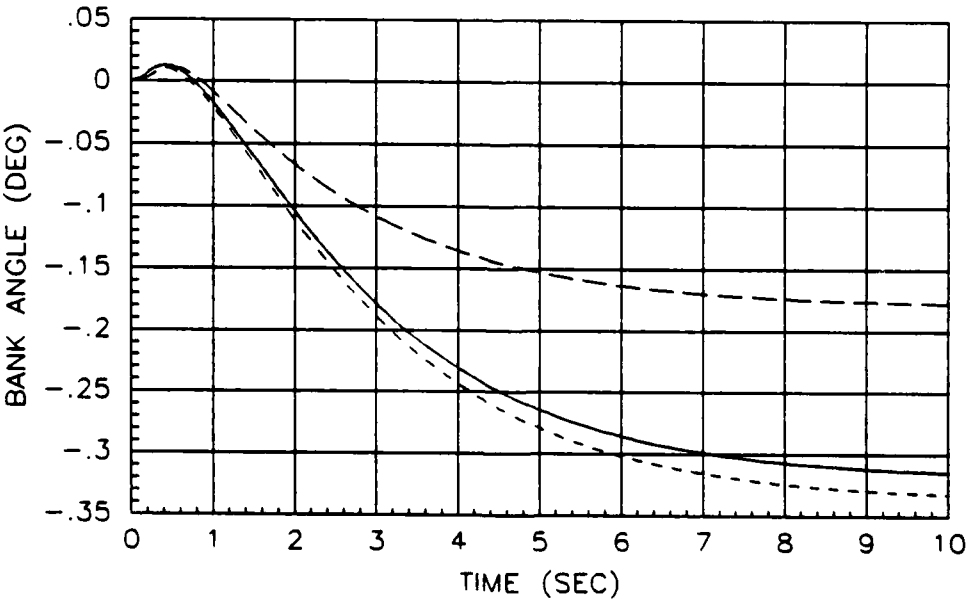

Fig. 4-4. Continuous System Bank Angle Responses

Table 4-2

Sideslip Command - Continuous System

Response	F.C.	Peak Value	Final Value	Rise Time (sec)	Settling Time (sec)
β (deg)	1	4.9	4.9	4.95	8.38
	2	4.9	4.9	4.95	8.39
	3	4.9	4.9	4.94	8.38
ϕ (deg)	1	-0.319	-0.319	--	--
	2	-0.337	-0.337	--	--
	3	-0.179	-0.179	--	--

Table 4-3

Bank Angle Command - Hybrid System

Response	F.C.	Peak Value	Final Value	Rise Time (sec)	Settling Time (sec)
ϕ (deg)	1	30.0	30.0	3.52	6.16
	2	30.0	30.0	3.52	6.17
	3	30.0	30.0	3.51	6.11
β (deg)	1	-0.0029	0.0015	--	--
	2	-0.0019	0.0015	--	--
	3	0.0361	0.0178	--	--

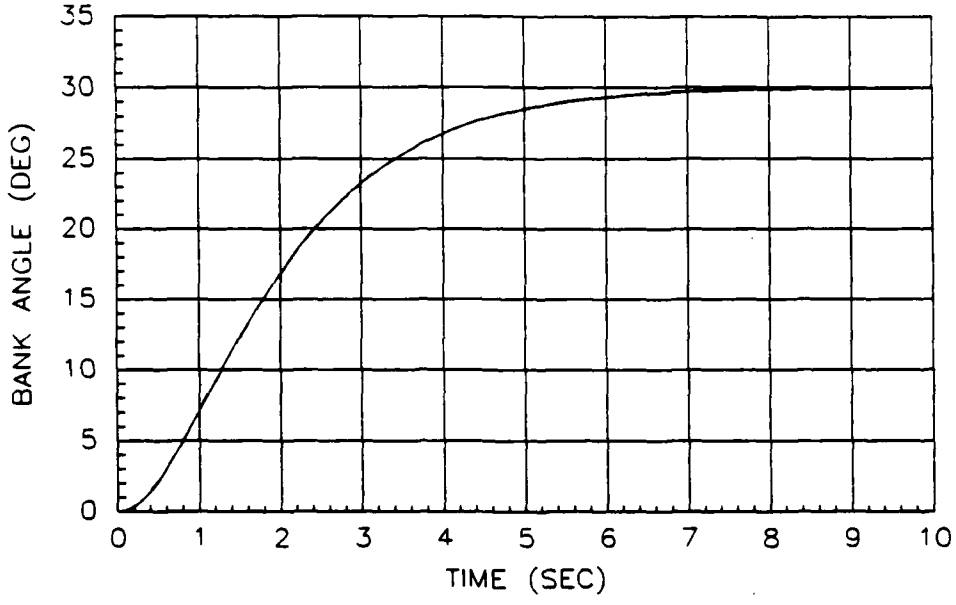

Fig. 4-5. Hybrid System Bank Angle Responses (compare to Fig. 4-1)

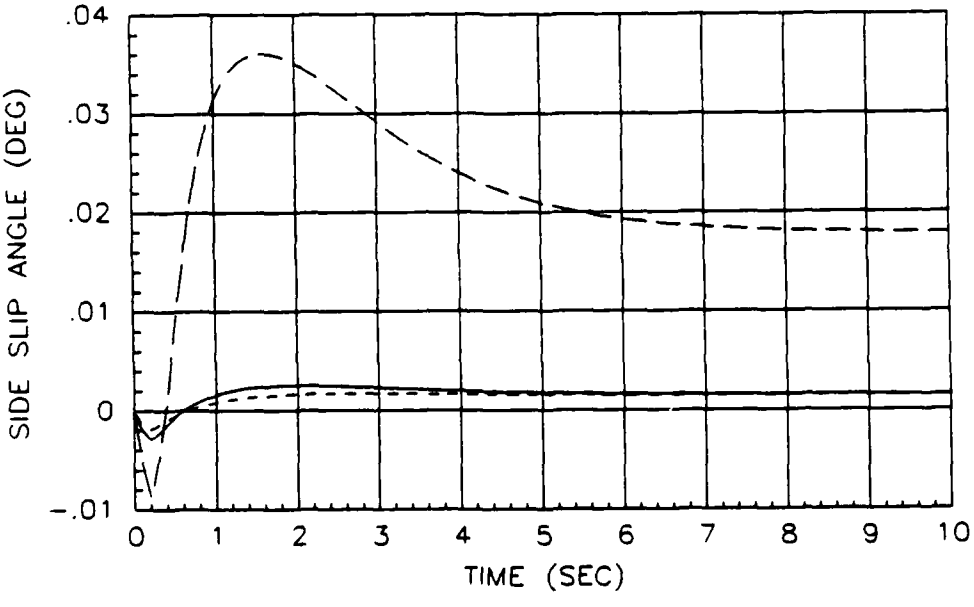

Fig. 4-6. Hybrid System Sideslip Responses (compare to Fig. 4-2)

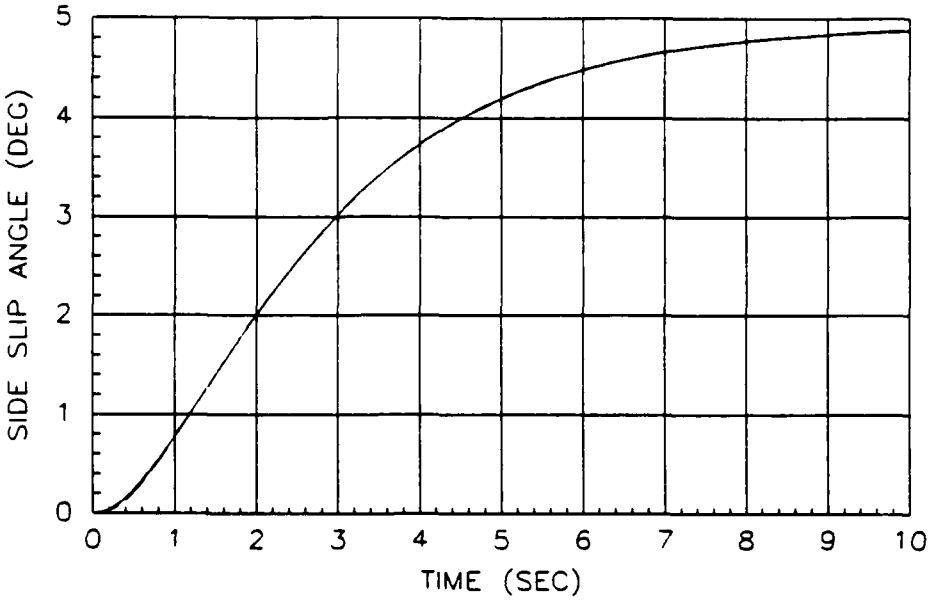

Fig. 4-7. Hybrid System Sideslip Responses (compare to Fig. 4-3)

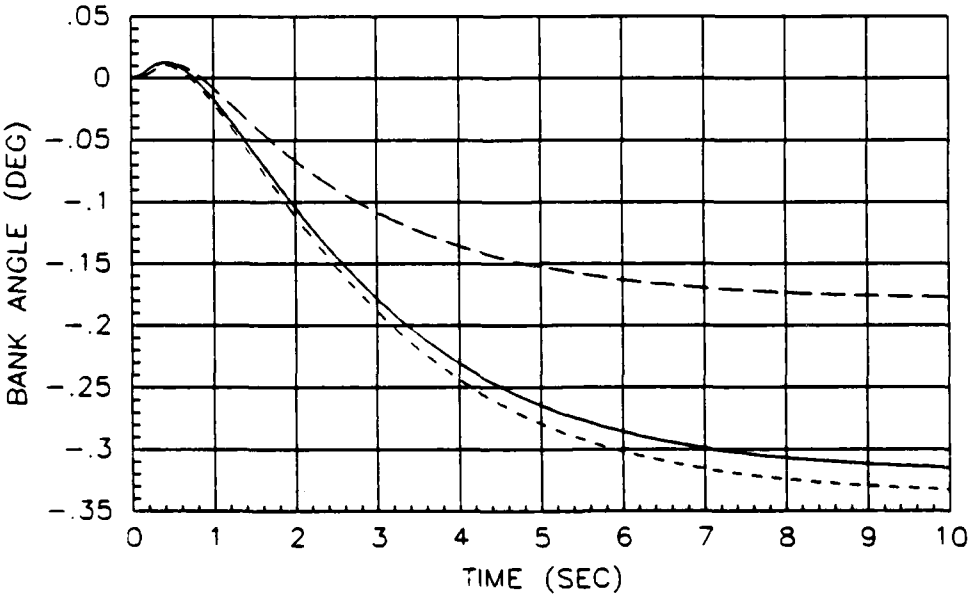

Fig. 4-8. Hybrid System Bank Angle Responses (compare to Fig. 4-4)

Figure 4-8. The sideslip response figures of merit for the hybrid system are shown in Table 4-4. Comparison of both the response plots and figures of merit shows that the hybrid system performance is essentially equivalent to the continuous system.

Table 4-4

Sideslip Command - Hybrid System

Response	F.C.	Peak Value	Final Value	Rise Time (sec)	Settling Time (sec)
β (deg)	1	4.9	4.9	4.95	8.39
	2	4.9	4.9	4.95	8.39
	3	4.9	4.9	4.92	8.36
ϕ (deg)	1	-0.319	-0.319	--	--
	2	-0.337	-0.337	--	--
	3	-0.179	-0.179	--	--

IV-4 KC-135 Longitudinal Mode Responses

A single maneuver is performed for the longitudinal mode rigid and elastic body aircraft. Two different inputs were used in reference 1 for the rigid body aircraft simulations. The input for F.C. 3 was a 4 degree pitch angle command which ramps to 4 degrees in 1 second and remains at 4 degrees thereafter. For F.C.'s 1 and 2, a similar input was used but the command only ramps to 1 degree. The reason for the two different inputs is explained in reference 1 (1:131).

To allow a direct comparison to be made with the results of reference 1, the simulations in this thesis investigation use the same inputs as those in reference 1. For the elastic body simulations, the input for all three F.C.'s is a 1 degree pitch command which rises to 1 degree in 1 second (the same as reference 1). Also note that the rigid and elastic body responses are shown on the same plots. As reported in reference 1, there was very little difference between the rigid and elastic body responses for the continuous system due to the small magnitudes of the first and second body bending modes (1:97). As seen in the responses on the following pages, there is very little difference between the rigid and elastic body responses for the hybrid system as well.

The continuous system responses and figures of merit for the KC-135 longitudinal mode are shown in Appendix F. A comparison between these responses and the those contained in reference 1 show that the specifications are met and that the two continuous systems are equivalent.

The responses to the pitch angle command for the hybrid system are shown in Figures 4-9 through 4-11. The pitch angle response is shown in Figure 4-9. The pitch angle response is similar to the tracking responses of the lateral mode in that there is a slow initial rise followed by a more rapid increase in the output. The perturbation altitude and perturbation velocity responses are shown in Figures 4-10 and 4-11, respectively. Note that, as in the continuous system, the magnitudes of the altitude and velocity responses are

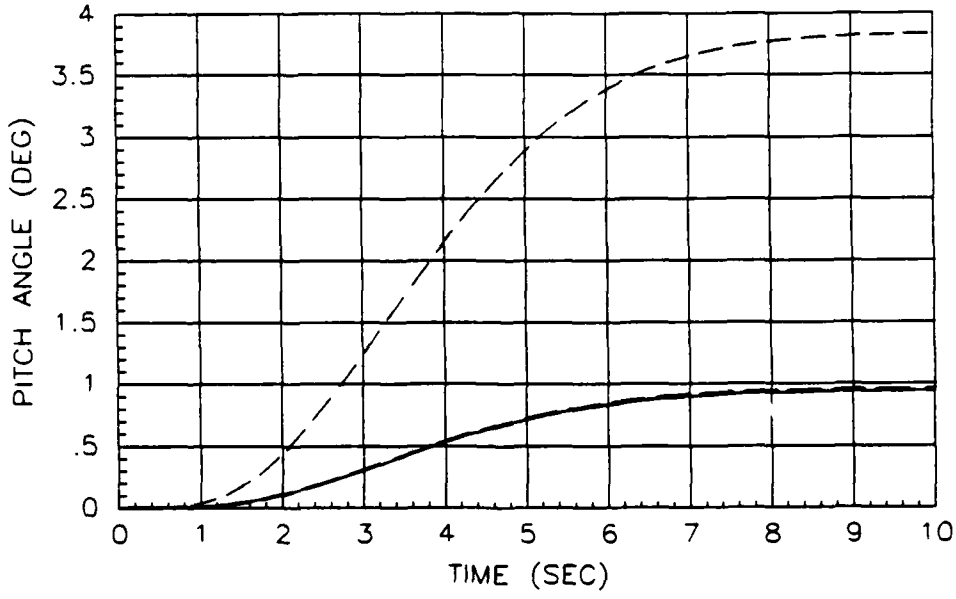

Fig. 4-9. Hybrid System Pitch Angle Responses (compare to Fig. F-1)

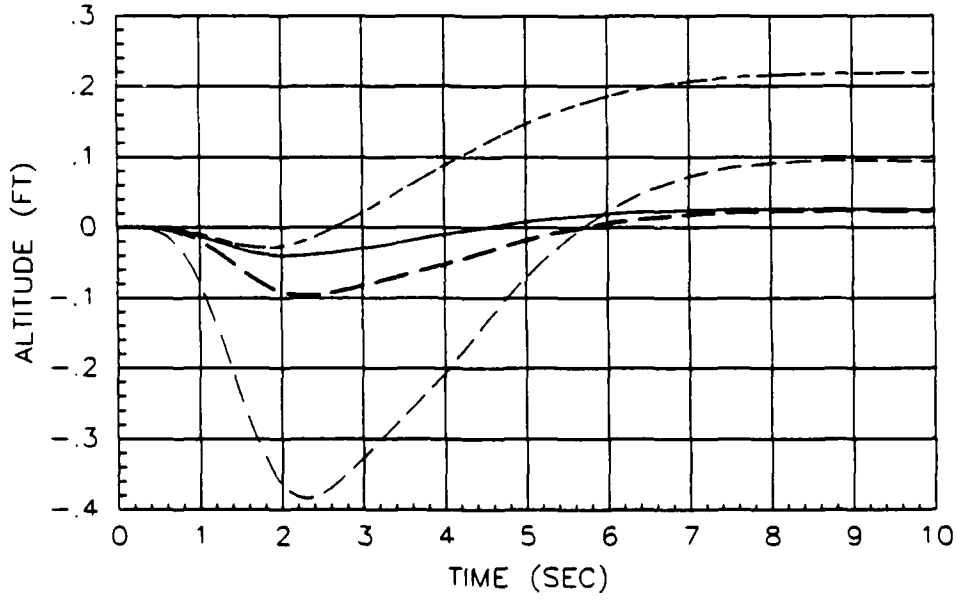

Fig. 4-10. Hybrid System Altitude Responses (compare to Fig. F-2)

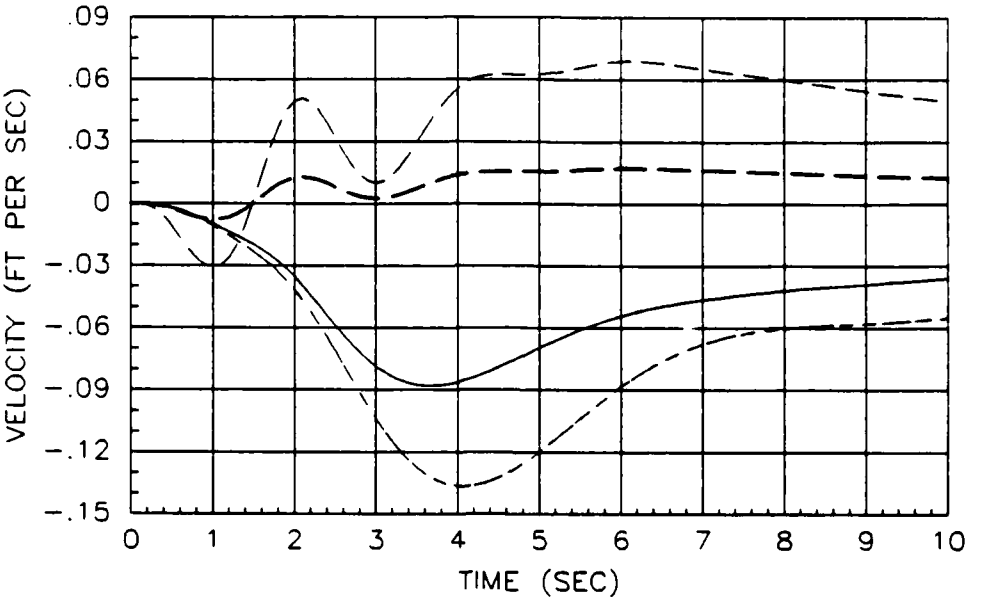

Fig. 4-11. Hybrid System Velocity Responses (compare to Fig. F-3)

small. Table 4-5 shows the time response characteristics for the rigid body pitch angle command responses while Table 4-6 shows the corresponding results for the elastic body.

IV-5 F-16 Simulation Responses

Stable responses are obtained for F.C.'s 1 and 2 only for the F-16 as discussed in Chapter 3. Therefore the plots for the F-16 contain responses for F.C.'s 1 and 2 only and for each of these two F.C.'s there are 6 CSC modes plotted. The input for the first maneuver is a pitch rate pulse command of 10 degrees per second and the input for the second maneuver is a roll rate pulse command of 50 degrees per second. In both cases, the input is removed at 5 seconds into the simulation.

Table 4-5

Pitch Angle Command - Hybrid System (Rigid Body)

Response	F.C.	Peak Value	Final Value	Rise Time (sec)	Settling Time (sec)
	1	1.0	1.0	4.35	8.28
θ (deg)	2	1.0	1.0	4.35	8.27
	3	3.9	3.9	4.38	8.32
	1	-0.040	0.026	--	--
h (ft)	2	0.222	0.222	--	--
	3	-0.384	0.093	--	--
	1	-0.088	-0.007	--	--
u (ft/sec)	2	-0.137	-0.010	--	--
	3	0.069	0.015	--	--

The continuous domain designs in reference 2 used a response model, as shown in Appendix D (Tables D-13 and D-16), to develop disturbance rejection bounds needed for the QFT design process. These models were expressed in terms of angle rate variables, similar to the tracking response models. To evaluate the disturbance rejection performance of the designs, a total angle was used rather than angle rate. For example, if pitch rate is commanded, then pitch rate is the tracking response and roll rate is the disturbance rejection response. In reference 2, the performance of the disturbance rejection response was evaluated by comparing the roll angle to the

Table 4-6

Pitch Angle Command - Hybrid System (Elastic Body)

Response	F.C.	Peak Value	Final Value	Rise Time (sec)	Settling Time (sec)
	1	1.0	1.0	4.36	8.28
θ (deg)	2	1.0	1.0	4.36	8.27
	3	1.0	1.0	4.38	8.34
	1	-0.040	0.026	--	--
h (ft)	2	0.222	0.222	--	--
	3	-0.095	0.023	--	--
	1	-0.088	-0.007	--	--
u (ft/sec)	2	-0.137	-0.010	--	--
	3	0.017	0.004	--	--

roll angle specification. Because of the state limitation of the computer program used in reference 2, the roll angle was estimated by graphically calculating the area under the roll rate response curves resulting from cross-coupling (2:60). As shown in the above referenced tables, it is desired that roll angle be less than five degrees when pitch rate is commanded. Similarly, when roll rate is commanded, it is desired that the pitch angle be less than three degrees.

The computer program used for this thesis investigation has no state limitations, therefore angle (versus angle rate) disturbance rejection responses are obtained directly by

integrating the angle rate responses. Thus only the angle response curves are shown.

As in the case of the KC-135, continuous domain simulations are performed for the F-16. These responses and their associated figures of merit are shown in Appendix F. A comparison of these continuous system responses with those of reference 2 shows that the systems performed similarly although several of the performance discrepancies reported in reference 2 (referenced earlier in this chapter) are not experienced. Again, this is most probably due to the use of the full order compensators in this investigation.

Pitch Rate Command Response - Hybrid System

The pitch rate command responses are shown in Figures 4-12 and 4-13. Figure 4-12 shows the pitch rate response. The figure shows a relatively quick response, as desired for a fighter aircraft. The roll angle resulting from the pitch rate command is shown in Figure 4-13. From the figure it can be seen that the maximum roll angle is approximately 3.2 degrees, well below the 5 degree specification. The figures of merit for the pitch rate responses are shown in Table 4-6.

Roll Rate Command Response - Hybrid System

The responses to the roll rate command are shown in Figures 4-14 and 4-15. The roll rate response is shown in Figure 4-14 where the response is similar to that for pitch rate. The pitch angle response is shown in Figure 4-15. The maximum roll angle is approximately -1.9 degrees which

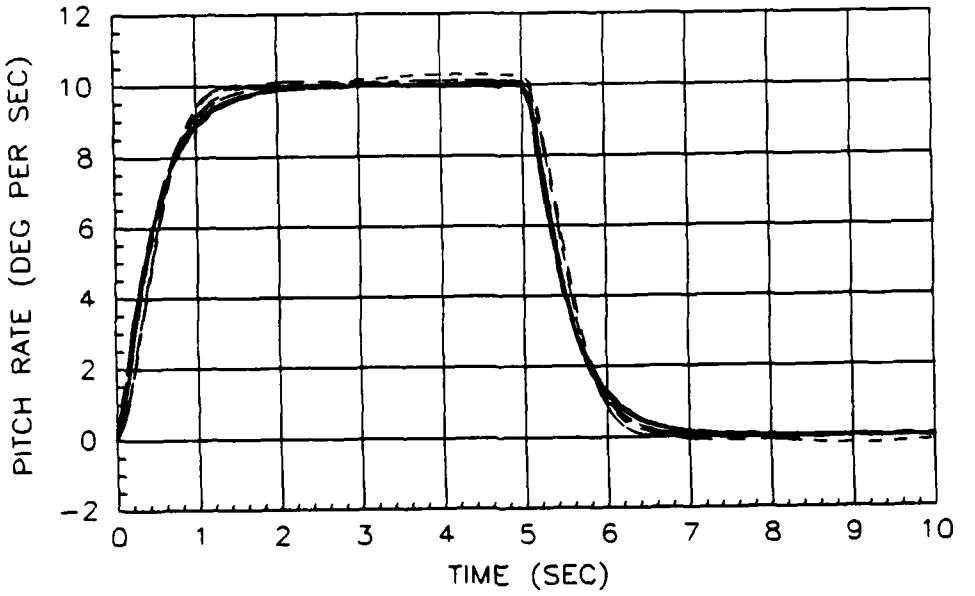

Fig. 4-12. Hybrid System Pitch Rate Responses (compare to Fig. F-4)

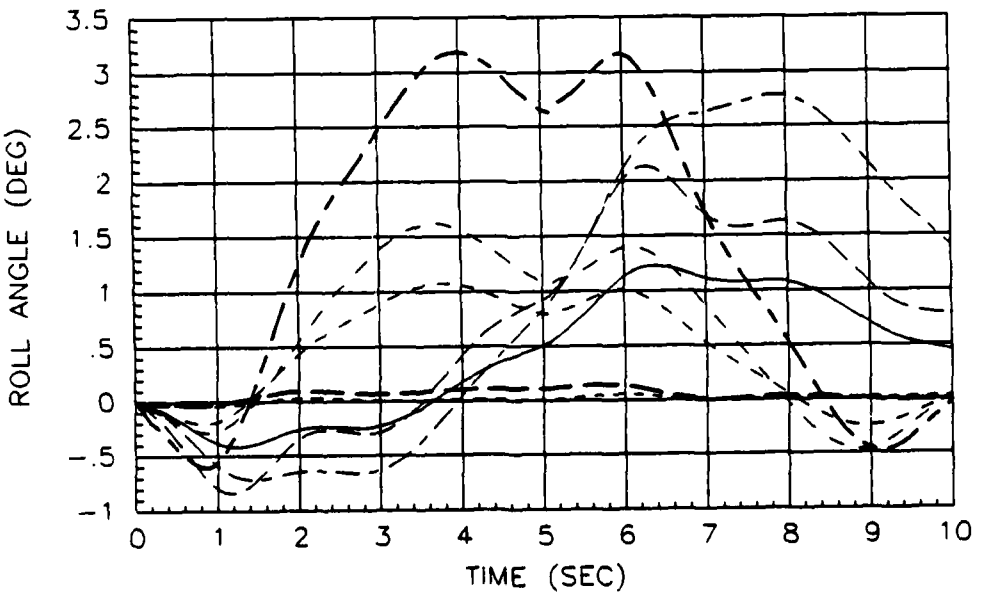

Fig. 4-13. Hybrid System Roll Angle Responses (compare to Fig. F-5)

Table 4-7

Pitch Rate Response Characteristics - Hybrid System

F.C.	CSC Mode	Peak Value (deg/sec)	Rise Time (sec)	Settling Time (sec)
1	1	10.02	0.92	1.75
	2	10.12	0.78	1.25
	3	10.02	0.93	1.76
	4	10.12	0.79	1.25
	5	10.30	0.83	2.53
	6	10.02	0.93	1.75
2	1	10.00	1.01	1.77
	2	10.02	0.88	1.50
	3	10.00	1.01	1.78
	4	10.13	0.83	1.32
	5	10.03	0.88	1.45
	6	10.00	1.01	1.77

Table 4-8

Roll Rate Response Characteristics - Hybrid System

F.C.	CSC Mode	Peak Value (deg/sec)	Rise Time (sec)	Settling Time (sec)
1	1	50.85	1.52	2.46
	2	50.63	1.58	2.71
	3	51.15	1.56	2.47
	4	51.11	1.67	3.17
	5	50.79	1.73	3.73
	6	51.45	1.42	4.45
2	1	50.84	1.46	2.22
	2	50.92	1.46	3.51
	3	50.84	1.45	2.18
	4	51.17	1.45	2.19
	5	51.07	1.44	4.03
	6	51.15	1.35	2.03

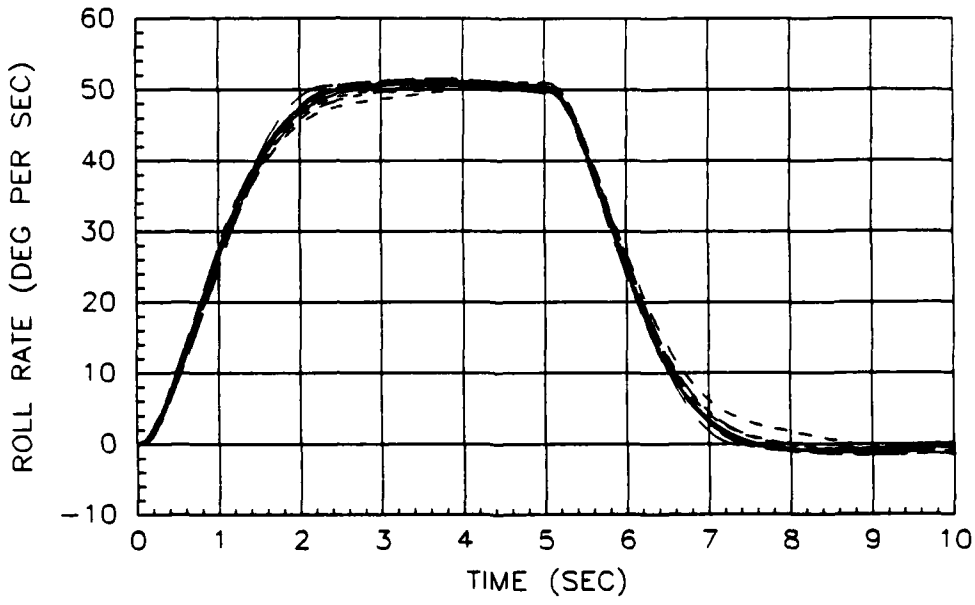

Fig. 4-14. Hybrid System Roll Rate Responses (compare to Fig. F-6)

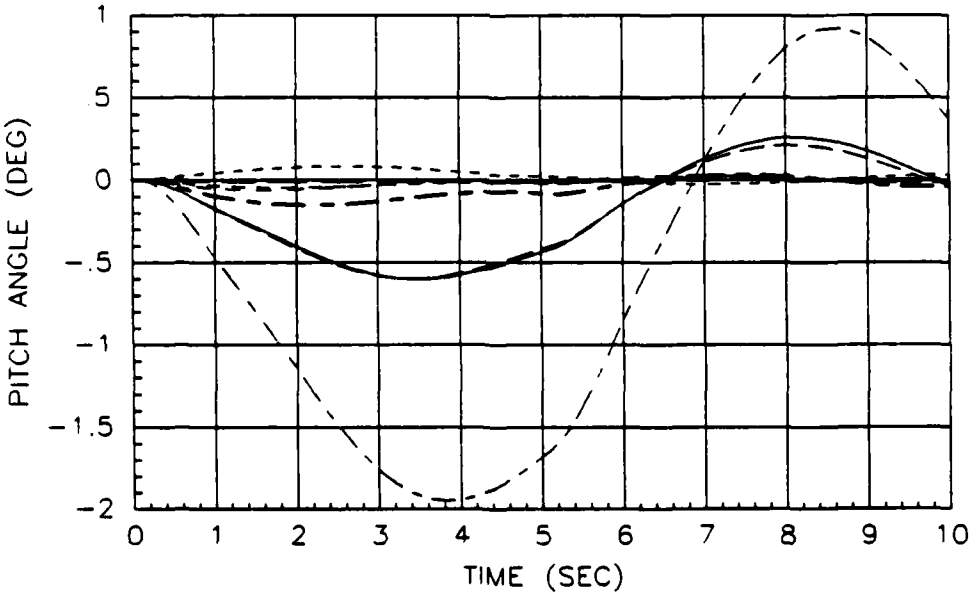

Fig. 4-15. Hybrid System Pitch Angle Responses (compare to Fig. F-7)

meets the 3 degree specification. The roll rate figures of merit are shown in Table 4-7. Examination of the response data shows that the specifications are met for both F.C.'s 1 and 2, demonstrating partial robustness.

IV-6 Summary

The responses for the KC-135 illustrate that all performance objectives are met for the hybrid system. The response data also shows that there is very little variation over all F.C.'s thereby demonstrating the robustness of the digital controllers. The performance of the KC-135 hybrid "infinite" wordlength system matches that of the continuous system well. The close agreement between the continuous and hybrid system responses suggests that a slower sampling rate might produce acceptable results as well. The F-16 responses show that for F.C.'s 1 and 2 the desired responses are achieved. The variation over the two F.C.'s is very small, thereby achieving limited robustness.

V. Implementation Phase

V-1 Introduction

This chapter discusses the digital implementation of the KC-135 lateral and longitudinal mode control systems. In the implementation phase both the sampling and finite wordlength effects encountered in a digital control system are considered. Some of the effects of finite wordlength are briefly discussed. The primary means by which these effects are considered is the use of a computer program which emulates the finite wordlength arithmetic of microprocessor. The development of and the theory behind this computer program are presented. The last portion of this chapter is devoted to the results obtained from simulations performed using the finite wordlength simulation program. Included in this discussion is the choice of a microprocessor wordlength which provides the required control system performance.

V-2 Finite Wordlength

In a digital control system the control compensator is implemented on a microprocessor (digital computer). The calculation of the discrete compensation signal which drives the analog plant is performed by the digital computer and because of the finite wordlength of the digital computer, errors are generated during this calculation (9:319). In this sense "error" means that the discrete compensation signal is different than the corresponding analog compensation signal (which is considered to be exact). Most of these errors can

generally be attributed to three different sources: quantization of the analog input to the digital controller (9:320), quantization of the compensator coefficients (9:336) and the quantization of the results of arithmetic operations (9:330). In all three cases the errors occur because a "number" with high accuracy (e.g. "infinitely" accurate analog signal or a number with many decimal digits) must be represented with a relatively small number (finite) of binary bits. Analytical methods exist which allow the generation of models for each of the error sources mentioned above. Usually these error models are described by nonlinear functions or stochastic processes. These models can be used to determine the effect of the error sources. Rather than use error models, this thesis investigation uses computer simulations to examine control system performance where the effects of microprocessor errors are included in the simulation.

The implementation structure of the digital controller can affect the performance of the digital control system. A k^{th} order digital controller is shown in Equation (5-1) where some of the numerator coefficients may be zero.

$$G(z) = \frac{Y(z)}{R(z)} = \frac{a_0 + a_1 z^{-1} + \ldots + a_k z^{-k}}{1 + b_1 z^{-1} + \ldots + b_k z^{-k}} \qquad (5\text{-}1)$$

Equation (5-1) may be rewritten as in Equation (5-2) where this form is generally called the k^{th} order difference (recurrence) equation. Implementation of a direct structure would involve programing the microprocessor such that the

coefficients in Equation (5-2), a_i and b_i, appear as multipliers in the computer code where i = 1,2,3,...k. Different direct structures exist but the simplest form is coding the microprocessor exactly as is seen in Equation (5-2) (called the direct form 1 or 1D). The effects of the last two error

$$Y(z) = a_0R(z) + a_1z^{-1}R(z) + \ldots + a_kz^{-k}R(z) - b_1z^{-1}Y(z) - b_2z^{-2}Y(z) - \ldots - b_kz^{-k}Y(z) \quad (5\text{-}2)$$

sources mentioned previously can be decreased by implementing the k^{th} order compensator as second-order sections connected either in a cascade or parallel structure. Many different cascade and parallel structures exist with each having various advantages and disadvantage (8:360,471). In this study the digital controllers are coded using the 1D structure discussed above.

V-3 Microprocessor Emulation

The implementation of the difference equation on a microprocessor, and also in digital controller simulation, involves the relatively simple computer operations of addition, multiplication and memory storage and retrieval. To show more explicitly what must be stored and retrieved in the computer memory, Equation (5-2) is modified to

$$y(n) = a_0r(n) + a_1r(n-1) + \ldots + a_kr(n-k) - b_1y(n-1) - b_2y(n-2) - \ldots - b_ky(n-k) \quad (5\text{-}3)$$

where y(n) is the difference equation output at the current

AD-A164 209 STUDY OF THE EFFECTS OF DISCRETIZING QUANTITATIVE FEEDBACK THEORY ANALOG.. (U) AIR FORCE INST OF TECH WRIGHT-PATTERSON AFB OH SCHOOL OF ENGI.. J S COUCOULES 2/3

UNCLASSIFIED DEC 85 AFIT/GE/ENG/85D-10 F/G 1/3 NL

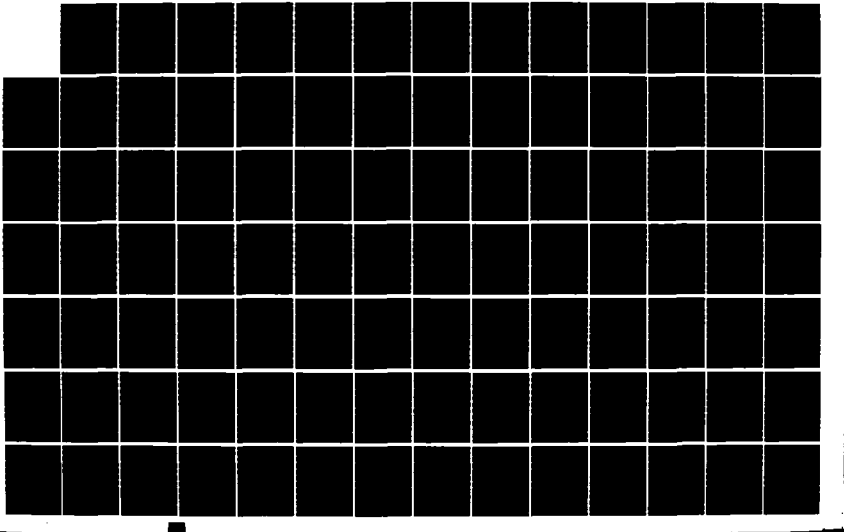

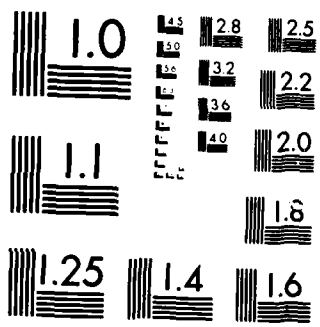

sampling period and r(n) is the difference equation input at the current sampling period. Note that the products of the delay operators (z^{-1}, z^{-2}, ect.) and the input and output of Equation (5-2) are now replaced by y(n-i) and r(n-i) in Equation (5-3) which represent the difference equation output and input at the i^{th} preceding sample period. Thus the previous inputs and outputs of the difference equation must be stored and subsequently retrieved from memory in order to compute the difference equation at the n^{th} (present) sample period.

A microprocessor represents numbers inherently as integers. Despite this fact the programmer of a microprocessor has the freedom to assign an implied radix point anywhere in the binary word. This leads to fixed-point arithmetic as a natural means of computing the difference equation. Fixed-point arithmetic is generally different from that of mainframe computers that are used to perform dynamic system simulations. The mainframes performing these simulations are usually configured to use floating-point arithmetic. Thus if a microprocessor based digital controller is to be accurately emulated in a simulation program on a mainframe, the computations must be done in such a way as to generate the same results as generated by the microprocessor.

A microprocessor simulation tool was developed in reference 23 which applied numerical analysis techniques to software to obtain a desired accuracy with the constraints of a given fixed wordlength and number representation. Although

this tool (a computer program) can perform much of the analysis needed for this study, it was designed primarily as a stand-alone tool and could not be integrated with other simulation software without considerable time and effort. Thus, a new microprocessor simulation tool is developed to aid in this study. An algorithm is suggested in reference 16 to perform analysis similar to that provided in reference 23. This algorithm is used to write the microprocessor emulation program (actually a FORTRAN subroutine) utilized in this thesis investigation. The following discussion of the theory of the algorithm paraphrases that of reference 16.

The emulation of fixed-point microprocessor calculations can be achieved by performing all calculations with floating-point arithmetic and then shifting the numbers binarily and taking the integer part. This is essentially the same as performing truncated calculations using integer arithmetic with an implied decimal point, as is the normal operating mode of a microprocessor. The radix point can be placed in any location desired. Rounding, rather than truncation, can be emulated by adding $\pm.5$ prior to taking the integer part. The above discussion can be expressed in equation form as

$$N(x) = IP\{[x]2^p + [r]sgn(x)\} \qquad (5-4)$$

where x is a decimal number, p is the number of binary places desired to the right of the radix point, r is 0 for truncation and 0.5 for rounding, IP{ } is the integer part function and sgn( ) is the sign function (16:247). Note that any portion

of the decimal number smaller than the least significant bit (LSB) of the microprocessor word is truncated or rounded off (depending on the value of r).

By manipulating all numbers involved in the calculation of the difference equation with Equation (5-4), all computations are performed with integers that represent fixed-point numbers. Thus the arithmetic is the same as that performed in the microprocessor which is being emulated. Specifically, Equation (5-4) must be applied to the difference equation input and the coefficients. If overflows are managed correctly, then the result of adding integers is the same as would be obtained from the microprocessor. If the computer wordlength is L+1 (one bit is reserved for the sign bit), the magnitude of the sum of any two integers cannot exceed 2^L-1. If a positive overflow occurs, then the magnitude of the number is set to 2^L-1. If a negative overflow occurs, then the magnitude must be set to 2^L. Note that it is assumed that the microprocessor manages overflows as described above. In some microprocessors this saturation capability is available as a inherent function (such as the Texas Instruments TMS32010) and on others it must be implemented in the microprocessor code.

Additional massaging must be performed on the results of multiplications. When two fixed-point numbers are multiplied, a fixed-point number results which has twice the number of binary digits to the right of the radix. To properly massage this number using truncation, the programmer of the microprocessor shifts the results binarily to the

right by the number of binary digits assumed to the right of the radix. The same manipulation is performed when rounding is desired except that prior to performing the shifting operation, the programmer adds 1 to the resulting product. The process described above for manipulating products can be implemented on a mainframe computer using the following function:

$$T(x) = IP\{[x]2^{-p} + [r]sgn(x)\} \qquad (5\text{-}5)$$

where x is now the result of performing multiplication using floating-point arithmetic on two numbers which have already been massage by Equation (5-4) (16:247). Note that IP{ }, sgn( ), r and p are as defined previously. Floating-point arithmetic must be used to perform all computations inside the braces of Equation (5-5). Multiplications can also produce overflows. If an overflow does occur, the number resulting from the application of Equation (5-5) must be manipulated in the same fashion as discussed previously for the addition operation. Examples illustrating the application of Equations (5-4) and (5-5) to specific numbers are given in reference 16.

A FORTRAN subroutine is written (24) which implements the algorithm discussed above. $MATRIX_X$ does not call this subroutine directly. If $MATRIX_X$ is "told" that a FORTRAN subroutine is to be used in a simulation, it calls a generic utility subroutine. This utility subroutine then calls all user written subroutines. The source code for the utility

subroutine is provided in skeleton form with the $MATRIX_X$ executable (compiled) code. After compiling the two subroutines they must be linked to an image of the $MATRIX_X$ executable code. A listing of both subroutines and a brief discussion of the microprocessor emulation subroutine is contained in Appendix G. Pseudocode is included in the subroutine as well.

The capabilities of the subroutine can be summarized as follows: Any microprocessor wordlength can be specified up to approximately 60 bits (Quad precision functions must be used for higher wordlengths). Either truncation or rounding can be chosen for quantizations. The subroutine accepts a floating-point input which is considered to be an "infinite" precision number equivalent to the analog error signal of the control system at the present sample period ($E^*(s)$ in Figure 2-3). The subroutine then generates the present output of the difference equation as a floating-point number (compensation signal). It is assumed that the wordlength of the analog-to-digital (A/D) converter is the same as the microprocessor wordlength. This is done for simplicity but the subroutine can be modified rather easily to remove this limitation in future studies. Thus $MATRIX_X$ performs the sampling operation, the subroutine performs the "A/D conversion" (quantizes the input), and $MATRIX_X$ models the ZOH at the digital controller output using Equation (2-1). Therefore the diagrams of the system models contained in Chapter II are still applicable except that the microprocessor emulation

subroutine is performing the compensator calculations using finite wordlength fixed-point arithmetic.

V-4 Implementation Phase Results

This section contains the responses for both the lateral and longitudinal mode of the KC-135 with the effects of finite wordlength included in the simulations. The results are obtained using the microprocessor emulation subroutine discussed in the previous section. The inputs to both modes of the aircraft are the same as that described in Sections IV-3 and IV-4 (i.e. the same maneuvers are performed).

V-4-1 KC-135 Lateral Mode Responses

The lateral mode responses are obtained using a microprocessor wordlength of 32 bits with 17 bits to the right of the radix point (17 BRR). Rounding rather than truncation is used in the simulations generating these plots. All performance specifications are met using this configuration as is shown later in the section. Thirty-two bits is a relatively standard wordlength. The number of BRR (17 bits) is chosen because this number provides similar performance for the longitudinal mode simulations and thus a common configuration is achieved for the entire aircraft. Simulations are run using several different combinations of rounding/truncation and numbers of BRRs with the overall wordlength kept at 32 bits. The "qualitative results" of these simulations as a function of BRR and truncation/rounding is shown in Table 5-1.

Table 5-1

KC-135 Lateral Mode Microprocessor Configuration Study

Wordlength	Bits Right of Radix Point (BRR)	System Performance	
		Rounding	Truncation
32	24	unacceptable	unacceptable
	20	unacceptable	unacceptable
	18	unacceptable	unacceptable
	17	acceptable	acceptable
	10	acceptable	acceptable
	6	acceptable	acceptable
	4	acceptable	unacceptable
	3	unacceptable	unacceptable

In Table 5-1, "acceptable" system performance means that all specifications are met while "unacceptable" means that either some or all of the specifications are not met or that the system is unstable. From the table it can be seen that the selection of truncation or rounding for the lateral mode makes little difference in the overall performance. Also from the table it is seen that the fewest number of BRR for acceptable performance is 4. This implies that at least 4 bits are needed to maintain the necessary precision. Examination of the table also reveals that the fewest number of bits to the left of the radix point that results in acceptable performance is 15 (32 - 17). This implies that at least 15 bits are needed to provide the necessary magnitude (maximum integer). Thus it appears that a 19 bit microprocessor probably provides acceptable performance. Examination of Equations (3-11) and (3-12) show that the compensator gains

for the KC-135 lateral mode are relatively high. If the majority of this gain is implemented outside the digital controller (e.g. analog amplifier) it is quite probable that a 16 bit (common wordlength) microprocessor achieves acceptable performance since the required number of "magnitude bits" is reduced. The above analysis is accomplished using the rule of thumb that approximately 3.5 bits are required to represent each decimal digit.

Bank Angle Command Response

The figures of merit for the bank angle command are given in Table 5-2. The bank angle command responses are shown in Figures 5-1 and 5-2. The bank angle response is shown in Figure 5-1 and the sideslip response is shown in Figure 5-2. Examination of Table 5-2 shows that all performance specifications are met. Also, the responses shown in Figure 5-1 have the shape desired for the tracking response as discussed in Chapter IV. Comparison with the continuous domain response data from Chapter IV, repeated here as Table 5-3, shows that the results are very similar.

Sideslip Command Response

The figures of merit for the sideslip command are given in Table 5-4. As with the bank angle command responses, all specifications are met for the sideslip command responses. The sideslip command responses are presented in Figures 5-3 and 5-4. The sideslip response to a sideslip command is shown in Figure 5-3. Figure 5-4 shows the bank angle response

Table 5-2

Bank Angle Command - Finite Wordlength

Response	F.C.	Peak Value	Final Value	Rise Time (sec)	Settling Time (sec)
ø (deg)	1	30.0	30.0	3.52	6.16
	2	30.0	30.0	3.52	6.17
	3	30.0	30.0	3.51	6.11
β (deg)	1	-0.0030	0.0015	--	--
	2	-0.0019	0.0015	--	--
	3	0.0361	0.0178	--	--

Table 5-3

Bank Angle Command - Continuous System

Response	F.C.	Peak Value	Final Value	Rise Time (sec)	Settling Time (sec)
ø (deg)	1	30.0	30.0	3.53	6.17
	2	30.0	30.0	3.52	6.17
	3	30.0	30.0	3.51	6.14
β (deg)	1	0.0025	0.0015	--	--
	2	-0.0019	0.0015	--	--
	3	0.0361	0.0178	--	--

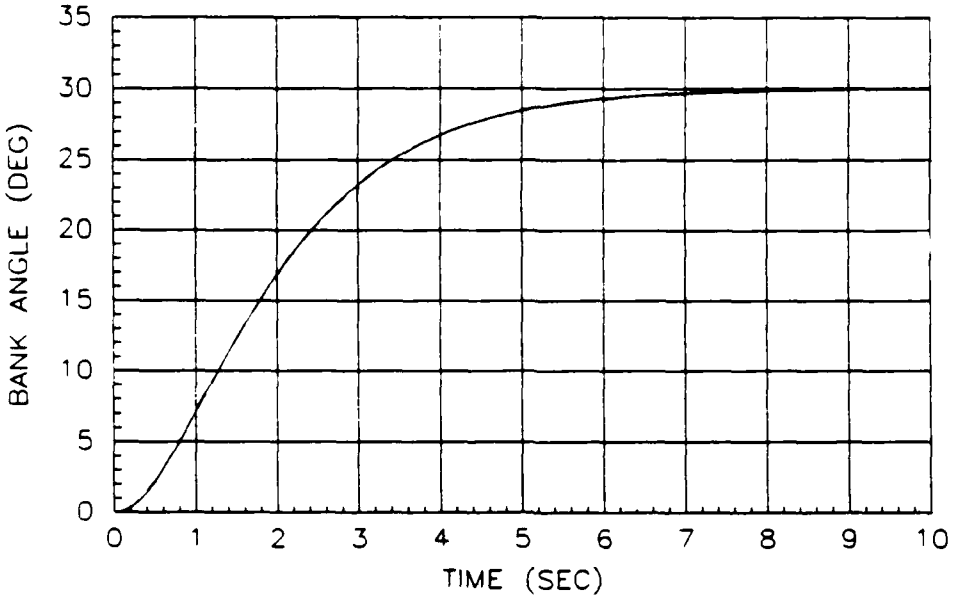

Fig. 5-1. Bank Angle Responses
(compare to Fig. 4-1)

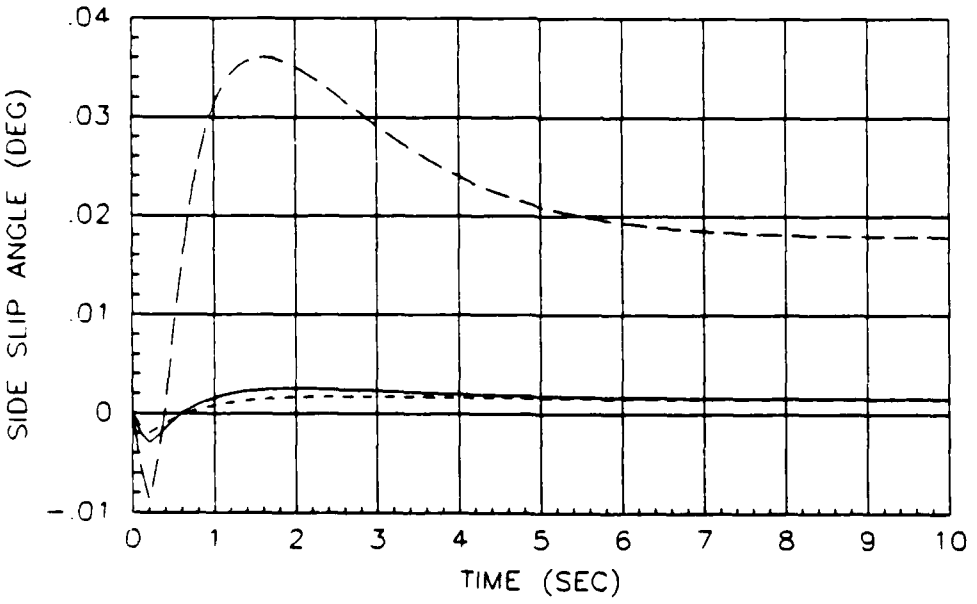

Fig. 5-2. Sideslip Responses
(compare to Fig. 4-2)

Table 5-4

Sideslip Command - Finite Wordlength

Response	F.C.	Peak Value	Final Value	Rise Time (sec)	Settling Time (sec)
	1	4.9	4.9	4.95	8.38
β (deg)	2	4.9	4.9	4.95	8.39
	3	4.9	4.9	4.95	8.35
	1	-0.319	-0.319	--	--
ϕ (deg)	2	-0.337	-0.337	--	--
	3	-0.179	-0.179	--	--

Table 5-5

Sideslip Command - Continuous System

Response	F.C.	Peak Value	Final Value	Rise Time (sec)	Settling Time (sec)
	1	4.9	4.9	4.95	8.38
β (deg)	2	4.9	4.9	4.95	8.39
	3	4.9	4.9	4.94	8.38
	1	-0.319	-0.319	--	--
ϕ (deg)	2	-0.337	-0.337	--	--
	3	-0.179	-0.179	--	--

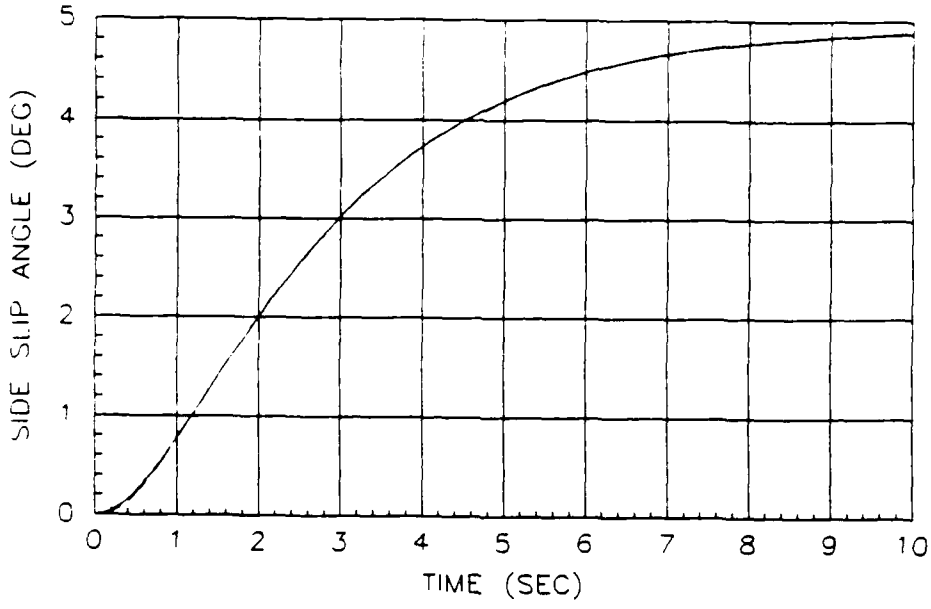

Fig. 5-3. Sideslip Responses
(compare to Fig. 4-3)

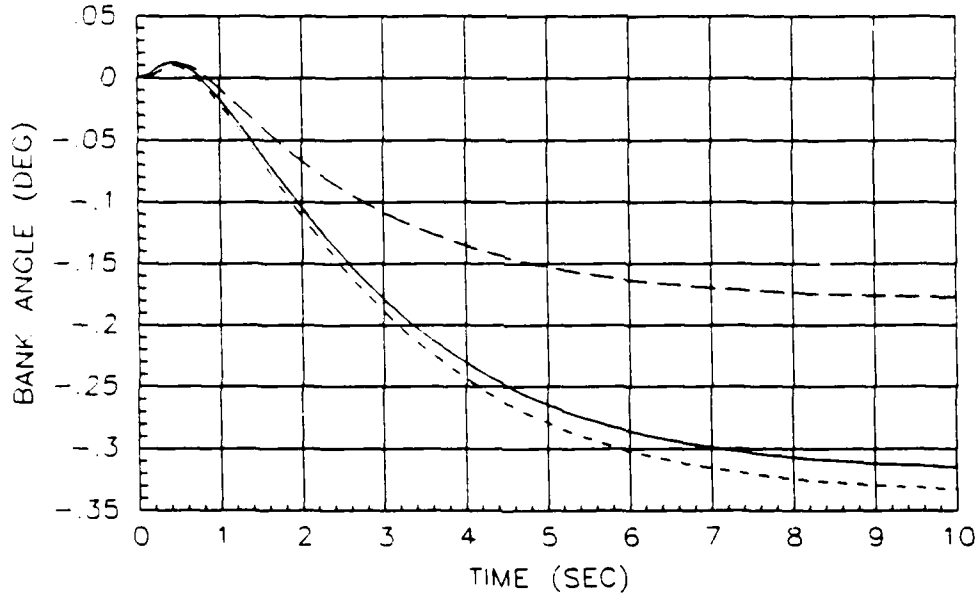

Fig. 5-4. Bank Angle Responses
(compare to Fig. 4-4)

to a sideslip command. Note that the continuous system figures of merit (from Chapter IV) for a sideslip command are repeated in Table 5-5. As is seen from the figures and the tables there is very little variation between the finite wordlength responses and the continuous responses.

V-4-2 KC-135 Longitudinal Mode Response As discussed above the longitudinal mode responses are obtained using a microprocessor configuration consisting of: a 32 bit wordlength, 17 BRR and rounding. Several simulations are run using various configurations of BRR and truncation/rounding. The qualitative results of these simulations are displayed in Table 5-6. The table reveals that about the same number of bits are required for the integer magnitude as is needed for the lateral mode. A major difference from the lateral mode is that 12 BRR is needed (versus 4) to

Table 5-6

KC-135 Longitudinal Mode Microprocessor Configuration Study

Wordlength	Bits Right of Radix Point (BRR)	System Performance	
		Rounding	Truncation
32	25	unacceptable	unacceptable
	20	unacceptable	unacceptable
	18	acceptable	unacceptable
	17	acceptable	acceptable
	14	acceptable	acceptable
	12	acceptable	unacceptable
	10	acceptable	unacceptable

maintain the needed precision. This can be partly attributed to the fact that the longitudinal mode plant equations contain unstable (right-half plane) poles and demand more precision to control them than the lateral mode. The table also shows more variation in the results between the use of truncation or rounding. Rounding provides a larger range of acceptable performance. Performing a similar analysis as is done for the lateral mode reveals that a minimum of 26 bits can produce the same results shown in the responses on the following pages. It is possible, but less likely, that a 16 bit microprocessor can achieve acceptable results for the longitudinal mode. Implementing a majority of the compensator gain outside the digital controller might allow a 16 bit microprocessor especially considering that the magnitude of the gain for one of the longitudinal compensators is higher than the maximum lateral compensator gain.

The figures of merit for the rigid body longitudinal mode responses are shown in Table 5-7. The elastic body figures of merit are shown in Table 5-8. The pitch command responses for the longitudinal mode are shown in Figures 5-4 through 5-6. The pitch angle response is shown in Figure 5-4. Figure 5-5 shows the perturbation altitude response and Figure 5-6 shows the perturbation velocity response. Note that as before both the rigid and elastic body responses for all three F.C.'s are shown on the same figure. The response characteristics given in both tables indicates the all performance specifications are met. Examination of the tracking response

curves shows that the desired response shape has been achieved. Also, comparison of the finite wordlength responses with the continuous system responses (Appendix F) shows only a small amount of variation.

Table 5-7

Pitch Angle Command (Rigid Body)

Response	F.C.	Peak Value	Final Value	Rise Time (sec)	Settling Time (sec)
	1	1.0	1.0	4.35	8.27
θ (deg)	2	1.0	1.0	4.35	8.28
	3	3.9	3.9	4.38	8.32
	1	-0.040	0.025	--	--
h (ft)	2	0.221	0.221	--	--
	3	-0.384	0.095	--	--
	1	-0.088	-0.041	--	--
u (ft/sec)	2	-0.139	-0.063	--	--
	3	0.072	0.053	--	--

Table 5-8

Pitch Angle Command (Elastic Body)

Response	F.C.	Peak Value	Final Value	Rise Time (sec)	Settling Time (sec)
	1	1.0	1.0	4.36	8.27
θ (deg)	2	1.0	1.0	4.36	8.28
	3	3.9	3.9	4.33	7.78
	1	-0.040	0.025	--	--
h (ft)	2	0.221	0.221	--	--
	3	-0.101	0.024	--	--
	1	-0.088	-0.043	--	--
u (ft/sec)	2	-0.138	-0.064	--	--
	3	0.019	0.014	--	--

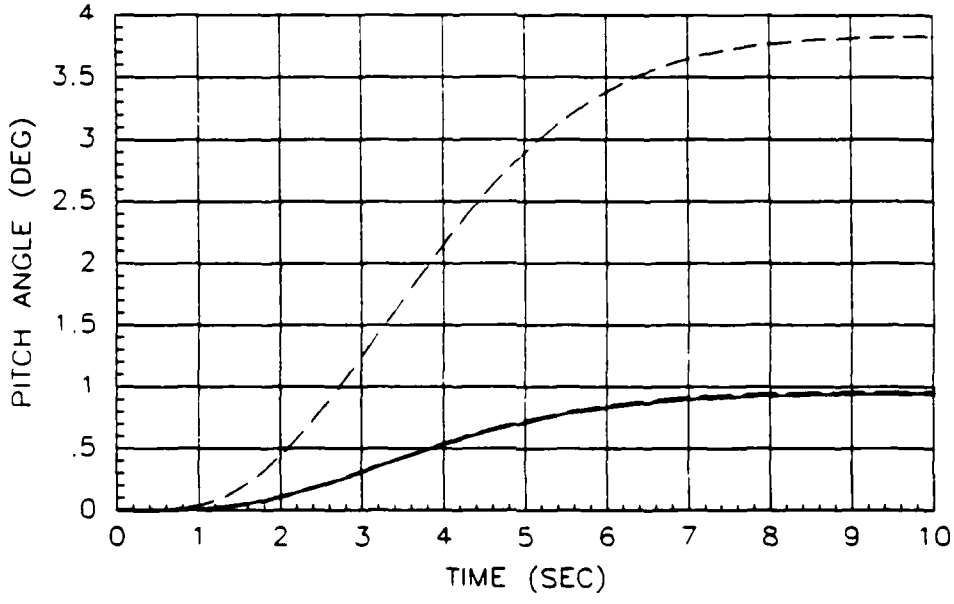

Fig. 5-5. Pitch Angle Responses
(compare to Fig. F-1)

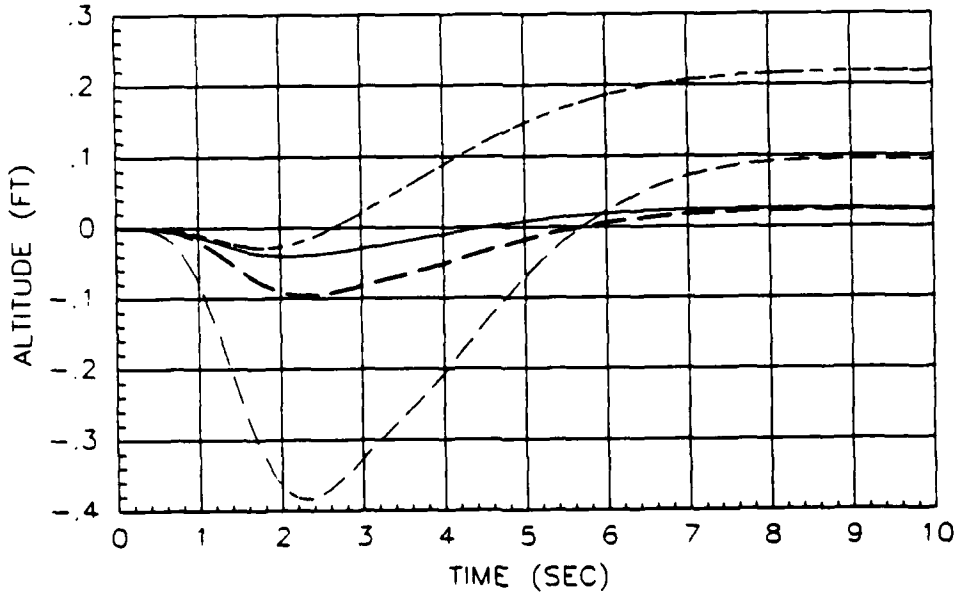

Fig. 5-6. Altitude Responses
(compare to Fig. F-2)

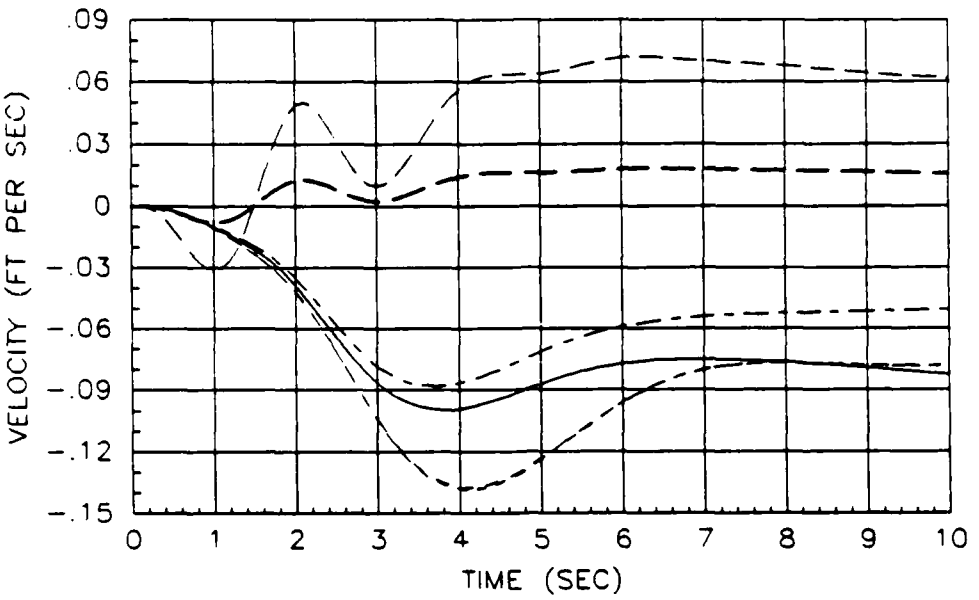

Fig. 5-7. Velocity Responses
(compare to Fig. F-3)

V-5 Summary

The response data presented in this chapter shows that the sampled-data finite wordlength KC-135 control system achieves all performance specifications and performs similarly to the continuous system. As with the continuous system, the elastic body responses show that the addition of the first and second body bending modes makes very little difference as compared to the rigid body aircraft. This performance has been achieved using a fairly standard microprocessor wordlength of 32 bits. An empirical analysis indicates that a smaller wordlength (possibly 16 bits) will achieve "acceptable" performance.

VI. Conclusions and Recommendations

VI-1 Discussion

The primary purpose of this thesis investigation is to extend two quantitative feedback theory analog multivariable control system designs to the discrete domain. In addition to extending the analog designs to digital designs, another objective is to determine what design guidelines, if any, can be established which might predict the "success" or "failure" of extending an existing analog QFT design to the discrete domain.

The preceding chapters indicated that in one case (the KC-135) the analog system can be extended to a digital system which meets all specifications and achieves essentially the same performance as the continuous system. For the other case (AFTI/F-16), specifications are met for only one out of four flight conditions. Simulations show that the system is unstable at the other three flight conditions for reasons to be discussed later. Performing "cut and try" (i.e. trial and error) modifications to one of the F-16 digital controllers improved the performance so that a stable system is achieved and specifications are met for two out of four flight conditions.

In both cases the Tustin transformation, in conjunction with a PCT system approximation, is used to extend the analog systems to digital systems. Depending upon the locations of the compensator s-plane poles and zeros, the frequency domain

characteristics of some real poles and zeros can be lost or severely warped by the Tustin transformation. For the purposes of extending QFT analog designs to the digital domain, it is surmised that the criterion for this loss of effect occurs for poles and zeros which are located at $S \geq -2/T$. In addition, when this loss of effect occurs for compensator zeros, a poor performing or unstable system will likely result because of a net increase in phase lag. It should be stressed that the criterion for a successful extension of an analog QFT design to a digital one is based upon experience from extending only two QFT analog designs. Thus it is difficult to determine at this point whether the above criterion will affect the extension of analog QFT designs in most cases or in very few cases. It is clear however that the criterion will most likely come into play when there is a "relatively high degree" of uncertainty in the controlled plant (e.g. healthy KC-135 versus a reconfigurable F-16 with a larger flight envelope).

VI-2 Conclusions

Based upon the results and discussions of the previous chapters the following conclusions can be stated:

1. Use of the Tustin transformation and PCT approximation to extend existing QFT analog designs to the discrete domain provide acceptable system performance when all real compensator zeros are located at $S \geq -2/T$. This criterion may apply to real compensator poles as well depending upon the location of the Nichols chart bounds (other than the UHFB).

Thus, the empirical results of this thesis investigation show that if the criterion is met, the Tustin/PCT approximation effectively accounts for the problems associated with sampling, finite wordlength and ZOH delay inherent in a sampled-data control system.

2. If the above criterion is not met then the Tustin/PCT approximations provide "poor performance" (i.e. predefined performance specifications are not met) and possibly an unstable system. Improving the performance then requires the application of "cut and try" methods. In this situation, the system performance guarantees inherent in the QFT design technique are lost and acceptable performance may not be achieved for all plants in the parameter space.

3. The standard z transformation is not a useful tool in extending QFT analog control system designs to the discrete domain.

4. Using the extension method described in this study, realizable sample times (40 to 60 HZ) and microprocessor wordlengths (16 to 32 bits) provide acceptable performance for the resulting QFT digital control systems.

VI-3 Recommendations

1. The primary recommendation is to implement the QFT design technique directly in the discrete domain. It is a clear result of this thesis investigation that acceptable discrete system performance cannot be achieved systematically in all cases by extending analog QFT designs to the discrete domain using the Tustin/PCT approach. A significant and

desirable characteristic of the QFT technique is that effective multivariate control systems can be designed in a systematic and deterministic manner for plants that have uncertain parameters. Therefore to maintain these desirable characteristics the technique should be applied directly in the discrete domain. Either the z or w' domain could be used but the w' domain is recommended since standard frequency domain techniques can be used. Discrete domain design requires that the plant equations be transformed to the discrete domain which implies that a sample rate must be chosen. To avoid "false starts" it is suggested that the maximum tolerable sample rate be used initially. A possible method to get around this restriction would be to "parameterize" the plant equations as a function of the sample rate. This would provide a much more general technique but it may not prove to be very practical (i.e. the parameterized equations could prove difficult to work with due their complexity).

2. A secondary recommendation is to expand the scope of the work done in this thesis effort. Frequency prewarping could be applied to the compensators prior to applying the Tustin transformation. Instead of using the Tustin transformation the matched z transformation (8:339) could be tried. This transformation is relatively "simple" to apply and it will not generate real poles or zeros on the negative z-plane axis as does the Tustin.

Appendix A: Single Input-Single Output Theory

(This appendix was taken from Reference 1 with minor changes.)

Introduction

Appendices A and B present an overview of the Quantitative Feedback Technique used in the design of the multiple output flight control systems in this thesis. Examples are presented to aid in the understanding of the material. The technique is valid for the general nxn case. However, for simplicity, the examples below are either single loop, 2x2 or 3x3 systems.

The flight control problem involves a multiple input-multiple output (MIMO) plant requiring regulation and control due to parameter uncertainty and disturbances. The mathematical equations describing the motion of an aircraft are linearized about a point in the flight envelope or flight condition. Uncertainty arises as the linearized coefficients vary with airspeed and with altitude.

The Quantitative Feedback Synthesis Technique developed by Dr. Isaac Horowitz uses feedback to achieve closed-loop system response within performance tolerances despite plant uncertainty. The range of plant uncertainty and the output performance specifications are quantitative parameters in the design process (17:81). The fundamentals of the design method are presented in the discussion of the single input-

single output design. The multiple input-multiple output design procedure is described in Appendix B, using the fundamentals developed in Appendix A.

Problem Definition

The general single input-single output (SISO) problem involves a plant transfer function, P, with uncertain parameters (gain, poles, and zeros) known only to be members of finite sets. The design specifications dictate the desired response of the plant to inputs and/or disturbances. The problem is to obtain a controller forcing the plant output to satisfy performance tolerances over the range of plant uncertainty.

The basic SISO control loop structure is shown in Figure A-1.

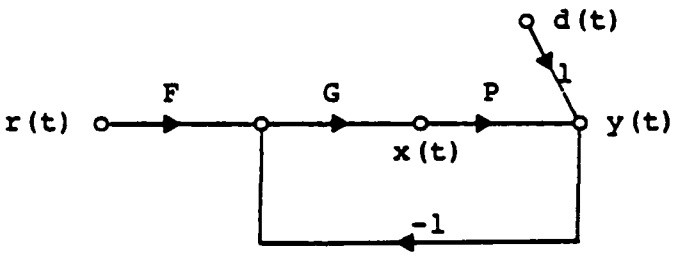

Figure A-1. Two Degrees-of-Freedom Control Loop

In this figure, r(t) is the command input to the system and d(t) is a disturbance input to be attenuated. P is the plant transfer function, the characteristics of which are not precisely known. The compensator, G, and the pre-

filter, F, are to be designed to force the system output, y(t), to be an element of a set of acceptable responses, despite the uncertainty in P and the disturbance input d(t). The plant input signal, x(t) is identified since it is generally of interest because of physical constraints. The signals, r(t) and y(t) are assumed measurable quantities and the latter is available for feedback. Access to both signals allows the use of the two degree-of-freedom structure of Figure A-1 and provides the designer with two independent compensator elements, F and G (18:13). It is also assumed that r(t), y(t), and (for now) P, such that y(t) = Px(t), are all Laplace transformable functions (18:8).

There are four transfer functions of interest in Figure A-1 where the loop transmission, L, is defined as L = GP. The system output due to the command disturbance inputs, respectively, are:

$$T_R = Y(s)/R(s) = \frac{F\ G\ P}{(1 + G\ P)} = \frac{F\ L}{(1 + L)} \qquad (A\text{-}1)$$

$$T_D = Y(s)/D(s) = \frac{1}{(1 + G\ P)} = \frac{1}{(1 + L)} \qquad (A\text{-}2)$$

and the plant input due to the command and disturbance inputs, respectively, are:

$$I_R = X(s)/R(s) = \frac{F\ G}{(1 + G\ P)} = \frac{F\ G}{(1 + L)} \qquad (A\text{-}3)$$

$$I_D = X(s)/D(s) = \frac{-G}{(1 + G\ P)} = \frac{-G}{(1 + L)} \qquad (A\text{-}4)$$

The design specifications may impose constraints on any or all of these transfer functions, but for the purpose of this example, only the first two are considered.

Design Specifications

The design specifications, or closed-loop system response tolerances, describe the upper and lower limits for acceptable output response to a desired input or disturbance. Any output response between the two bounds is assumed acceptable. The response specifications must be determined prior to applying the design method. Typically, response specifications are given in the time domain, such as the figures of merit M_p, t_s, t_p, and K_m based upon a step forcing function (10:346), or as a bounded region as shown in Figure A-2. Response to a step input is a good initial test of system response. Bounds (T_L) and (T_U) of the figure are the acceptable lower and upper limits of a system's tracking performance to a step input. Desired system response to a step disturbance generally requires maintaining the output below a given value, thus only an upper bound is necessary as shown by curve (T_D) in Figure A-2. Additional similar bounds are needed if other inputs are to be considered. The design technique is a frequency domain approach; therefore, the time domain specifications must be translated to bounds in the frequency domain. Desired control ratios, $T_{MR} = [Y/R]_{MR}$ and $T_{MD} = [Y/D]_{MD}$ are modeled to satisfy the performance specifications using the pole-zero placement method as described in

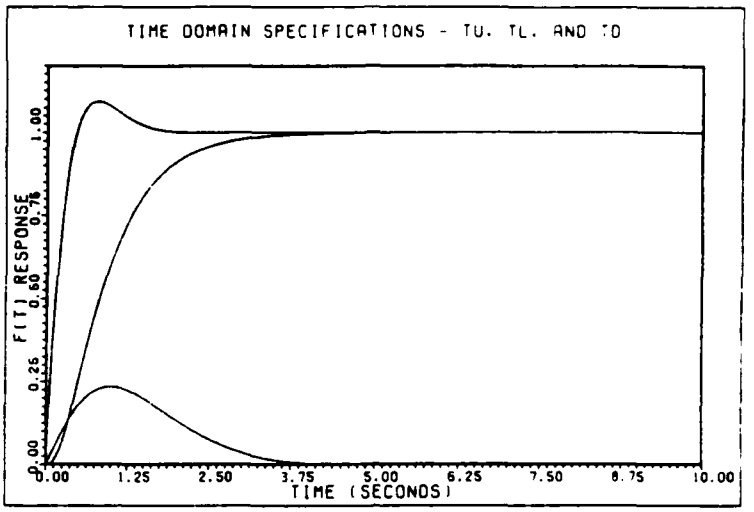

Fig. A-2. Time Domain Step Response Specifications

Section 12-2 of Reference 10. For response to a step input, a third-order model with one zero is suggested.

$$T_M = \frac{A(S + z_1)}{(S^2 + 2\zeta\omega_n S + \omega_n^2)\ (S + p_3)} \qquad \text{(A-5)}$$

The pole-zero pattern of Equation (A-5) is shown in Figure A-3. The locations of the roots are adjusted until the step response of the modeled control ratio matches the bound.

The frequency domain characteristics are considered during the response modeling. It is desirable to keep the magnitude difference (as a function of frequency) between the upper and lower bound models of $T_{MR}(j\omega)$ as large as possible at all frequencies. Choosing a lower bound model with a greater pole to zero ratio than the upper one ensures that the magnitude difference approaches infinity in the limit

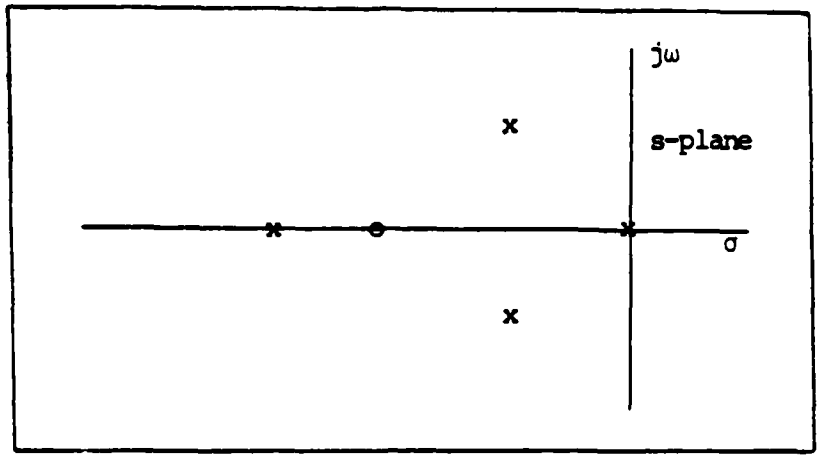

Fig. A-3. Third-Order Control Ratio Pole-Zero Pattern

as ω approaches infinity.

Errors made during this modeling process manifest themselves in one of two ways. First, if the worst acceptable response model is not really acceptable, the system may not meet the specifications over the assumed range of uncertainty in P. And, second, if the entire range of allowable outputs is not considered, the bandwidth of the compensation will be higher than necessary, increasing the cost of the compensator (18:5).

Once control ratios are obtained for each time response bound, a magnitude plot of the frequency response (Bode plot) for each $T_M(j\omega)$ is made on the same graph as shown in Figure A-4. These plots are the frequency domain representation of the design specifications on T_R and T_D. These derived frequency domain specifications are used to obtain the bounds on the loop transmission, $\underline{L}(j\omega)$, as described later.

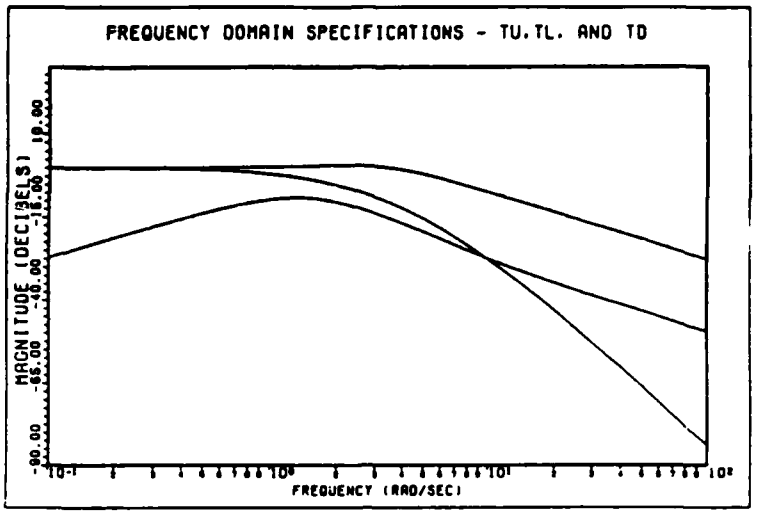

Fig. A-4. Frequency Domain Specifications

Nichols Chart

The primary tool used in the design of the compensator elements, G and F is the Nichols chart, shown in Figure A-5. If the open loop transmission of a unity feedback system (L=GP, assuming F=1 for now, in Figure A-1) is plotted using the horizontal and vertical scales on the chart, then at any given frequency, the magnitude and phase angle of T_R=L/(1+L) can be read directly from the curved scales. Conversely, any point corresponding to the magnitude and angle of T_R on the curved scales provides a point corresponding to the magnitude and angle of L on the horizontal and vertical scales (10:332-334). This correspondence between L and T_R on the Nichols chart is very important.

Likewise, the Nichols chart can be used for the disturbance response. Recall that T_D=1/(1+L). By way of Sidi's transformation, L=1/m (19:152-155) the system control

ratio due to the disturbance becomes $T_D=m/(1+m)$, which is of the same form as $T_R=L/(1+L)$. One could design the inverse of the loop transmission, m, directly on the Nichols chart, but it is much easier to realize that by turning the Nichols chart upside down, reflecting the vertical angle of L lines about the -180 degree line (i.e., -190 becomes -170, -210 becomes -150, etc) and reversing the signs on all magnitude lines, the chart can be used directly to design L itself. The horizontal

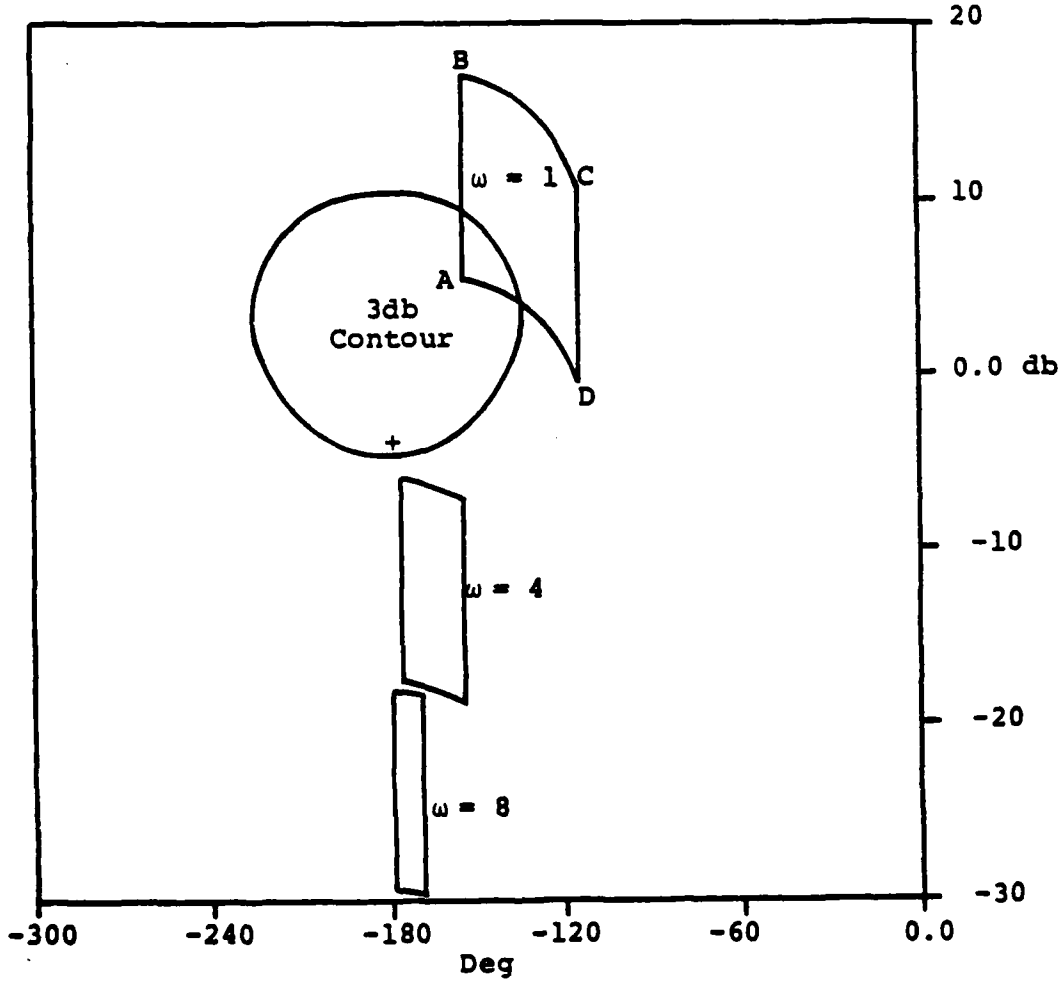

Fig. A-5. Nichols Chart with Plant Templates

and vertical lines still correspond to the magnitude and angle of L, and the curved magnitude lines correspond to the magnitude of (1+L) (19:155). For design purposes, only the magnitude of (1+L) is required. Therefore, the curved angle lines on the chart can be ignored. In practice, Sidi's transformation is merely implied by turning the Nichols chart upside down and modifying the scales as described above. The dummy variable, m, need not be considered further.

Plant Templates

A plant template is a plot on the Nichols chart of the range of uncertainty in the plant P at a given frequency (5:290). Consider the example $P(s) = K/s(s+a)$ where the gain K is described by: $2 < K < 8$, and the location of the second pole is given by: $0.5 < a < 2.0$. An infinite number of possible P's exist due to the variation of the parameters, K and a; however, each parameter is a member of a set with finite boundaries. Likewise, the magnitude and phase angle of all possible P's lie within finite boundaries when plotted at a given frequency. The plant template is obtained by plotting $Lm[\underline{P}(j\omega)]$ vs. $Ang[\underline{P}(j\omega)]$ for all possible $\underline{P}(j\omega)$'s, that is over the range of uncertainty at a given frequency on the Nichols chart. Note, only the outer edges of the template need be calculated. The plant transfer functions at the boundaries are found by holding one parameter constant at a boundary value, i.e., set K=2, and vary "a" in increments from 0.5 to 2.0. The frequency response at $\omega=1$ for the P's obtained above provides a set of points from A, (K=2, a=0.5),

to D, (K=2, a=2), on the Nichols chart as shown in Figure A-5. The process is continued until the complete template is formed. For example, for a=0.5, vary K from 2 to 8 to obtain the line from A, (a=0.5, K=2), to B, (a=0.5, K=8). Templates are needed for a number of frequencies taken at regular intervals, such as every octave. A set of templates is shown in the figure to demonstrate the change in size and location of the range of uncertainty in P for different frequencies.

Nominal Plant

To facilitate the shaping of the loop transmission, the designer needs a reference or nominal plant transfer function. This nominal plant, P_o, chosen by the designer, is nothing more than a reference plant to be used in the definition and shaping of the nominal loop transmission $L_o = GP_o$. There are no rules or constraints on the selection P_o. It doesn't even have to be from the set of possible P's, but it is usually convenient to choose P_o such that it lies at a recognizable point on the templates. It is convenient, as is the case with the example, to select P_o such that it lies at the lower, left hand corner of the templates. This choice for P_o keeps the bounds on L_o, to be described next, as near the center of the Nichols chart as possible. Once selected, the P_o point should be marked on each template, as in Figure A-5. For the example, the plant described by $P_o = 2/(s + 0.5)$ is chosen as the nominal plant.

Derivation of Bounds on L

The system step response y(t) is uniquely determined by the transfer function T(s). Likewise, T(s), for a stable, minimum phase system (no right-half-plane poles or zeros), is completely specified by the magnitude of the frequency response $\underline{T}(j\omega)$ as described in References 18 and 14. From the design specifications, the frequency response of the output $\underline{Y}(j\omega)$ can vary from the value of the bound (T_U) to the value on the bound (T_L) at a given frequency (see Figure A-4). For the given example, at the frequency, $\omega = 1$, assume that $\underline{Y}(j1)$ can vary from 0.7db to -0.8db. The relative variation in $\underline{Y}(j1)$ is (0.7)db - (-0.8)db or 1.5db. In general, the allowable relative change in $\underline{Y}(j\ )$ at a given frequency is expressed as:

$$\Delta Lm\ [Y(j\omega_i)] = Lm\ [T_U(j\omega_i)] - Lm\ (T_L(j\omega_i)] \qquad (A-6)$$

where $\underline{T}_U(j\omega)$ and $\underline{T}_L(j\omega)$ are the frequency domain bounds on $\underline{Y}(j\omega)$.

The relative change in the output is related to the control ratio as follows. From Figure A-1 and Equation (A-1), LmY = LmT = Lm[FL/(1+L)] where L = GP and it is assumed that no uncertainty exists in G and F. Then,

$$\Delta Lm\ [Y(j\omega_i)] = \Delta Lm\ [T(j\omega_i)] = \Delta Lm\ \frac{L(j\omega)}{[1 + L(j\omega_i)]} \qquad (A-7)$$

Likewise, the relative change in $\underline{L}(j\omega)$ is equal to the relative change in the plant.

$$\Delta Lm\ [L(j\omega_i)] = \Delta Lm\ [P(j\omega_i)] \qquad (A-8)$$

The variation in P arises due to parameter uncertainty, thus the problem is to find an L such that the relative change requirements on the closed-loop response are satisfied for the entire uncertainty range of P. The design specifications state the requirements on the closed-loop response $\underline{Y}(j\omega)$ and thus $\underline{T}(j\omega)$ as given by Equation (A-7). Constraints on the loop transmission $\underline{L}(j\omega)$ are desired (5:291; 18:18).

$\underline{L(j\omega)}$ Bounds on the Nichols Chart

The relative uncertainty in L is shown to be equal to the range of uncertainty in P by Equation (A-8). As described earlier, the plant template is a plot on the Nichols chart of the range of uncertainty in P at a given frequency. Because Lm (L) = Lm (P) + Lm (G) and also Ang (L) = Ang (G) + Ang (P), a template may be translated (but not rotated) horizontally or vertically on the Nichols chart, where horizontal and vertical translations correspond to the angle and magnitude requirements on $\underline{G}(j\omega)$ respectively at a given frequency (5:290). Drawing a line on each of the templates parallel to the horizontal or vertical grid lines (see Figure A-5) of the Nichols chart is suggested to maintain correct template orientation.

With the template corresponding to ω = 1 of Figure A-5, translate it to position 1 shown in Figure A-6. Since the template is the range of uncertainty in P and L = GP, where G is to be precisely determined, it follows that the

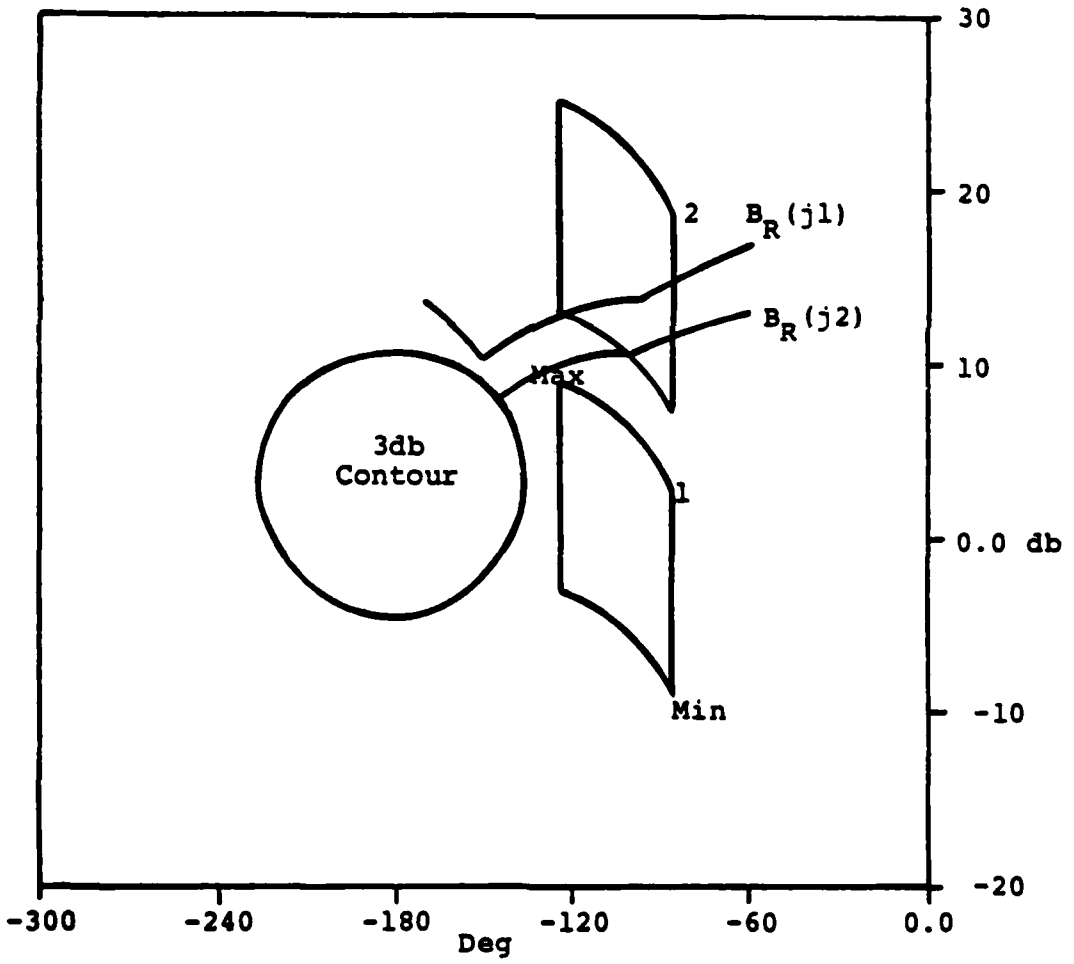

Fig. A-6. $L_o(j\omega_i)$ Bounds on the Nichols Chart

area now covered by the template corresponds to the variation in L and in T due to the uncertainty of P. Recall the correspondence between L and T on the Nichols chart. Using the curved magnitude contours, i.e., contours of constant $Lm[\underline{T}(j\omega)]$, read the maximum and minimum values of T covered by the template. If the difference between the maximum and minimum values is greater than the allowable variation in T at the frequency $\omega = 1$, that is ($\Delta Lm[\underline{T}(j1)]$ as given by Equation (A-7) and determined from Figure A-4, shift the template vertically, as shown in Figure A-6, until the difference is equal to $Lm[\underline{T}(j1)]$ (to position 2). Conversely, if the difference is less than that allowed, move the template vertically downward until the equality is obtained. When the position of the template achieves the equality (position 2 of the example), mark the nominal point P_o of the template on the Nichols chart. The point marked corresponds to a bound on the magnitude and phase angle values of $\underline{L}_o(j1)$ read from the horizontal and vertical scales of the Nichols chart, where the nominal loop transmission, $\underline{L}_o(j\omega_i)$ is given by:

$$\underline{L}_o(j\omega_i) = \underline{G}(j\omega_i)\underline{P}_o(j\omega_i) \qquad \text{(A-9)}$$

Repeat he process horizontally across the chart at different values of $Ang(L_o)$. The points marked on the chart form a curve, $\underline{B}_R(j\omega_i)$, representing the boundary of $\underline{L}_o(j\omega_i)$ at the given frequency of the template. As long as $\underline{L}_o(j\omega_i)$ lies outside or above the boundary, $\underline{B}_R(j\omega_i)$, corresponding to $\omega = \omega_i$ at the frequency $\omega = \omega_i$, the variation in T due to the

uncertainty in P is less than or equal to the relative change in T allowed by the design specifications at that frequency. Repeat this boundary, $\underline{B}_R(j\omega_i)$, derivation for various frequencies, ω_i using the corresponding plant templates to obtain a series of bounds on $\underline{L}_o(j\omega_i)$ (5:291292).

Likewise, the step disturbance response specification (line T_D on Figure A-4), is converted to bounds on $\underline{L}_o(j\omega)$. In order to effectively reject the disturbance the following inequality must be satisfied:

$$1/|[1 + L(j\omega)]| \leq |C(j\omega)| \qquad \text{(A-10)}$$

where $\underline{C}(j\omega)$ is the magnitude of the boundary, (T_D), on Figure A-4. Converting the magnitudes to decibels and rearranging terms, the inequality can be expressed as:

$$\text{Lm } [1 + L(j\omega)] \geq - \text{Lm } [C(j\omega)] \qquad \text{(A-11)}$$

Now a template is placed on the inverted Nichols chart such that its lowest point rests directly on the contour of constant Lm $[1 + \underline{L}(j\omega)]$ equal to -Lm $[\underline{C}(j\omega)]$ at the frequency, ω_i, for which the template is drawn. The point, P_o, is marked and the template slid along the same contour forming a bound, $\underline{B}_D(j\omega_i)$ for L_o. Bounds are formed for each frequency, in this manner using each template. Using the rectangular (Lm L) grid, transcribe the bounds, $\underline{B}_D(j\omega_i)$, on L_o onto the upright Nichols chart which already contains the command response bounds, $\underline{B}_R(j\omega)$, on L_o as shown in Figure A-7. For each frequency of interest, erase the lower of the

two L bounds, where the remaining bound is labeled, $\underline{B}_o(j\omega)$. The point here is that the worst case (most restrictive) bound must be used in shaping of L_o.

Universal Frequency Bound

The universal frequency (UF) bound ensures the loop transmission, L, has positive phase and gain margins, whose values depend on the oval of constant magnitude chosen (see Figure A-7). As the frequency, ω, increases, the plant templates become narrower and can be considered vertical lines as ω approaches infinity. The allowable variation in T increases with frequency also. The result is the bounds of $\underline{L}_o(j\omega_i)$ tend to become a very narrow region around the 0 db, -180 degree point (origin) of the Nichols chart at high frequency. To avoid placing closed-loop poles near the $j\omega$ axis resulting in oscillatory disturbance response, a UF bound is needed on the Nichols chart. With increasing ω, the bounds on L_o approximately follow the ovals encircling the origin. Choose one of the ovals near the origin. In Figure A-7, the contour of constant magnitude equal to 3db is used in this example. From the templates corresponding to high frequency, find the template with the greatest vertical displacement, Δv, in db. Δv may be accurately determined by finding the maximum change in $Lm[\underline{P}(j\omega)]$ in the limit as ω goes to infinity. Translate the lower half of the 3db oval down the length of the template, i.e., Δv db, as shown, thus obtaining the UF bound (see Figure A-7). (Note: Professor Horowitz refers to this bound as the Universal High Frequency

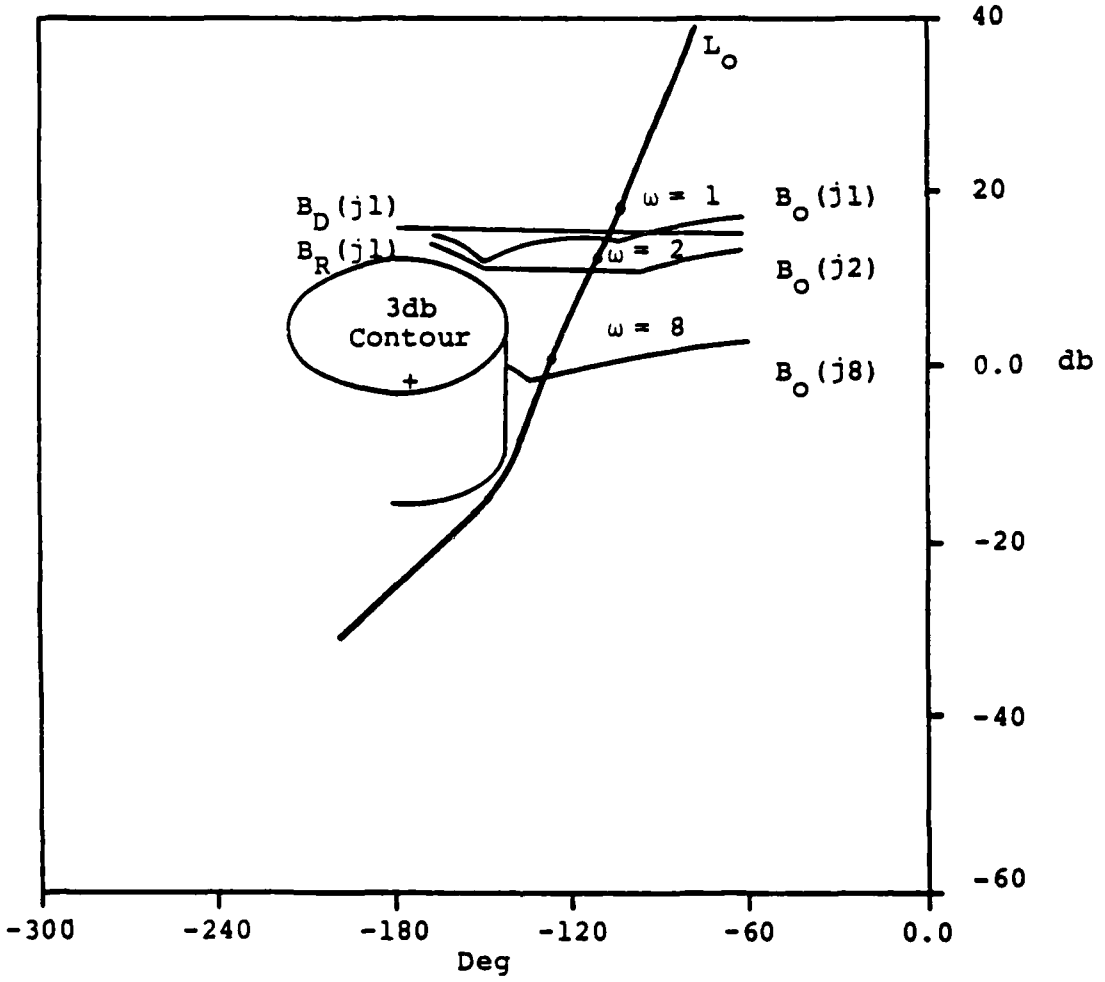

Fig. A-7. Nominal $\underline{L}_o(j\omega_i)$

(UHF) Bound) (18:20-22).

Shaping of the Nominal Loop Transmission

The shaping of a nominal loop transmission conforming to the boundaries of L_o is a most crucial step in the design process. A minimum bandwidth design has the value of L_o on its corresponding bound at each frequency. In practical designs, the goal is to have the value of L_o occurring above the corresponding bounds, but as close as possible to keep the bandwidth to a minimum. Figure A-7 shows a practical design for L_o. Note, any right-half-plane (rhp) poles and/or zeros of P_o must be included in L_o to avoid any attempt to cancel them with zeros of P_o as a starting point in the design of L_o is suggested, to avoid any implicit cancellation of roots in determining G.

Solving for G

The compensator, G, is obtained from the relation: $G = L_o/P_o$. If the L_o found above does not contain the roots of P_o, then the compensator G must cancel them. Note, cancellation occurs only for purposes of design using the nominal plant transfer function. In actual implementation, exact cancellation does not result (nor is it necessary) since P can vary over the entire uncertainty range.

Provided the nominal loop transmission, L_o, is shaped properly, i.e., meets the requirement of being on or above the bound, $B_o(j\omega_i)$, at each corresponding fre-

quency, the variation in T resulting from the uncertainty in P is guaranteed to be less than or equal to the allowable relative change in T allowed by the design specifications (5:291). The design of the pre-filter, F, is the final step in the design process.

Design of F

Design of a proper L_o only guarantees the variation in $\underline{T}(j\omega)$ is less than or equal to that allowed. The purpose of the pre-filter is to position $Lm[\underline{T}(j\omega)]$ within the frequency domain specifications. For the example given above, the magnitude of the frequency response must lie within the bounds shown in Figure A-4 which are redrawn in Figure A-8. One method for determining the bounds on the pre-filter, F, is as follows. Place the nominal plant of the $\omega = 1$ template on the

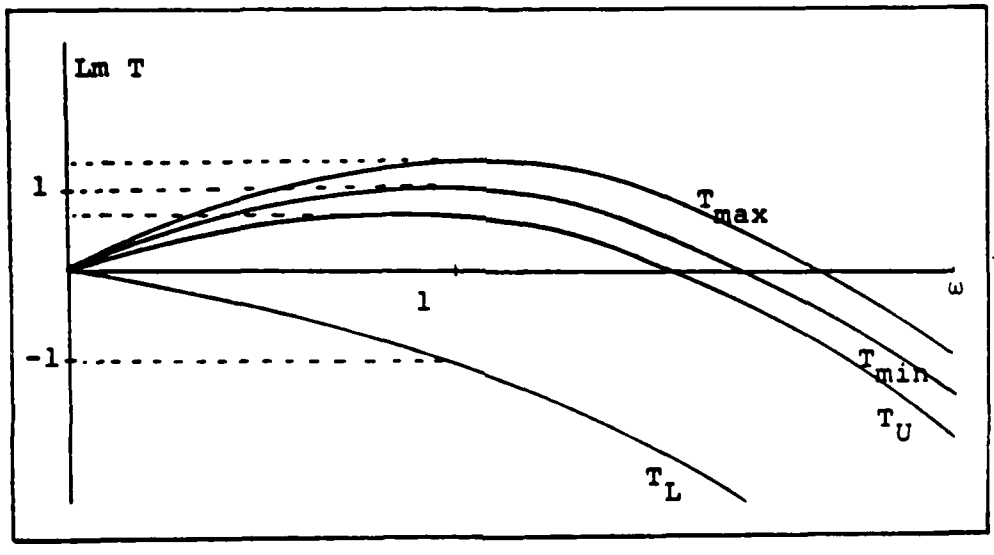

Fig. A-8. Requirements of F

Nichols chart where $\underline{L}_o(jl)$ point occurs. Record the maximum and minimum values of Lm(T), 1.2 and 1.0 in the example, obtained from the curved magnitude contours. Compare the values found above to the maximum and minimum values allowed by the frequency domain specifications of Figure A-4 at $\omega = 1$ (0.7db and -0.8db). Determine the range, in db, Lm(T) must be raised or lowered to fit within the bounds of the specifications. For example, at $\omega = 1$, the actual Lm(T) must be within $[Lm(T_U) = 0.7db] > Lm[\underline{T}(jl)] > [Lm(T_L) = -0.8db]$. But, from the plot of L_o, the actual range of Lm(T) is: 1.2db > $Lm[\underline{T}(jl)]$ > 1.0db. To lower $Lm[\underline{T}(jl)]$ from the actual range to the desired range, the pre-filter, Lm(F) is required: (0.7 - 1.2 db) > $Lm[\underline{F}(jl)]$ > (-0.8 - 1.0db), or -0.5db > $Lm[\underline{F}(jl)]$ > -1.8db (see Figure A-8). The process is repeated for each frequency corresponding to the templates used in the design of L_o. Therefore, in Figure A-9 the difference between the T_U and T_{max} curves and the difference between the T_L and T_{min} curves indicate the requirements for F as a function of frequency.

Bounds of F, $[Lm(T_U) - Lm(T_{max})] > Lm(F) > [Lm(T_L) - Lm(T_{min})]$, are plotted as a function of frequency as shown in Figure A-9. By use of the straight line approximation, determine a transfer function, F, such that its magnitude lies within these bounds. The transfer function obtained in this manner is the pre-filter, F (5:301).

The single loop design is complete with the design of F. The system response is guaranteed to remain within the

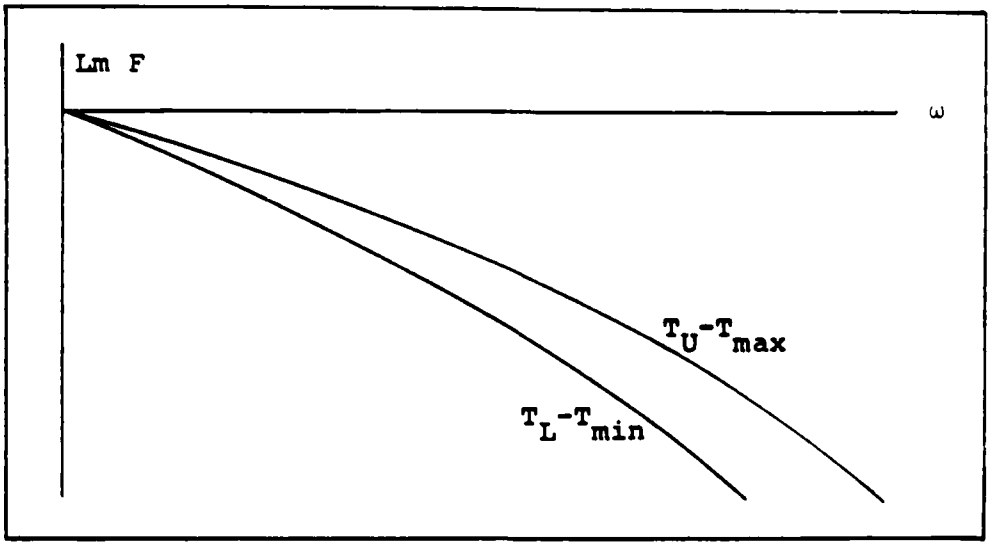

Fig. A-9. Frequency Bounds on the Pre-filter, F

bounds of the design specifications, provided the uncertainty in P stays within the range assumed at the beginning of the design process (5:288).

Summary

This appendix presents an overview of the SISO design technique of Professor Horowitz for single loop systems with uncertain plants. The technique is entirely based in the frequency domain, and makes considerable use of the Nichols and Bode plots. Much of the designing can be done by graphical methods.

Design specifications are translated into the frequency domain and constitute limits or boundaries on the frequency response of the system control ratio and the loop transmission. Two compensator elements, G and F, are synthesized to control the system response to inputs and disturbances.

Appendix B: Multiple Input-Multiple Output Theory

(This appendix was taken from Reference 1 with minor changes.)

Introduction

The design approach for each loop of the MIMO system is identical to that for the SISO system described in Appendix A. But first the MIMO system must be separated into SISO loops which are equivalent to the actual MIMO model.

In general, an nxn MIMO system can be represented in matrix notation as $\underline{y} = \underline{P}\underline{u}$, where $\underline{y}$ is the vector of plant outputs, $\underline{u}$ is the vector of plant inputs, and $\underline{P}$ is the plant matrix of transfer functions relating $\underline{u}$ to $\underline{y}$. This $\underline{P}$ matrix is formed from either the linear differential equations describing the system or directly from the system state space representation.

Professor Horowitz has shown, by the use of fixed point theory, that the inverse of the $\underline{P}$ matrix, referred to as $\underline{Q}'$, contains elements which are the inverses of n^2 single loop transfer functions equivalent to the original MIMO plant. The MIMO problem is then broken up into n loop designs and n pre-filter/disturbance problems, which are each handled as described in Appendix A (20:677).

The MIMO Plant

Consider the multiple input-multiple output plant of Figure B-1. The nx1 input vector, $\underline{u}$ produces an nx1 output

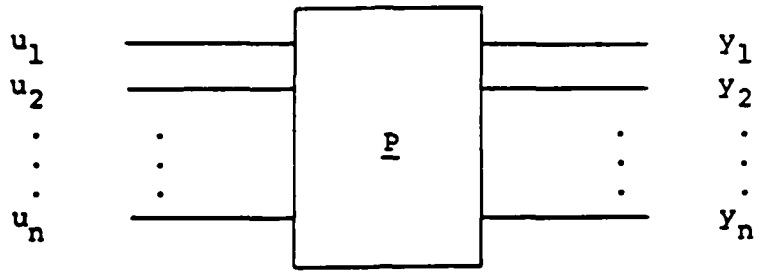

Fig. B-1. MIMO Plant

vector, $\underline{y}$. The relationship between $\underline{y}$ and $\underline{u}$ is described by the nxn plant matrix, $\underline{P}$, which is known only to be an element of a set of possible $\underline{P}$'s. It is assumed that the range of uncertainty in $\underline{P}$ can be determined, probably in the form of empirical data relating $\underline{u}$ to $\underline{y}$. Note that the input and output vectors are assumed to be of the same dimension. Although this may appear to be a restrictive assumption, it can be shown that with n inputs, at most n outputs can be independently controlled (21:530-536). Thus, if the existing model defines an unequal number of inputs and outputs, the first step is to modify the model such that the dimensions of the input and output vectors are equal. An example of such a modification is presented in reference 1 (1:33).

The plant matrix $\underline{P}$, can be derived directly from the set of coupled, linear, time-invariant differential equations describing the behavior of the plant in response to its inputs. Consider a general plant model of the form:

$$(a)y_1 + (bs + c)y_2 = (f)u_1 + (g)u_2$$
$$(ds)y_1 + (e)y_2 = (h)u_1 + (i)u_2 \qquad \text{(B-1)}$$

where a through i are the constant coefficients, Y's are the outputs, and the u's are the inputs to the plant. The system of Equation (B-1) can be represented in matrix notation as:

$$\begin{bmatrix} a & bs + c \\ ds & e \end{bmatrix} \underline{Y} = \begin{bmatrix} f & g \\ h & i \end{bmatrix} \underline{u} \qquad \text{(B-2)}$$

Define the matrix multiplying the output vector as $\underline{M}$ and the matrix multiplying the input vector as $\underline{N}$. The system is now described by:

$$\underline{My} = \underline{Nu} \qquad \text{(B-3)}$$

The plant matrix needed is defined by:

$$\underline{y} = \underline{Pu} \qquad \text{(B-4)}$$

Thus the plant matrix, $\underline{P}$ is simply:

$$\underline{P} = \underline{M}^{-1}\underline{N} \qquad \text{(B-5)}$$

The standard state space representation for a system is described by the equations (4:93):

$$\begin{aligned} \dot{\underline{x}} &= \underline{Ax} + \underline{Bu} \\ \underline{y} &= \underline{Cx} \end{aligned} \qquad \text{(B-6)}$$

The block diagram for this system is shown in Figure B-2.

Although any number of states may be represented, it is again assumed that the input and output vectors, $\underline{u}$ and $\underline{y}$ respectively, are of the same dimension. Assuming

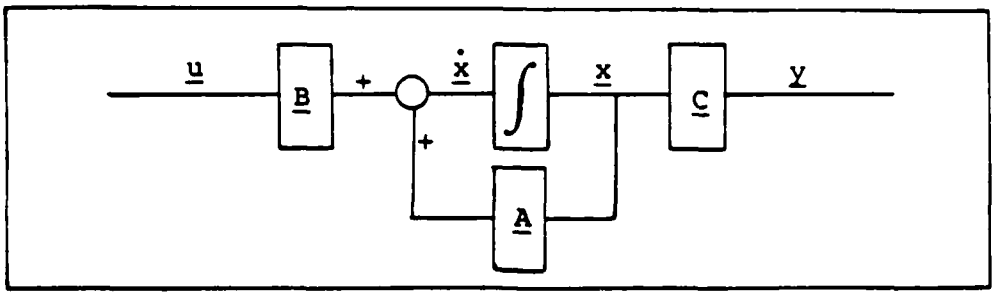

Fig. B-2. Standard State Space Diagram

the system is linearized and the A, B, and C matrices are time invariant, the plant matrix is:

$$P = C[sI - A]^{-1} B \qquad (B-7)$$

This plant matrix is actually a representative member of a set of possible plant matrices due to the uncertainty in the plant parameters. In practice, a finite set of P matrices are formed representing the plant under varying conditions.

MIMO Compensation

The compensation scheme for the MIMO system is similar to that of the SISO system of Appendix A. The basic MIMO control structure is shown in Figure B-3 where P is the uncertain plant matrix, G is a diagonal compensator matrix, and F is a pre-filter matrix. The design technique can accommodate designs involving a non-diagonal G matrix (4:14). The functions of G and F are identical to those of G and F of the SISO system of Appendix A. Figure B-4 shows a more detailed breakdown of a 2x2 MIMO system where:

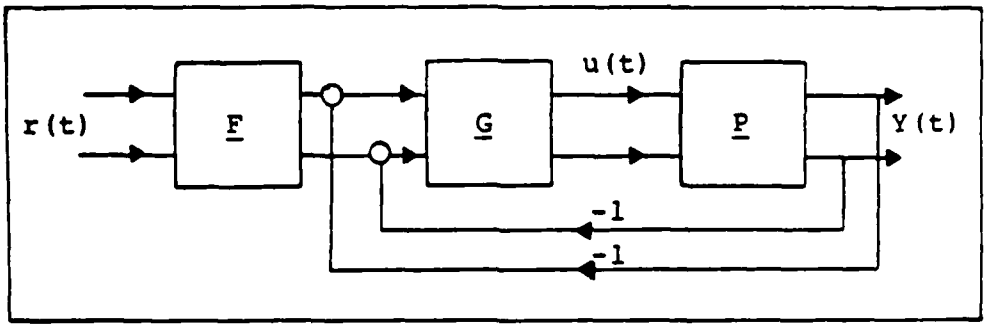

Fig. B-3. MIMO Control Structure

$$\underline{G} = \begin{bmatrix} g_1 & 0 \\ 0 & g_2 \end{bmatrix} \qquad \underline{F} = \begin{bmatrix} f_{11} & f_{12} \\ f_{21} & f_{22} \end{bmatrix} \qquad \underline{P} = \begin{bmatrix} p_{11} & p_{12} \\ p_{21} & p_{22} \end{bmatrix}$$

Constraints on the Plant Matrix

The set of $\underline{P}$ matrices must be tested to ensure that two critical conditions are met (17:86-90):

1. $\underline{P}$ must not be singular for any possible combination of plant parameters; i.e., $\underline{P}^{-1}$ must exist.

2. As $s \rightarrow \omega$, $|p_{11}p_{22}| > |p_{12}p_{21}|$ for all possible plants. This is the requirement for a 2x2 plant.

For explanation of the constraint inequality for the 3x3 system see the second half of this appendix. For higher cases see Reference 17.

The first condition is absolutely necessary to ensure controllability of the plant. The inverse of $\underline{P}$

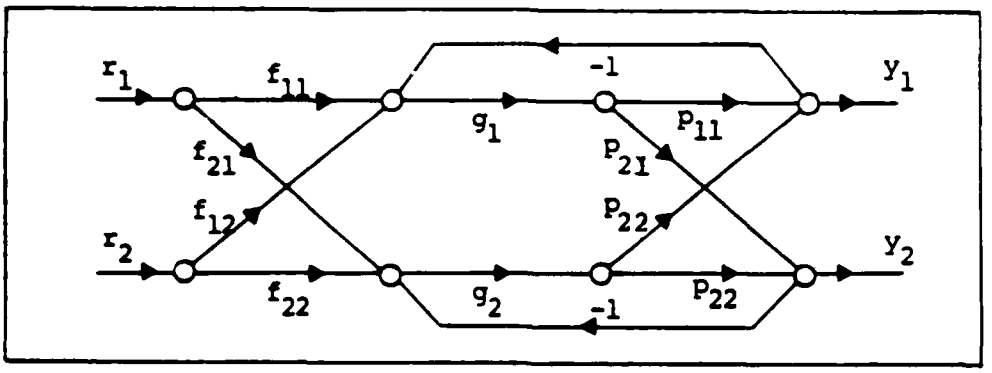

Fig. B-4. Two-by-Two MIMO System

produces the effective transfer functions used in the design. If condition 2 is not satisfied, it may be possible to change the ordering of the input or output vector which changes the ordering of the $\underline{P}$ matrix elements.

Effective SISO Loops

Now define a matrix $\underline{Q}' = \underline{P}^{-1}$ which has elements, q'_{ij}. The n^2 effective transfer functions needed are: $q_{ij} = 1/q'_{ij}$. Reference 17 contains the derivation and proof of this equivalence. The nxn MIMO system is now treated as n^2 SISO problems. Figure B-5 shows the four effective SISO loops resulting from the 2x2 MIMO system (20:682).

Each loop in Figure B-5 is handled as an individual SISO design problem in accordance with the procedures presented in Appendix A. The f's and g's are the compensator elements of $\underline{F}$ and $\underline{G}$ described previously. The disturbances, d_{ij} represent the interaction between the loops.

$$-d_{ij} = \sum_{k} \frac{b_{kj}}{q_{ik}} , \quad k \neq i \qquad \text{(B-8)}$$

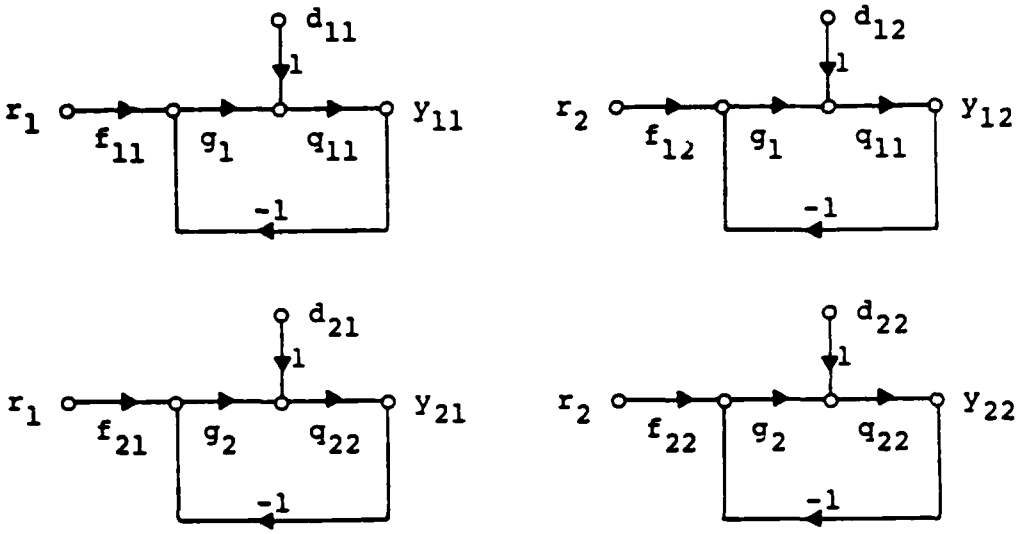

Fig. B-5. Effective SISO Loops

The b_{kj} in the above equation is the upper response bound, (T_U or T_D in Figure A-4), for the respective input/output relationship. These are obtained from the design specifications (20:681-684). Note that the first digit of the subscript of b_{kj} refers to the output and the second digit to the input. Thus, b_{kj} is a function of the response requirements on the output, y_k, due to the input, r_j.

A recent improvement in the design technique involves modification of the q's on the second and subsequent loops based on the g's already designed. This reduces the overdesign inherent in the early part of the design process. During the design of the final loop the exact equation, representing the loop and the interactions of the other loops, is used (22:977). The use of this improvement is demonstrated in the original continuous domain designs used in this thesis

investigation (1:33).

Basically Non-interacting (BNIC) Loops

When the response of an output, y_k, due to an input, r_j, is ideally zero, the y_{kj} loop is called a basically non-interacting (BNIC) loop (20:679). Due to loop interaction and plant uncertainty, this ideal response is not achievable. Therefore, the performance specifications describe maximum responses and the loop is handled exclusively as a disturbance rejection problem.

3x3 MIMO System Design Theory

The remainder of this appendix is devoted to the 3x3 MIMO system structure with extension to a general nxn system. Several methods are discussed of ways to reduce the complexity required in the design process. Finally, a discussion of the improved design technique is highlighted.

Control Structure

The system structure is similar to that of the 2x2 system discussed previously. The basic structure is shown in Figure B-6 where $\underline{P}$ is the uncertain plant matrix, $\underline{G}$ is the compensator matrix, and $\underline{F}$ is the pre-filter matrix. The purpose of $\underline{G}$ and $\underline{F}$ is identical to those of the SISO system. Figure B-7 shows the 3x3 MIMO structure with $\underline{G}$ being diagonal. The general form of the aircraft equations of motion, for a 3x3 MIMO system, are of the form:

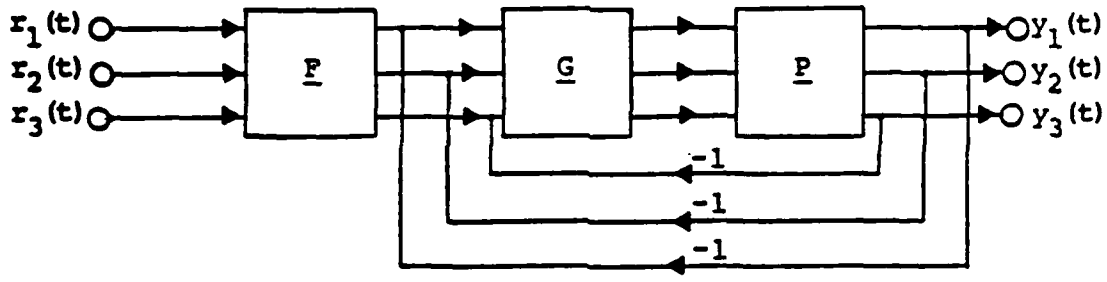

Fig. B-6. The 3x3 Multiple Input-Multiple Output Feedback Structure

$$(aS + b)Y_1 + (cS + d)Y_2 + (eS + f)Y_3 = gU_1 + hU_2 + iU_3 \qquad \text{(B-9)}$$

$$(jS + k)Y_1 + (lS + m)Y_2 + (nS + o)Y_3 = pU_1 = qU_2 + rU_3 \qquad \text{(B-10)}$$

$$(tS + v)Y_1 + (wS + x)Y_2 + (aaS + bb)Y_3 = ccU_1 + ddU_2 + eeU_3 \qquad \text{(B-11)}$$

where a through ee are constant coefficients. Equations (B-9) through (B-11) can be written in matrix notation as:

$$\begin{bmatrix} aS + b & cS + d & eS + f \\ jS + k & lS + m & nS + o \\ tS + v & wS + x & aaS + bb \end{bmatrix} \begin{bmatrix} Y_1 \\ Y_2 \\ Y_3 \end{bmatrix} = \begin{bmatrix} g & h & i \\ p & q & r \\ cc & dd & ee \end{bmatrix} \begin{bmatrix} U_1 \\ U_2 \\ U_3 \end{bmatrix} \qquad \text{(B-12)}$$

Equation (B-12) is of the form:

$$\underline{My} = \underline{Nu} \qquad \text{(B-13)}$$

where the output matrix $\underline{M}$ multiplies the output vector $\underline{y}$ and the input matrix $\underline{N}$ multiplies the input vector $\underline{u}$. Equation (B-13) is manipulated to

$$\underline{y} = \underline{M}^{-1}\underline{N}\underline{u} \tag{B-14}$$

where $$\underline{P} = \underline{M}^{-1}\underline{N} \tag{B-15}$$

is defined as the plant matrix. Thus equation (B-14) becomes

$$\underline{y} = \underline{P}\underline{u} \tag{B-16}$$

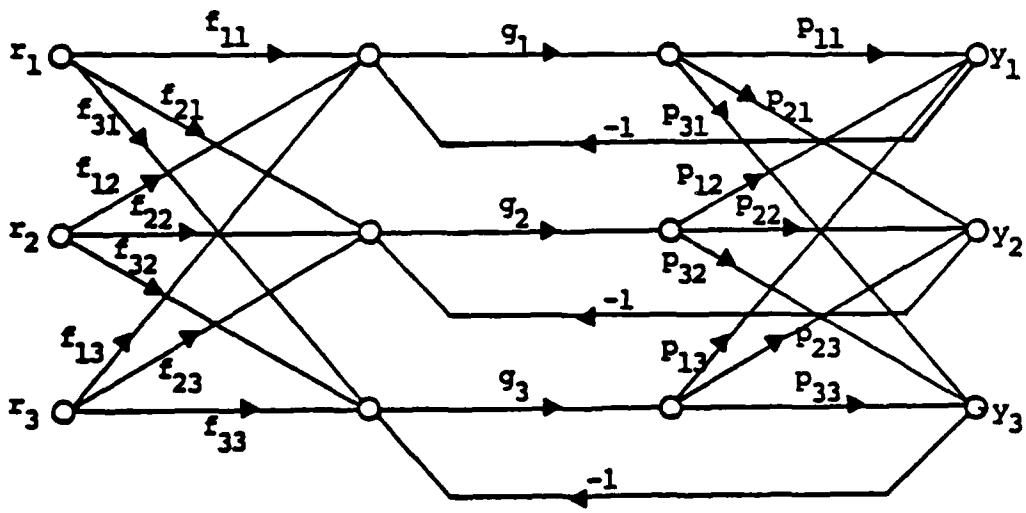

Fig. B-7. The Complete 3x3 MIMO Structure with Diagonal G

The remaining elements of the 3x3 MIMO system can be represented in matrix form as:

$$F = \begin{bmatrix} f_{11} & f_{12} & f_{13} \\ f_{21} & f_{22} & f_{23} \\ f_{31} & f_{32} & f_{33} \end{bmatrix} \quad ; \quad G = \begin{bmatrix} g_1 & 0 & 0 \\ 0 & g_2 & 0 \\ 0 & 0 & g_3 \end{bmatrix} \qquad \text{(B-17)}$$

In this thesis G is always a diagonal matrix but G can be a full matrix which gives the designer more flexibility in the design technique.

Constraints on the Plant Matrix

There are two constraints on the P matrix which must be satisfied. These constraints are:

1. The plant matrix P must be invertible. That is, P^{-1}, must exist (i.e., P must not be singular).
2. As $S \rightarrow \infty$

$$|p_{11}p_{22}p_{33}| > |p_{11}p_{23}p_{21}| + |p_{12}p_{21}p_{33}| + |p_{12}p_{23}p_{31}| + |p_{13}p_{22}p_{31}| + |p_{13}p_{21}p_{32}|$$

for all possible plants (20).

The first constraint ensures that the plant is controllable. If constraint 2 is not satisfied, then the original order of the input and output matrices may be changed to ensure that this constraint is met. It is to be noted that constraint 2 is not required for the improved design method. The only requirement is that the diagonal terms

do not change sign as $S \rightarrow \infty$ (i.e., q_{11}, q_{22}, through q_{ij} where i=j).

Effective SISO Loops

First define a matrix $Q'=p^{-1}$ having elements q'_{ij} and a matrix $Q=[q_{ij}]$ where $q_{ij}=1/q'_{ij}$. Thus q_{ij} are the n^2 effective transfer functions that are needed for the QFT technique. Using the above transformation the 3x3 system is now treated as n^2 (nine) SISO problems (20). Figure B-8 shows the resulting nine effective SISO loops. Note that the first subscript on d_{ij}, f_{ij} and y_{ij} refers to the ith output and the second subscript to the jth input. Since $q_{ij}=1/q'_{ij}$, Q can be represented in matrix form as

$$Q = \begin{bmatrix} q_{11} & q_{12} & q_{13} \\ q_{21} & q_{22} & q_{23} \\ q_{31} & q_{32} & q_{33} \end{bmatrix} \qquad \text{(B-18)}$$

Using Figure B-8 the input/output relationship is defined as:

$$t_{ij} = y_{ij}/r_j \qquad \text{(B-19)}$$

where $r_j = 1$

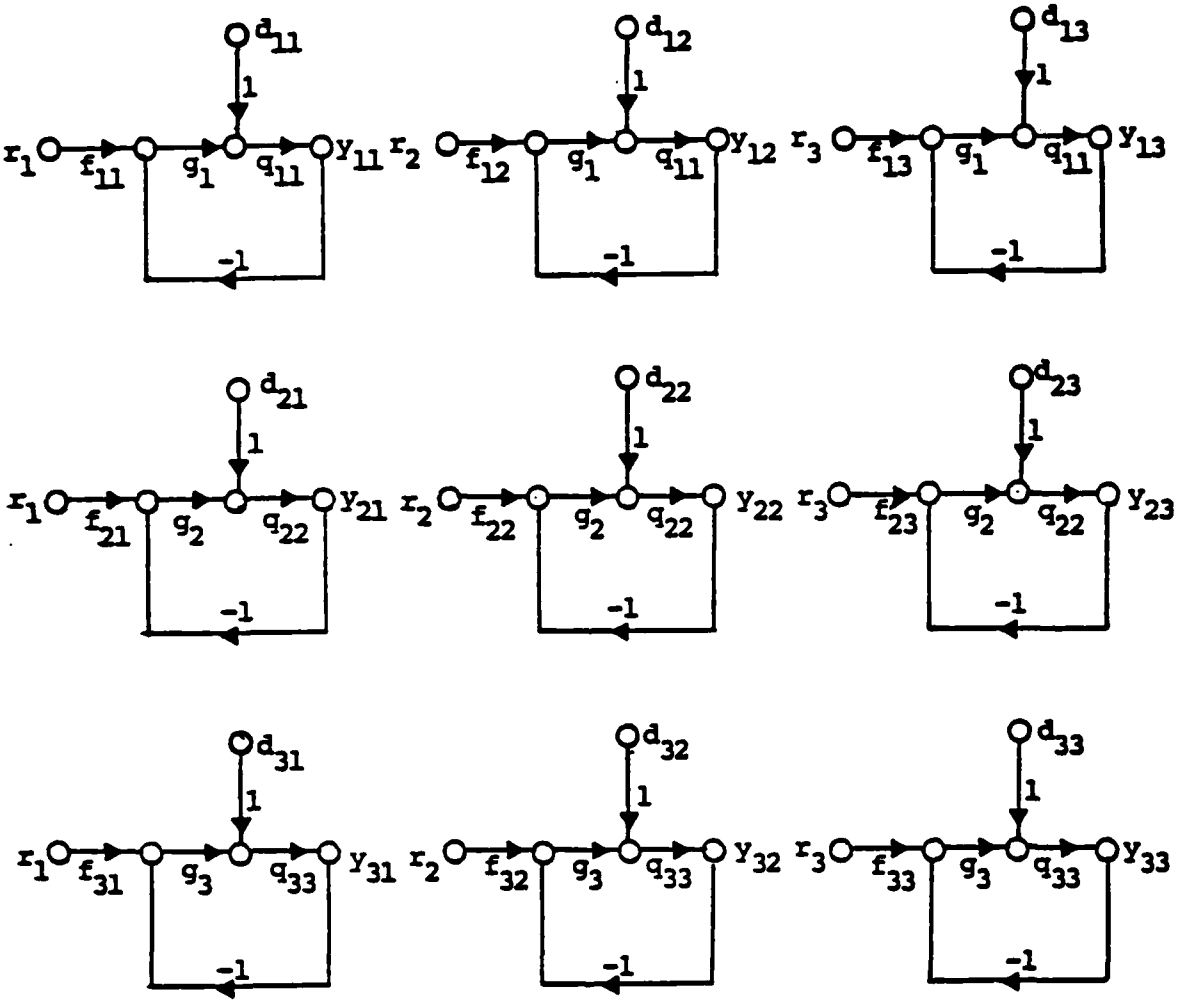

Fig. B-8. The Final Equivalent Single Loop Feedback Structure which Replaces the 3x3 MIMO System

Therefore the final equations for the nine SISO effective loops are:

$$t_{11} = \frac{f_{11}g_1q_{11}}{1 + g_1q_{11}} + \frac{q_{11}d_{11}}{1 + g_1q_{11}} \qquad \text{(B-20)}$$

$$t_{12} = \frac{f_{12}g_1q_{11}}{1 + g_1q_{11}} + \frac{q_{11}d_{12}}{1 + g_1q_{11}} \qquad \text{(B-20a)}$$

$$t_{13} = \frac{f_{13}g_1q_{11}}{1 + g_1q_{11}} + \frac{q_{11}d_{13}}{1 + g_1q_{11}} \qquad \text{(B-20b)}$$

$$t_{21} = \frac{f_{21}g_2q_{22}}{1 + g_2q_{22}} + \frac{q_{22}d_{21}}{1 + g_2q_{22}} \qquad \text{(B-20c)}$$

$$t_{22} = \frac{f_{22}g_2q_{22}}{1 + g_2q_{22}} + \frac{q_{22}d_{22}}{1 + g_2q_{22}} \qquad \text{(B-20d)}$$

$$t_{23} = \frac{f_{23}g_2q_{22}}{1 + g_2q_{22}} + \frac{q_{22}d_{23}}{1 + g_2q_{22}} \qquad \text{(B-20e)}$$

$$t_{31} = \frac{f_{31}g_3q_{33}}{1 + g_3q_{33}} + \frac{q_{33}d_{31}}{1 + g_3q_{33}} \qquad \text{(B-20f)}$$

$$t_{32} = \frac{f_{32}g_3q_{33}}{1 + g_3q_{33}} + \frac{q_{33}d_{32}}{1 + g_3q_{33}} \qquad \text{(B-20g)}$$

$$t_{33} = \frac{f_{33}g_3q_{33}}{1 + g_3q_{33}} + \frac{q_{33}d_{33}}{1 + g_3q_{33}} \qquad \text{(B-20h)}$$

where:

$$d_{11} = -\left[t_{21}/q_{12} + t_{31}/q_{13}\right] \qquad \text{(B-21)}$$

$$d_{12} = -\left[t_{22}/q_{12} + t_{32}/q_{13}\right] \qquad \text{(B-21a)}$$

$$d_{13} = - [t_{23}/q_{12} + t_{33}/q_{13}] \qquad \text{(B-21b)}$$

$$d_{21} = - [t_{11}/q_{21} + t_{31}/q_{23}] \qquad \text{(B-21c)}$$

$$d_{22} = - [t_{12}/q_{21} + t_{32}/q_{23}] \qquad \text{(B-21d)}$$

$$d_{23} = - [t_{13}/q_{21} + t_{33}/q_{23}] \qquad \text{(B-21e)}$$

$$d_{31} = - [t_{11}/q_{31} + t_{21}/q_{32}] \qquad \text{(B-21f)}$$

$$d_{32} = - [t_{12}/q_{31} + t_{22}/q_{32}] \qquad \text{(B-21g)}$$

$$d_{33} = - [t_{13}/q_{31} + t_{33}/q_{32}] \qquad \text{(B-21h)}$$

Finally, the above equations can be written in a general form for any n^2 equivalent single loop feedback structure (20:680). Thus in general form:

$$t_{ij} = \frac{f_{ij}g_i q_{ii} + d_{ij}q_{ii}}{1 + g_i q_{ii}} \qquad \text{(B-22)}$$

where: $d_{ij} = - \sum_k T_{kj}/q_{ik}$ and $k \neq j$

Equation (B-22) can be expressed as

$$t_{ij} = \frac{f_{ij}L_i + d_{ij}q_{ii}}{1 + L_i} \qquad \text{(B-23)}$$

where: $L_i = g_i q_{ii}$

Simplification of the Single-Loop Structure

The single-loop structure in Figure B-8 has two components, one due to the input r_j (assume r_j=1) and one due to the disturbance input d_{ij}. Therefore, the control ratio t_{ij} is the sum of control ratios each involving the jth input and can be written:

$$t_{ij} = \tau_{ij} + \tau_{d_{ij}} \tag{B-24}$$

$$\tau_{ij} = \frac{f_{ij}L_i}{1 + L_i} \quad ; \quad \tau_{d_{ij}} = \frac{d_{ij}q_{ii}}{1 + L_i} \tag{B-25}$$

For a fixed $\underline{P}$ which is an element of the universal set $\underline{P}$, $|d_{ij}|_{max}$ occurs at

$$|d_{ij}|_{max} = \sum_{k\neq i} |t_{kj}/q_{ik}|_{max} \tag{B-26}$$

Since the relative phases of t_{kj}/q_{ik} are not known, the design process must use the extreme cases:

$$\sum_{k\neq i} \frac{|t_{kj}|_{max}}{|q_{ik}|} = \sum_{k\neq i} \frac{|b_{ij}|}{|q_{ik}|} \triangleq d_{ij} \tag{B-27}$$

The term b_{ij} is the control ratio that represents the maximum allowable magnitude of the output due to the disturbance input which is one of the required design specifications.

Performance Tolerances

The performance tolerances are divided into two separate portions. One set of tolerances for the inter-

acting loop (tracking loop) and a second tolerance for the Basically Non-Interacting (BNIC) loop (Appendix A). Thus, for the BNIC loop it is necessary that:

$$|\tau_{ij}(j\ ) + \tau_{d_{ij}}(j\omega)\ _{max}| \leq |\tau_{ij}|_{max} + |\tau_{d_{ij}}|_{max}$$

$$= |\tau_{d_{ij}}|_{max} \leq b_{ij}(\omega) \qquad \text{(B-28)}$$

The above equation can be justified since the relative phase of the two terms ($\tau_{ij}(j\omega)$ and $\tau_{d_{ij}}(j\omega)$) are not known. Then $\tau_{ij}(j\omega)$ can be forced to zero by simply selecting f_{ij}, for i=j, to be zero. $b_{ij}(j\omega)$ are the upper bounds for the design specification on the disturbance rejection (20:681). The performance tolerance for the interacting loop is:

$$a_{ij}(\omega) \leq |\tau_{ij}(j\omega) + \tau_{d_{ij}}(j\omega)| \leq b_{ij}(\omega) \qquad \text{(B-29)}$$

where a_{ij} and b_{ij} are the upper and lower bounds of the design specifications for the interacting loop. Applying the above tolerances to the BNIC loop results in the following inequality:

$$|T_{ij}| = \frac{|q_{ii}|\ \ |d_{ij}|}{|1 + L_i|} \leq |b_{ij}| \qquad \text{(B-30)}$$

where for the 3x3 system

$$|d_{ij}| = |b_{kj}/q_{jk} + b_{ki}/q_{ik}| \qquad k \neq i$$

Rearranging Equation (B-30) yields the following inequality:

$$|1 + L_i| \geq \frac{|b_{kj}/q_{jk} + b_{ki}/q_{ik}|}{|b_{ij}|} \times |qii| \qquad \text{(B-31)}$$

Equation (B-31) is used in the design of all BNIC loops, which generates the required bounds on the loop transmission for a disturbance input.

The interacting loop tolerance generates the following conditions which must be satisfied in the design:

$$\tau_{ij} = \frac{f_{ij}L_i}{1+L_i} \quad ; \quad \tau_{d_{ij}} = \frac{d_{ij}q_{ii}}{1+L_i} \qquad \text{(B-32)}$$

where the bounds on $\tau_{d_{ij}}$ are found exactly as outlined above and the bounds on τ_{ij} are determined using the plant uncertainty (templates) and the given tolerances a_{ij} and b_{ij} on the interacting loop. It must be noted that the tolerances given by a_{ij} and b_{ij} are for the bounds on the entire interacting loop. Therefore, the tolerances must be divided between the interacting and BNIC cases. If one of the equations of Equation (B-32) is much more dominant than the other, then the entire bounds can be dedicated to that particular portion. The designer is cautioned that if one of τ_{ij} or $\tau_{d_{ij}}$ dominates, it must be verified over the entire frequency range of interest.

Improved Design Technique

The improved technique reduces the inherent overdesign. The unimproved technique does not exploit the correla-

tion between the t_{ij} of the system. With the improved technique this correlation between the t_{ij}'s is taken into account for the second and subsequent loop design. This technique is highlighted using a 3x3 MIMO system as an example.

Assume that loop one is the first loop to be designed. Therefore the general equation for these three SISO problems is obtained from Equation (B-22) (22:977-988) and is given as:

$$t_{1j} = \frac{f_{1j}L_1 + d_{1j}q_{11}}{1 + L_1} \qquad j = 1, 2, 3 \qquad \text{(B-33)}$$

$$L_1 = g_1 q_{11} \; ; \quad d_{1k} = \sum_{k \neq 1}^{3} t_{1j}/q_{1k}$$

Using Equation (B-33) the elements L_1 and f_{1j} are designed such that t_{1j}'s are stable and meet the desired tolerances or specifications. With loop one design completed, the second loop design can now be accomplished. The general equations for loop two are obtained using Equation (B-22). The resulting equation is:

$$t_{2j} = \frac{f_{2j}L_2 + d_{2j}q_{22}}{1 + L_2} \qquad \text{(B-34)}$$

$$d_{2j} = \sum_{k \neq 1}^{3} t_{2j}/q_{2k} \qquad j = 1,2,3$$

By solving for t_{1j} in Equation (B-33) and substituting these into Equation (B-34) it can be shown (22) that

$$t_{2j} = \frac{f_{2j}L_{2e} + d_{2e}}{1 + L_{2e}} \tag{B-35}$$

where $$L_{2e} = \frac{q_2 q_{22}}{1 - \gamma_{12}/(1+L_1)} \tag{B-35a}$$

$$\gamma_{12} = \frac{q_{11}q_{22}}{q_{12}q_{21}} \tag{B-35b}$$

$$q_{22e} = \frac{q_{22}\ (1 + L_1)}{(1 + L_1) - \gamma_{12}} \tag{B-35c}$$

$$d_{2j} = \frac{L_{2e}}{g_2}\left[t_{3j}\left(\frac{q_{11}}{q_{21}q_{13}(1 + L_1)}\right) - \frac{f_{1j}L_i}{q_{21}(1 + L_1)}\right] \tag{B-35d}$$

Using equations (B-35a) through (B-35d) the elements L_{2e} and f_{2j} can be designed to meet the desired tolerances since L_1 and f_{1j} are known from the first loop design.

The final loop is accomplished in a similar manner as the second loop design. The resulting equations are:

$$t_{3j} = \frac{f_{3j}L_{3e} + d_{3e}}{(1 + L_{3e})} \tag{B-36a}$$

$$L_{3e} = \frac{L_3\epsilon}{\epsilon - \Lambda} \tag{B-36b}$$

$$L_{3e} = q_{33e}q_3 \tag{B-36c}$$

$$q_{33e} = \frac{q_{33}\epsilon}{\epsilon - \Lambda} \tag{B-36d}$$

$$\Lambda = \gamma_{23}(1 + L_1) + \gamma_{13}(1 + L_2) - (\gamma_{12}u_1 + \gamma_{13}u_2) \quad \text{(B-36e)}$$

$$\epsilon = (1 + L_1)(1 + L_2) - \gamma_{12} \quad \text{(B-36f)}$$

$$u_1 = \frac{q_{21}q_{33}}{q_{23}q_{31}} \quad ; \quad u_2 = \frac{q_{31}q_{22}}{q_{32}q_{21}} \quad \text{(B-36g)}$$

$$\gamma_{12} = \frac{q_{11}q_{22}}{q_{12}q_{21}} \quad ; \quad \gamma_{23} = \frac{q_{22}q_{33}}{q_{23}q_{32}} \quad \text{(B-36h)}$$

$$\gamma_{13} = \frac{q_{11}q_{33}}{q_{13}q_{31}} \quad \text{(B-36i)}$$

$$d_{3i} = \frac{f_{1i}L_1q_{33}n_1 + f_{2i}L_2q_{33}n_2}{\epsilon - \Lambda} \quad \text{(B-36j)}$$

$$n_1 = \frac{q_{22}}{q_{21}q_{31}} - (1 + L_2)/q_{31} \quad \text{(B-36k)}$$

$$n_2 = \frac{q_{11}}{q_{12}q_{31}} - (1 + L_1)/q_{32} \quad \text{(B-36l)}$$

In Equations (B-36a) through (B-36l) L_1, L_2, f_{1j}, f_{2j}, are all known; therefore, the only unknowns are f_{3i} and g_3. These now constitute single-loop uncertainty problems and can be designed using the methods outlined in Appendix A. The required elements are designed to the desired tolerances or specifications. This completes the improved 3x3 MIMO design technique. If all loops are designed to meet the given tolerances, then the desired response from the MIMO system is guaranteed.

Equilibrium and Tradeoffs

Equilibrium exists when it is impossible to reduce the burden on any L_i, without increasing it on some other L_j (20:683). This simply states that some of the design tolerances may be decreased or increased for certain loops without making it more difficult on other loops. This results in only one column of the equivalent SISO systems being dominant. However, after equilibrium is reached, it may be desirable to sacrifice one loop for the sake of another. This involves "tradeoffs" between the different loops. It should be noted that these tradeoffs, when used, always make it harder to meet specifications on one loop when reduction is accomplished in another.

Summary

This Appendix describes the design technique used in the design of single input-single output and multiple input-multiple output systems. First, the SISO system technique is outlined and, second, the technique is expanded to the MIMO system.

The appendix describes the multiple input-multiple output plant and the corresponding plant matrix. Guidelines are presented for finding the $\underline{P}$ matrix, which relates the input vector to the output vector.

The division of the MIMO system into separate SISO loops is presented using the inverse of the $\underline{P}$ matrix. After the equivalent SISO loops are determined, each is designed in accordance with the SISO design theory pre-

sented in Appendix A.

Finally, the guidelines for reducing the MIMO system to a simple SISO system problem is illustrated with a 3x3 design overview with extension to any general n^2 MIMO system.

Appendix C: Plant Transfer Functions

Introduction

Appendix C contains the input-output matrices for the KC-135 F.C.'s 2 and 3 for both the lateral and longitudinal modes. The individual plant transfer functions for F.C.'s 2 and 3 of the KC-135 lateral mode are also listed. The individual plant transfer functions for all three F.C.'s of the KC-135 longitudinal mode are presented. The plant transfer funcitons for all four of the F-16 flight conditions are listed in this appendix as well.

KC-135 Lateral Mode Input-Output Matrices

Flight Condition 2

$$\begin{bmatrix} (S^2+.920643S-.016597) & (.3974S+6.25223) \\ (.0399458S^2+.06167S+.00821) & -(S^2+.272719S+1.88298) \end{bmatrix} \begin{bmatrix} \phi \\ \beta \end{bmatrix}$$

$$= \begin{bmatrix} .46223 & 1.111 \\ (.0007655S+.02546) & -(.0273552S+1.3286) \end{bmatrix} \begin{bmatrix} \delta_w \\ \delta_r \end{bmatrix} \qquad (C\text{-}1)$$

Flight Condition 3

$$\begin{bmatrix} (S^2+1.09665S-.09548) & (.69382S+2.4876) \\ (.031645S^2+.22835S+.03271) & -(S^2+.368629S+.609055) \end{bmatrix} \begin{bmatrix} \phi \\ \beta \end{bmatrix}$$

$$= \begin{bmatrix} .37757 & .36189 \\ (.0024207S+.01926) & -(.03819S+.46618) \end{bmatrix} \begin{bmatrix} \delta_w \\ \delta_r \end{bmatrix} \qquad (C\text{-}2)$$

KC-135 Lateral Mode Plant Transfer Functions

Flight Condition 2

$$P_{11} = \frac{.462534(S+.152381 \pm j.439295)}{(S+.00958403)(S+.970805)(S+.114426 \pm j1.46457)} \quad (C-3)$$

$$P_{12} = \frac{1.10013(S+2.20360)(S-2.56358)}{(S+.00958403)(S+.970805)(S+.114426 \pm j1.46457)} \quad (C-4)$$

$$P_{21} = \frac{-.0007655(S+.487457)(S-1.06261)}{(S+.00958403)(S+.970805)(S+.114426 \pm j1.46457)} \quad (C-5)$$

$$P_{22} = \frac{.027355(S+.950937)(S+50.1706)(S-.00990664)}{(S+.00958403)(S+.970805)(S+.114426 \pm j1.46457)} \quad (C-6)$$

Flight Condition 3

$$P_{11} = \frac{.37925(S+.209057 \pm j.830047)}{(S+.0193202)(S+1.30868)(S+.0796150 \pm j.954940)} \quad (C-7)$$

$$P_{12} = \frac{.33539(S+1.30164)(S-2.15152)}{(S+.0193202)(S+1.30868)(S+.0796150 \pm j.954940)} \quad (C-8)$$

$$P_{21} = \frac{-.002421(S+.210775)(S+7.57616)(S-3.67045)}{(S+.0193202)(S+1.30868)(S+.0796150 \pm j.954940)} \quad (C-9)$$

$$P_{22} = \frac{.03819(S+1.31034)(S+12.3458)(S-.0528804)}{(S+.0193202)(S+1.30868)(S+.0796150 \pm j.954940)} \quad (C-10)$$

KC-135 Longitudinal Mode Input-Output Matrices

Rigid Body

Flight Condition 2

$$\begin{bmatrix} .041S & (.5601S-1.113) & (S+.0029) \\ (-.0743S^2-.03555S) & (.0063S+.479) & .0049 \\ -.1789S & (S^2+.8149S+2.4608) & -.0091 \end{bmatrix} \begin{bmatrix} h \\ \theta \\ u \end{bmatrix}$$

$$= \begin{bmatrix} .010498 & -.0798 & .034 \\ -.0186 & .0273 & 0 \\ -1.758 & .218 & 0 \end{bmatrix} \begin{bmatrix} \delta_e \\ \delta_{sb} \\ \delta_T \end{bmatrix} \qquad \text{(C-11)}$$

Flight Condition 3

$$\begin{bmatrix} .1031S & (.166S-.9848) & (S+.0234) \\ (-.2438S^2-.1899S) & (.0335S+.7784) & .0592 \\ -.2619S & (S^2+1.092S+1.074) & -.0318 \end{bmatrix} \begin{bmatrix} h \\ \theta \\ u \end{bmatrix}$$

$$= \begin{bmatrix} .0065 & -.0631 & .1268 \\ -.0375 & .0646 & 0 \\ -.9218 & .0954 & 0 \end{bmatrix} \begin{bmatrix} \delta_e \\ \delta_{sb} \\ \delta_T \end{bmatrix} \qquad \text{(C-12)}$$

Elastic Body

The general form of the elastic body input-ouput matrices is given in Equation (C-13). The individual elements (a through f) of the input-output matrices are given in Equations (C-14) through (C-16).

$$\begin{bmatrix} a & b & 0 \\ c & d & 0 \\ 0 & 0 & 1 \end{bmatrix} \begin{bmatrix} h \\ \Theta \\ u \end{bmatrix} = \begin{bmatrix} e & 0 & 0 \\ f & 0 & 0 \\ 0 & 0 & 0 \end{bmatrix} \begin{bmatrix} \delta_e \\ \delta_{sb} \\ \delta_T \end{bmatrix} \qquad \text{(C-13)}$$

Flight Condition 1

$$a = -.0769S^2 - (.00023/A + .000113/B)S \qquad \text{(C-14a)}$$

$$b = (1 + .00241/A - .0031/B)S + .00299/A + .0031/B \qquad \text{(C-14b)}$$

$$c = -(.00022/A + .00106/B)S \qquad \text{(C-14c)}$$

$$d = S^2 + (.0023/A - .02912/B)S + .00286/A + .0137/B \qquad \text{(C-14d)}$$

$$e = .000576/A + .000749/B \qquad \text{(C-14e)}$$

$$f = .00055/A + .00704/B \qquad \text{(C-14f)}$$

$$A = S^2 + 1.318S + 134.074 = (S + .659 \pm j11.5603) \qquad \text{(C-14g)}$$

$$B = S^2 + 1.112S + 545.026 = (S + .556 \pm j23.3392) \qquad \text{(C-14h)}$$

Flight Condition 2

$$a = -.0743S^2 - (.000038/A + .000011/B)S \qquad \text{(C-15a)}$$

$$b = (1 + .00046/A - .01748/B)S + .00051/A + .0015/B \qquad \text{(C-15b)}$$

$$c = (.00189/A - .000121/B)S \qquad \text{(C-15c)}$$

$$d = S^2 - (.02276/A + .1903/B)S + .00163/A - .02537/B \qquad \text{(C-15d)}$$

$$e = .000083/A + .00187/B \qquad \text{(C-15e)}$$

$$f = -.0041/A + .0203/B \qquad \text{(C-15f)}$$

$$A = S^2 + 1.848S + 93.164 = (S + .924 \pm j9.60782) \qquad \text{(C-15g)}$$

$$B = S^2 + 1.196S + 517.212 = (S + .598 \pm j22.7344) \qquad \text{(C-15h)}$$

Flight Condition 3

$$a = -.2438S^2 - (.00122/A + .00059/B)S \quad \text{(C-16a)}$$

$$b = (1 + .00401/A - .00517/B)S + .00499/A + .00244/B \quad \text{(C-16b)}$$

$$c = (-.00366/A + .00178/B)S \quad \text{(C-16c)}$$

$$d = S^2 + (.00121/A - .01548/B)S + .0015/A + .00731/B \quad \text{(C-16d)}$$

$$e = .000961/A + .00125/B \quad \text{(C-16e)}$$

$$f = .00029/A + .00374/B \quad \text{(C-16f)}$$

$$A = S^2 + 1.893S + 131.014 = (S + .9465 \pm j11.4069) \quad \text{(C-16g)}$$

$$B = S^2 + 1.229S + 547.77 = (S + .6145 \pm j23.3964) \quad \text{(C-16h)}$$

KC-135 Longitudinal Mode Plant Transfer Functions

Rigid Body

Flight Condition 1

$$P_{11} = \frac{.277230(S+.0136689)(S-6.15013)(S+6.35439)}{S(S-.0568942)(S+.0599089)(S+.647974\pm j1.66670)} \quad \text{(C-17)}$$

$$P_{12} = \frac{-.416125(S-.0731283\pm j.0712002)(S+.877711)}{S(S-.0568942)(S+.0599089)(S+.647974\pm j1.66670)} \quad \text{(C-18)}$$

$$P_{13} = \frac{.00315410(S+.384350\pm j1.95325)}{S(S-.0568942)(S+.0599089)(S+.647974\pm j1.66670)} \quad \text{(C-19)}$$

$$P_{21} = \frac{-1.64900(S+.00813148)(S+.500895)}{(S-.0568942)(S+.0599089)(S+.647974\pm j1.66670)} \quad \text{(C-20)}$$

$$P_{22} = \frac{.1733(S-.0633967)(S+.0871544)}{(S-.0568942)(S+.0599089)(S+.647974\pm j1.66670)} \quad \text{(C-21)}$$

$$P_{23} = \frac{.00051975(S+1.84759)}{(S-.0568942)(S+.0599089)(S+.647974\pm j1.66670)} \quad \text{(C-22)}$$

$$P_{31} = \frac{.011619(S+.294472)(S-1.75751)(S+77.6744)}{(S-.0568942)(S+.0599089)(S+.647974\pm j1.66670)} \quad (C-23)$$

$$P_{32} = \frac{-.0827(S-.0389887)(S+.486976)(S+1.76180)}{(S-.0568942)(S+.0599089)(S+.647974\pm j1.66670)} \quad (C-24)$$

$$P_{33} = \frac{.0495(S-.00163560)(S+.648795\pm j1.66352)}{(S-.0568942)(S+.0599089)(S+.647974\pm j1.66670)} \quad (C-25)$$

Flight Condition 2

$$P_{11} = \frac{.250336(S+.0150531)(S-6.41871)(S+6.62877)}{S(S-.0499167)(S+.0625482)(S+.641481\pm j1.55626)} \quad (C-26)$$

$$P_{12} = \frac{-.367429(S+.00725990)(S-.828748)(S+1.60330)}{S(S-.0499167)(S+.0625482)(S+.641481\pm j1.55626)} \quad (C-27)$$

$$P_{13} = \frac{.00224226(S+.413300\pm j1.78313)}{S(S-.0499167)(S+.0625482)(S+.641481\pm j1.55626)} \quad (C-28)$$

$$P_{21} = \frac{-1.758(S+.00890135)(S+.446262)}{(S-.0499167)(S+.0625482)(S+.641481\pm j1.55626)} \quad (C-29)$$

$$P_{22} = \frac{.218(S-.0110571)(S+.186891)}{(S-.0499167)(S+.0625482)(S+.641481\pm j1.55626)} \quad (C-30)$$

$$P_{23} = \frac{.0003094(S+1.77430)}{(S-.0499167)(S+.0625482)(S+.641481\pm j1.55626)} \quad (C-31)$$

$$P_{31} = \frac{.010498(S+.256483)(S-1.73052)(S+95.5837)}{(S-.0499167)(S+.0625482)(S+.641481\pm j1.55626)} \quad (C-32)$$

$$P_{32} = \frac{-.0798(S-.308874)(S+.315440)(S+2.62745)}{(S-.0499167)(S+.0625482)(S+.641481\pm j1.55626)} \quad (C-33)$$

$$P_{33} = \frac{.034(S+.00793446)(S+.642379\pm j1.55311)}{(S-.0499167)(S+.0625482)(S+.641481\pm j1.55626)} \quad (C-34)$$

Flight Condition 3

$$P_{11} = \frac{.153815(S+.105056)(S-4.12352)(S+4.32065)}{S(S-.136952)(S+.192094)(S+.919587\pm j1.02075)} \quad (C-35)$$

$$P_{12} = \frac{-.264971(S-.148416)(S+.208363)(S+1.06381)}{S(S-.136952)(S+.192094)(S+.919587\pm j1.02075)} \quad (C-36)$$

$$P_{13} = \frac{.030790(S+.554997\pm j1.08817)}{S(S-.136952)(S+.192094)(S+.919587\pm j1.02075)} \quad (C-37)$$

$$P_{21} = \frac{-.9218(S+.0604067)(S+.697985)}{(S-.136952)(S+.192094)(S+.919587\pm j1.02075)} \quad (C-38)$$

$$P_{22} = \frac{.0954(S-.127425)(S+.181287)}{(S-.136952)(S+.192094)(S+.919587\pm j1.02075)} \quad (C-39)$$

$$P_{23} = \frac{.00403224(S+2.77876)}{(S-.136952)(S+.192094)(S+.919587\pm j1.02075)} \quad (C-40)$$

$$P_{31} = \frac{.0065(S+.446838)(S-4.80063)(S+27.3263)}{(S-.136952)(S+.192094)(S+.919587\pm j1.02075)} \quad (C-41)$$

$$P_{32} = \frac{-.0631(S-.164207)(S+.156521)(S+1.69664)}{(S-.136952)(S+.192094)(S+.919587\pm j1.02075)} \quad (C-42)$$

$$P_{33} = \frac{.1268(S+.000194722)(S+.935361\pm j1.00664)}{(S-.136952)(S+.192094)(S+.919587\pm j1.02075)} \quad (C-43)$$

Elastic Body

Flight Condition 1

$$P_{e11} = \frac{-.0172302(S+.000012507)(S-3.11866)}{S(S-.000629852)(S+.00030929\underline{1}+j.000362912)}$$

$$\frac{(S-.690542\underline{+}j17.3342)}{(S+.659000\underline{+}j11.5603)(S+.556000\underline{+}j23.3392)} \quad \text{(C-44)}$$

$$P_{e21} = \frac{.007590(S+.0000095)}{(S-.000629852)(S+.00030929\underline{1}+j.000362912)}$$

$$\frac{(S+.651531\underline{+}j12.783921)}{(S+.659000\underline{+}j11.5603)(S+.556000\underline{+}j23.3392)} \quad \text{(C-45)}$$

$$P_{c11} = \frac{.277230(S+.0000038)(S+.0146521)(S+6.35534)}{S(S+.0599089)(S-.000629852)(S-.0568942)}$$

$$\frac{(S-6.15050)(S-.000531746\underline{+}j.00384070)}{(S+.000309291\underline{+}j.000362912)(S+.647974\underline{+}j1.66670)} \quad \text{(C-46)}$$

$$P_{c21} = \frac{-1.64900(S+.0000043)(S+.0102544)(S+.500952)}{(S+.0599089)(S-.000629852)(S-.0568942)}$$

$$\frac{(S-.00110205\underline{+}j.00453225)}{(S+.000309291\underline{+}j.000362912)(S+.647974\underline{+}j1.66670)} \quad \text{(C-47)}$$

Flight Condition 2

$$P_{e11} = \frac{-.0262853(S+1.13826)(S-.0000215)}{S(S+.0000087)(S+.924000\underline{+}j9.60782)}$$

$$\frac{(S-3.80642\underline{+}j9.41610)}{(S+.598000\underline{+}j22.7344)(S-.0003104\underline{1}+j.0154348)} \quad \text{(C-48)}$$

$$P_{e21} = \frac{.0162(S+4.90139)(S-.00024978)}{(S+.0000087)(S+.924000\pm j9.60782)}$$

$$\frac{(S-2.88813)}{(S+.598000\pm j22.7344)(S-.0003104l\pm j.0154348)} \qquad \text{(C-49)}$$

$$P_{c11} = \frac{.250336(S+.0149432)(S+6.62950)(S-6.41928)}{S(S+.0625482)(S-.0499167)(S+.641481\pm j1.55626)}$$

$$\frac{(S-.00024721\pm j.0153769)}{(S-.00031041\pm j.0154348)} \qquad \text{(C-50)}$$

$$P_{c21} = \frac{-1.75800(S+.446247)(S+.00872367)}{(S+.0625482)(S-.0499167)(S+.641481\pm j1.55626)}$$

$$\frac{(S-.00021654\pm j.0153884)}{(S-.00031041\pm j.0154348)} \qquad \text{(C-51)}$$

Flight Condition 3

$$P_{e11} = \frac{-.0090689(S+.0000283)(S-.948309)}{S(S+.0000425)(S+.00873567)(S-.00875316)}$$

$$\frac{(S+.364981\pm j17.5884)}{(S+.946518\pm j11.4069)(S+.614516\pm j23.3964)} \qquad \text{(C-52)}$$

$$P_{e21} = \frac{.00403(S-.0000651)}{(S+.0000425)(S+.00873567)(S-.00875316)}$$

$$\frac{(S+.922475\pm j12.6551)}{(S+.946518\pm j11.4069)(S+.614516\pm j23.3964)} \qquad \text{(C-53)}$$

$$P_{c11} = \frac{.153815(S+.00004381)(S+.00832179)(S+.105105)}{S(S+.00004252)(S+.00873567)(S+.192094)(S-.00875316)}$$

$$\frac{(S+4.32110)(S-.00841569)(S-4.12404)}{(S-.136952)(S+.919587\pm j1.02075)} \qquad \text{(C-54)}$$

$$P_{c21} = \frac{-.921800(S+.00006170)(S+.00791259)(S+.0606049)}{(S+.00004252)(S+.00873567)(S+.192094)(S-.00875316)}$$

$$\frac{(S+.697999)(S-.00817314)}{(S-.136952)(S+.919587\pm j1.02075)} \qquad \text{(C-55)}$$

F-16 Plant Transfer Functions

Note that due to symmetry, $P^a_{ij} = P^b_{ij}$.

Flight Condition 1

$$P^a_{11} = \frac{q}{\delta^a_1} = \frac{-1.118S(S+.01822)(S+.4568)}{(S-.3633)(S+1.3)(S+.07683\pm j.2065)} \qquad \text{(C-56)}$$

$$P^a_{12} = \frac{q}{\delta^a_2} = \frac{.1209S(S+.06537)(S+.2589)}{(S-.3633)(S+1.3)(S+.07683\pm j.2065)} \qquad \text{(C-57)}$$

$$P^a_{22} = \frac{p}{\delta^a_2} = \frac{-2.239S(S+.205\pm j.853)}{(S+.1041)(S+.6835)(S+.2741\pm j1.909)} \qquad \text{(C-58)}$$

$$P^a_{21} = \frac{p}{\delta^a_1} = \frac{-2.142S(S+.3017\pm j1.562)}{(S+.1041)(S+.6835)(S+.2741\pm j1.909)} \qquad \text{(C-59)}$$

Flight Condition 2

$$P^a_{11} = \frac{-2.931S(S+.01004)(S+.5502)}{(S-1.167)(S+2.028)(S+.006472\pm j.07803)} \qquad \text{(C-60)}$$

$$P^a_{12} = \frac{-.1059S(S+.006697)(S+1.861)}{(S-1.167)(S+2.028)(S+.006472\pm j.07803)} \qquad \text{(C-61)}$$

$$P^a_{22} = \frac{-8.723S(S+.219\pm j1.607)}{(S+.07795)(S+.8265)(S+.211\pm j1.953)} \qquad \text{(C-62)}$$

$$P^a_{21} = \frac{-6.792S(S+.2442\pm j2.101)}{(S+.07795)(S+.8265)(S+.211\pm j1.953)} \quad \text{(C-63)}$$

Flight Condition 3

$$P^a_{11} = \frac{-12.03S(S+.01262)(S+1.51)}{(S-.9645)(S+3.223)(S+.007553\pm j.05384)} \quad \text{(C-64)}$$

$$P^a_{12} = \frac{-3.236S(S+.01254)(S+1.646)}{(S-.9645)(S+3.223)(S+.007553\pm j.05384)} \quad \text{(C-65)}$$

$$P^a_{22} = \frac{-25.53S(S+.3541\pm j2.927)}{(S+.02719)(S+2.697)(S+.391\pm j2.962)} \quad \text{(C-66)}$$

$$P^a_{21} = \frac{-25.36S(S+.3749\pm j3.578)}{(S+.02719)(S+2.697)(S+.391\pm j2.962)} \quad \text{(C-67)}$$

Flight Condition 4

$$P^a_{11} = \frac{-16.45S(S+.02996)(S+1.097)}{(S+.01516\pm j.02343)(S+.8012\pm j6.592)} \quad \text{(C-68)}$$

$$P^a_{12} = \frac{-2.925S(S+.03459)(S+.6861)}{(S+.01516\pm j.02343)(S+.8012\pm j6.592)} \quad \text{(C-69)}$$

$$P^a_{22} = \frac{-7.084S(S+.4083\pm j4.916)}{(S+.03448)(S+2.171)(S+.4996\pm j3.129)} \quad \text{(C-70)}$$

$$P^a_{21} = \frac{-23.3S(S+.3774\pm j3.848)}{(S+.03448)(S+2.171)(S+.4996\pm j3.129)} \quad \text{(C-71)}$$

Appendix D: Time Response Models

Introduction

This appendix contains the response models used in the continuous domain QFT designs for the KC-135 and F-16 aircraft. These responses will also serve as the basis for judging the performance of the discrete designs of this thesis.

KC-135 Lateral Mode Response Models

Bank Angle Command

Table D-1 contains the upper bound bank angle time response, b_{11}, for a bank angle command of 30 degrees.

TABLE D-1

b_{11}--Time Domain Specifications
KC-135 Lateral Mode

Rise time = 2.29 seconds
Settling time = 4.24 seconds
Peak value = 30.0 degrees
Final value = 30.0 degrees

The lower bound bank angle response for a bank angle command of 30 degrees is shown in Table D-2.

TABLE D-2

a_{11}--Time Domain Specifications
KC-135 Lateral Mode

Rise time = 5.21 seconds
Settling time = 9.51 seconds
Peak value = 30.0 degrees
Final value = 30.0 degrees

The maximum acceptable response for the sideslip response due to a bank angle command is contained in Table D-3.

TABLE D-3

b_{12}--Time Domain Specifications
KC-135 Lateral Mode

Settling time = 15 seconds
Peak time = 1 second
Peak value = 1.0 degrees
Final value = 0.0 degrees

Sideslip Command

The upper bound for the sideslip response to a 5 degree sideslip command is shown in Table D-4.

TABLE D-4

b_{22}--Time Domain Specifications
KC-135 Lateral Mode

Rise time = 4.91 seconds
Settling time = 8.90 seconds
Peak value = 5.0 degrees
Final value = 5.0 degrees

Table D-5 outlines the worst acceptable response or lower bound for sideslip response with a 5 degree sideslip command.

TABLE D-5

a_{22}--Time Domain Specifications
KC-135 Lateral Mode

Rise time = 7.87 seconds
Settling time = 14.4 seconds
Peak value = 5.0
Final value = 5.0

Table D-6 shows the maximum allowable time response characteristics for bank angle response to a sideslip command of 5 degrees.

TABLE D-6

b_{21}--Time Domain Specifications
KC-135 Lateral Mode

Peak time = .681 seconds
Settling time = 20 seconds
Peak value = 2.0
Final value = 0.0

KC-135 Longitudinal Mode Response Models

Pitch Angle Command

Table D-7 shows the upper bound pitch angle response for a 4 degree pitch angle command input.

TABLE D-7

b_{22}--Time Domain Specifications
KC-135 Longitudinal Mode

Rise time = 2.93 seconds
Settling time = 6.26 seconds
Peak value = 4.08
Final value = 4.00

The lower bound pitch angle response for a 4 degree pitch angle command is shown in Table D-8.

TABLE D-8

a_{22}--Time Domain Specifications
KC-135 Longitudinal Mode

Rise time = 5.08 seconds
Settling time = 10.1 seconds
Peak value = 4.00
Final value = 4.00

Table D-9 shows the maximum allowable response for perturbation altitude, h, due to a pitch angle command of 4 degrees.

TABLE D-9

b_{12}--Time Domain Specifications
KC-135 Longitudinal Mode

Rise time = 2.11 seconds
Settling time = 9.92 seconds
Peak value = 0.5
Final value = 0

The maximum response for perturbation velocity, u, due to a pitch angle command is outlined in Table D-10.

TABLE D-10

b_{32}--Time Domain Specifications
KC-135 Longitudinal Mode

Peak time = 1.94 seconds
Settling time = 9.76 seconds
Peak value = 1.00
Final value = 0

F-16 Response Models

Pitch Rate Command

The upper bound pitch rate response to a pitch rate command of 10 degrees per second is contained in Table-11.

TABLE D-11

b_{11}--Time Domain Specifications, F-16

Rise time = 0.33 seconds
Settling time = 1.5 seconds
Peak value = 11.0 deg/sec

The lower bound on the pitch rate response for a 10 degree per second pitch angle command is shown in Table D-12.

TABLE D-12

a_{11}--Time Domain Specifications, F-16

Rise time = 1.63 seconds
Settling time = 3.01 seconds
Peak value = 10.0 deg/sec

The maximum allowable roll rate response for a pitch rate command is shown in Table D-13.

TABLE D-13

b_{21}--Time Domain Specifications, F-16

Rise time = 0.70 seconds
Settling time = 4.30 seconds
Peak value = 2.344 deg/sec
Total roll angle $\leq$ 5 deg

Roll Rate Command

The maximum response for roll angle due to a 50 degree per second roll rate command shown in Table D-14.

TABLE D-14

b_{22}--Time Domain Specifications, F-16

Rise time = 0.65 seconds
Settling time = 3.01 seconds
Peak value = 55.00 deg/sec

The lower bound for the roll rate response to a roll rate command of 50 degrees per second is shown in Table D-15.

TABLE D-15

a_{22}--Time Domain Specifications, F-16

Rise time = 3.23 seconds
Settling time = 6.00 seconds
Peak value = 50.0 deg/sec

The maximum allowable response for pitch rate when roll rate is commanded is shown in D-16.

TABLE D-16

b_{12}-Time Domain Specifications, F-16

Rise time = 0.65 seconds
Settling time = 4.30 seconds
Peak value = 1.4 deg/sec
Total pitch angle $\leq$ 3.0 deg

Appendix E: Continuous and Discrete Compensators

Introduction

This appendix contains the continuous and discrete compensators for the longitudinal mode of the KC-135 and the F-16 aircraft. The continuous domain compensators are modified to counter the effects of the ZOH, as discussed in Chapter III. The KC-135 longitudinal mode compensators are used for both the rigid and elastic body models. The sampling rates for the KC-135 and F-16 are selected as 40 Hz and 60 Hz respectively. Also included are the S domain prefilters for the F-16 and both modes of the KC-135 as originally designed in references 1 and 2.

Continuous Domain Prefilters

KC-135 Lateral Mode

$$F_{11}(s) = \frac{.9}{(S+.9)(S+1)} \qquad \text{(E-1)}$$

$$F_{22}(s) = \frac{.512}{(S+.512)(S+1)} \qquad \text{(E-2)}$$

KC-135 Longitudinal Mode

$$F_{22}(s) = \frac{.3506}{(S+.5)(S+.54\pm j.64)} \qquad \text{(E-3)}$$

F-16

$$F_{11}(s) = \frac{2}{S+2} \qquad \text{(E-4)}$$

$$F_{22}(s) = \frac{2.78}{(S+1.334\pm j1.00022)} \qquad \text{(E-5)}$$

Continuous Domain Compensators

KC-135 Longitudinal Mode

$$G_1(s) = \frac{-18.1875(S+4)(S+80)}{(S+24\pm j32)} \qquad \text{(E-6)}$$

$$G_2(s) = \frac{5.62(10^7)(S+1)(S+80)}{(S+30)(S+390\pm j520)} \qquad \text{(E-7)}$$

$$G_3(s) = \frac{2680(S+2)(S+.01846)(S+80)}{S(S+.5)(S+10)(S+18\pm j24)} \qquad \text{(E-8)}$$

F-16

$$G_1(s) = \frac{-19916.667(S+.3)(S+1.1)(S+1.167)(S+2.028)(S+20)}{S^2(S+.0107)(S+.4845)(S+.5)^2(S+35)}$$

$$\frac{(S+120)(S+430)(S+.006472\pm j.07803)}{(S+87)(S+636\pm j848)} \qquad \text{(E-9)}$$

$$G_2(s) = \frac{-18750(S+.03448)(S+.3)(S+2.171)(S+12.9)(S+120)^2}{S^2(S+.2)(S+3.46)(S+48)(S+.62\pm j6.07582)}$$

$$\frac{(S+.4996\pm j3.12896)}{(S+450\pm j600)} \qquad \text{(E-10)}$$

Digital Controllers

KC-135 Longitudinal Mode

$$G_1(z) = \frac{-20.6453z(z-.904762)}{(z-.405405\pm j.432432)} \qquad \text{(E-11)}$$

$$G_2(z) = \frac{13477.3z(z-.975309)(z+1)}{(z-.454545)(z+.846937\pm j.169347)} \qquad \text{(E-12)}$$

$$G_3(z) = \frac{.476851z(z-.999539)(z-.951220)}{(z-1)(z-.987578)(z-.777778)}$$

$$\frac{(z+1)^2}{(z-.540275\pm j.377210)} \qquad \text{(E-13)}$$

F-16

$$G_1(z) = \frac{-9.11983z(z+1)(z-.995012)(z-.981833)(z-.980737)}{(z-1)^2(z-.999822)(z-.991957)(z-.991701)^2}$$

$$\frac{(z-.966762)(z-.714286)(z+.563636)}{(z-.548387)(z-.159420)}$$

$$\frac{(z-.999891\pm j.001300)}{(z+.859419\pm j.157689)} \qquad \text{(E-14)}$$

$$G_2(z) = \frac{-10.2585z^2(z+1)(z-.999425)(z-.995012)(z-.964460)}{(z-1)^2(z-.996672)(z-.943949)(z-.428571)}$$

$$\frac{(z-.805869)(z-.990366\pm j.051683)}{(z-.984684\pm j.099972)(z+.800263\pm j.210250)} \qquad \text{(E-15)}$$

Appendix F: Continuous System Simulation Responses

Introduction

This appendix contains the simulation responses for the KC-135 longitudinal mode and the F-16 continuous systems. For the KC-135 longitudinal mode, continuous system simulations are performed only for the rigid body. The KC-135 lateral mode continuous system responses are shown in Chapter IV.

The continuous system response data in this appendix and in Chapter IV is compared with the original continuous system performance in references 1 and 2 as an empirical validation of the plant and compensator data as well as the general simulation setup used in this study. The continuous response data is also compared with the hybrid system responses to assess the hybrid system performance.

KC-135 Longitudinal Mode Responses - Continuous System

The pitch angle command responses are shown in Figures F-1 through F-3. The pitch rate response is shown in Figure F-1. Figure F-2 shows the perturbation altitude response and Figure F-3 shows the perturbation velocity response. The rigid body response characteristics for the pitch angle command are shown in Table F-1. As noted in Section IV-4, comparison of these responses with the specifications shows that the desired robust performance is achieved.

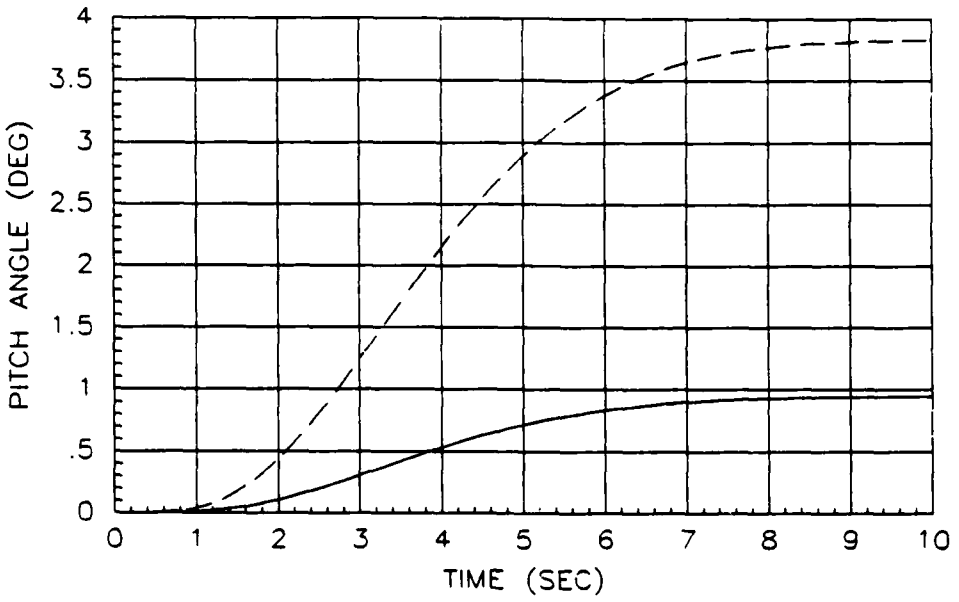

Fig. F-1. Continuous System Pitch Angle Responses

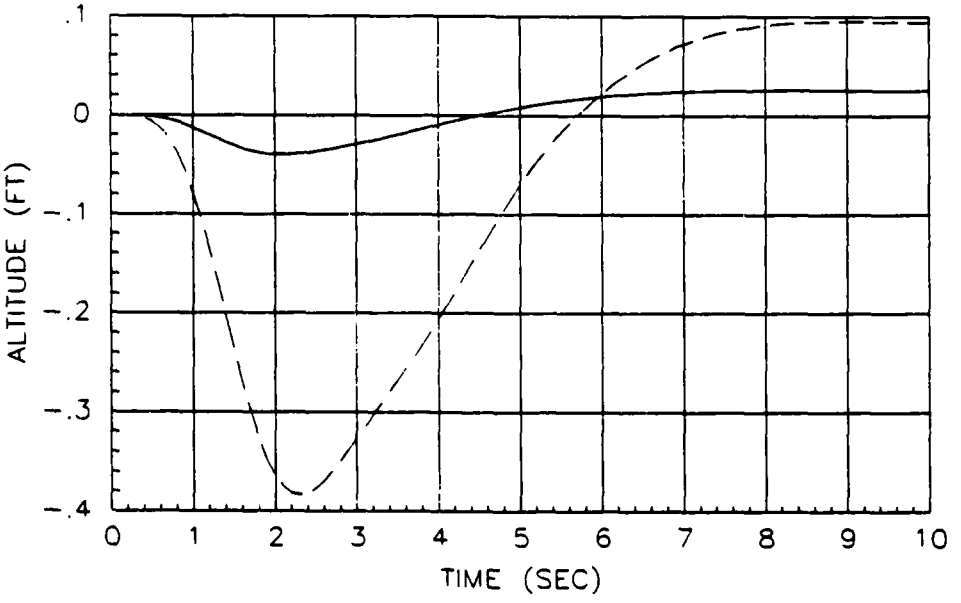

Fig. F-2. Continuous System Altitude Responses

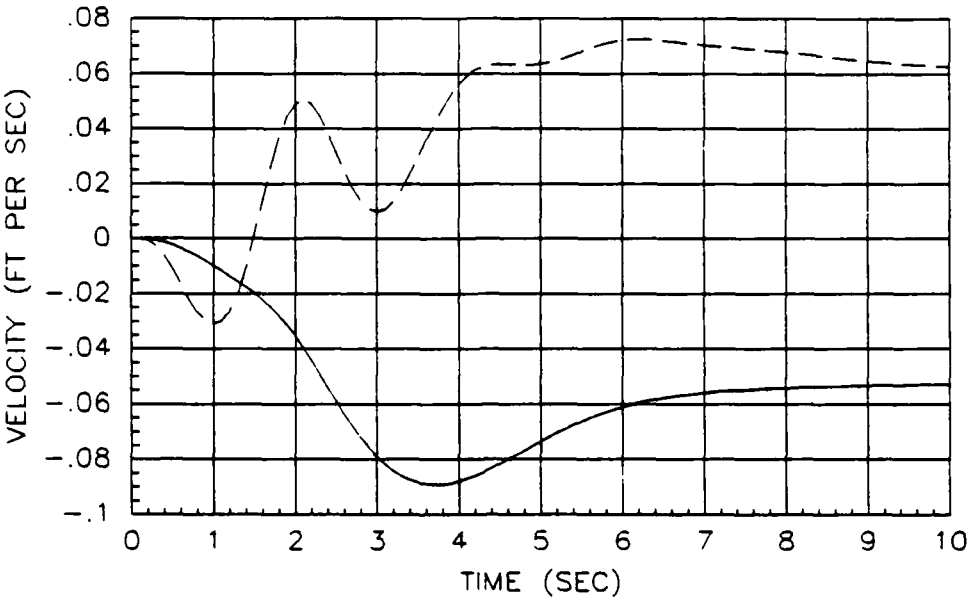

Fig. F-3. Continuous System Velocity Responses

Table F-1

Pitch Angle Command - Continuous System (Rigid Body)

Response	F.C.	Peak Value	Final Value	Rise Time (sec)	Settling Time (sec)
θ (deg)	1	1.0	1.0	4.37	8.27
	2	1.0	1.0	4.36	8.22
	3	3.9	3.9	4.38	8.31
h (ft)	1	-0.040	0.025	--	--
	2	0.221	0.221	--	--
	3	-0.384	0.095	--	--
u (ft/sec)	1	-0.089	-0.045	--	--
	2	-0.138	-0.067	--	--
	3	0.073	0.052	--	--

F-16 Pitch Rate Response - Continuous System

The pitch rate command response for the F-16 is shown in Figures F-4 and F-5. The pitch rate response is shown in Figure F-4 and the roll angle response is shown in Figure F-5. Note that all four F.C.'s are included in these response plots. From Figure F-5, the maximum roll angle for the pitch rate command is approximately 2.8 degrees which meets the 5 degree specification. The figures of merit for the pitch rate command responses are shown in Table F-2. Examination of the continuous system response data shows that in general, the specifications are met. In some instances the settling time specification is not met, but as discussed in reference 2 the specifications can be met by fine tuning the prefilter, F_{11}. Note that the maximum delta in the settling time is 1.33 seconds which is less than the delta in the response models (1.5 secs). The pitch rate response data in reference 2 showed a 2.14 second delta in the settling time which theoretically should not occur. It is highly probable that the use of reduced order compensators in reference 2 caused the discrepancy.

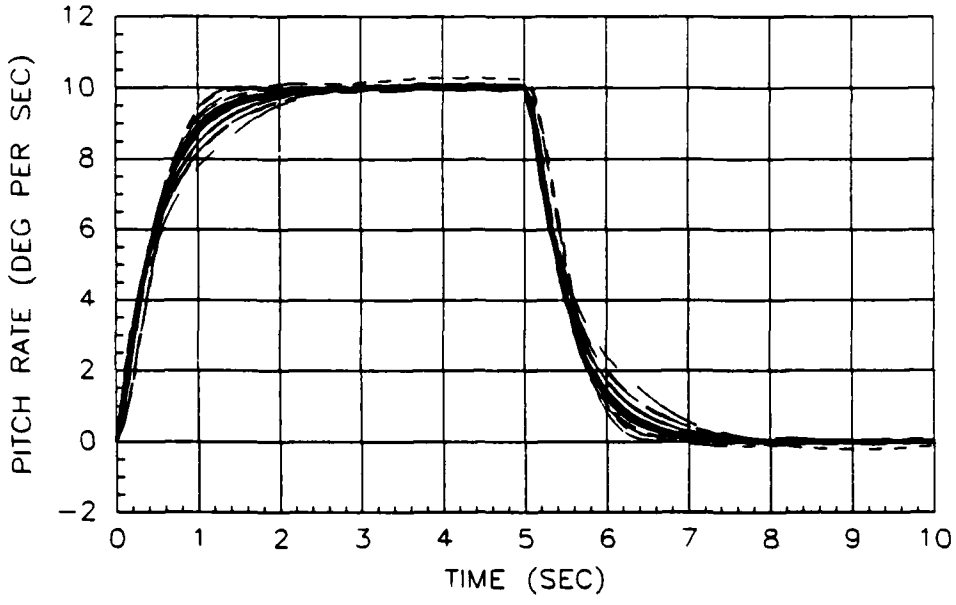

Fig. F-4. Continuous System Pitch Rate Responses

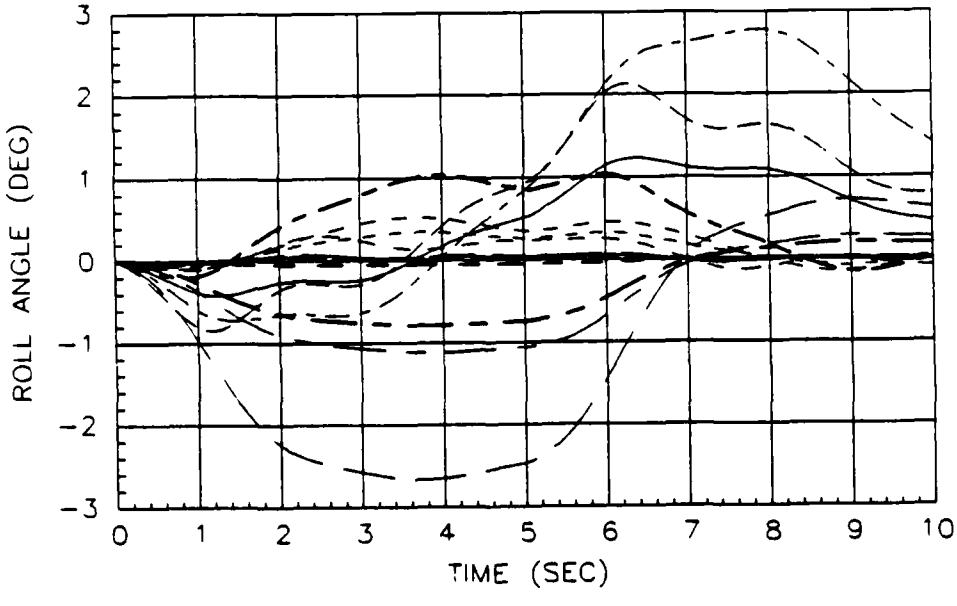

Fig. F-5. Continuous System Roll Angle Responses

Table F-2

Pitch Rate Response Characteristics - Continuous System

F.C.	CSC Mode	Peak Value (deg/sec)	Rise Time (sec)	Settling Time (sec)
1	1	10.02	1.00	1.80
	2	10.12	0.77	1.25
	3	10.02	0.90	1.80
	4	10.12	0.71	1.25
	5	10.30	0.85	2.50
	6	10.02	0.90	1.75
2	1	10.00	1.02	1.75
	2	10.02	0.90	1.50
	3	10.00	1.02	1.79
	4	10.13	0.82	1.34
	5	10.03	0.86	1.45
	6	10.00	1.02	1.75
3	1	10.00	1.09	1.92
	2	9.99	1.04	1.88
	3	10.00	1.08	1.94
	4	10.03	1.02	1.60
	5	10.00	1.05	1.92
	6	10.00	1.08	1.99
4	1	10.02	1.28	2.17
	2	10.05	1.38	2.38
	3	10.02	1.22	2.17
	4	10.12	1.57	2.58
	5	10.05	1.35	2.40
	6	10.02	1.28	2.17

F-16 Roll Rate Command Response - Continuous System

The roll rate command responses are shown in Figures F-6 and F-7. Figure F-6 shows the roll rate response and Figure F-7 shows the pitch angle response. The maximum pitch angle is approximately -1.9 degrees. The pitch angle specification is 3 degrees, therefore this specification is met. Table F-3 shows the roll rate response characteristics. The

response data shows that all specifications are met except the settling time where an explanation similar to that given above applies here.

Table F-3

Roll Rate Response Characteristics - Continuous System

F.C.	CSC Mode	Peak Value (deg/sec)	Rise Time (sec)	Settling Time (sec)
1	1	50.85	1.53	2.45
	2	50.63	1.59	2.70
	3	51.15	1.56	2.47
	4	51.11	1.67	3.18
	5	50.79	1.73	3.72
	6	51.53	1.42	4.45
2	1	50.77	1.47	2.25
	2	50.81	1.48	2.25
	3	50.78	1.44	2.23
	4	50.87	1.47	2.24
	5	50.86	1.45	2.24
	6	50.68	1.44	2.18
3	1	50.75	1.48	2.24
	2	50.74	1.46	2.26
	3	50.75	1.48	2.21
	4	50.80	1.50	2.26
	5	50.74	1.48	2.26
	6	50.81	1.48	2.28
4	1	50.77	1.48	2.27
	2	50.76	1.49	2.37
	3	50.78	1.49	2.27
	4	50.78	1.48	2.27
	5	50.78	1.48	2.28
	6	50.81	1.48	2.28

AD-A164 209 STUDY OF THE EFFECTS OF DISCRETIZING QUANTITATIVE FEEDBACK THEORY ANALOG..(U) AIR FORCE INST OF TECH WRIGHT-PATTERSON AFB OH SCHOOL OF ENGI.. J S COUCOULES 3/3

UNCLASSIFIED DEC 85 AFIT/GE/ENG/85D-10 F/G 1/3 NL

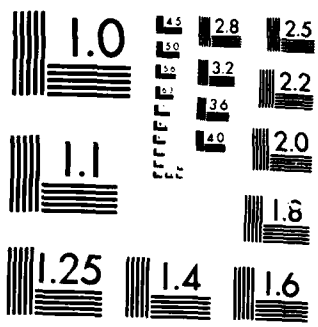

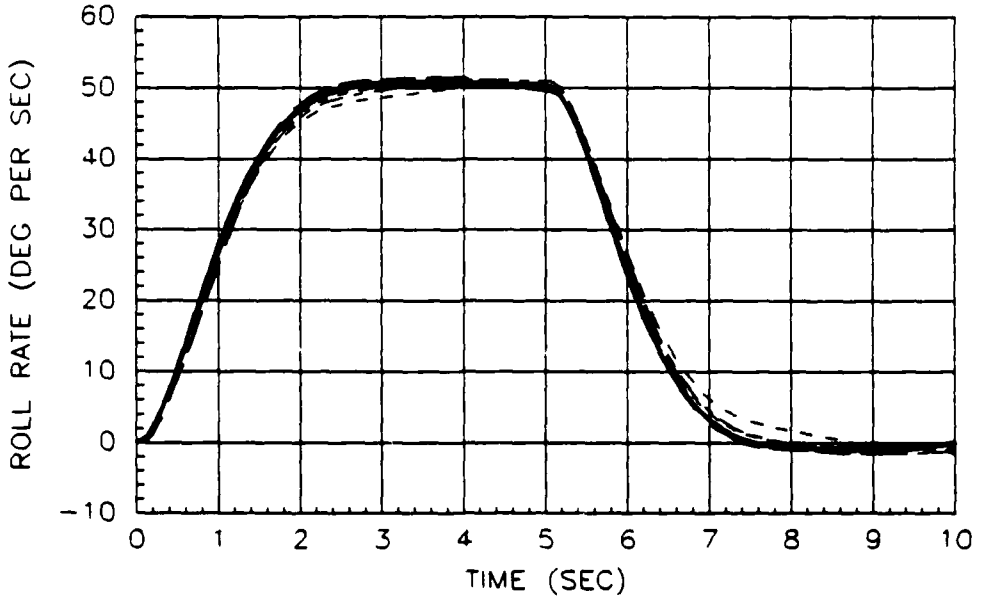

Fig. F-6. Continuous System Roll Rate Responses

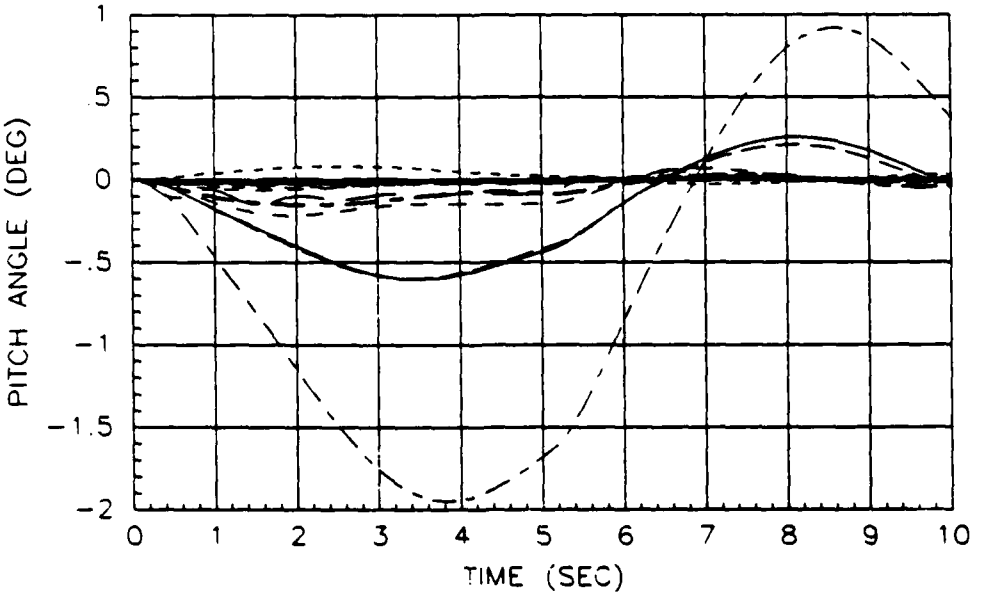

Fig. F-7. Continuous System Pitch Angle Responses

Appendix G: Microprocessor Emulation Program

Introduction

This appendix contains the microprocessor emulation subroutine code listing. Also included is the code listing for the utility "hook" subroutine provided with the $MATRIX_X$ executable code (7:SB 6-2). A brief discussion of each subroutine is given below.

Hook Subroutine

A detailed explanation of this subroutine and its use is contained in reference 7 (7:SB 6-4). Essentially the entire code of this subroutine is provided with the $MATRIX_X$ code. The name of the subroutine is UPDFTN. If more than one user written FORTRAN subroutine is to be interfaced with $MATRIX_X$ then this UPDFTN must be modified slightly. The version of UPDFTN shown below has been modified to allow three different subroutines to be called from $MATRIX_X$ (actually from System Build) where their names can be seen in the calling statements in the code. All parameters sent from System Build to the microprocessor emulation subroutine (i.e. the "user" defined subroutine) pass untouched through subroutine UPDFTN. It is very important that none of the UPDFTN code be changed (from the template provided with $MATRIX_X$) except in very specific areas. These areas are explained in reference (7). The code for UPDFTN is given below.

```
      SUBROUTINE UPDFTN ( NUMBER, NAME, T, U, NU, X, XDOT, NX, Y, NY,
     +                                  RP, IP, DELX, DELY, ERROR )
C
C ------------------------------------------------------------------------
C !            SYSTEM_BUILD FORTRAN FUNCTION EVALUATION HOOK              !
C !                                                                       !
C ! Used by MATRIXX, An ANSI77 version, A subset of System_Build.        !
C ------------------------------------------------------------------------
C                                                                 DBV 09/05/84
      DOUBLE PRECISION T,     U(1),    X(1),    Y(1)
      DOUBLE PRECISION RP(1), XDOT(1), DELX(1), DELY(1)
      INTEGER          IP(1), BLOCK
      CHARACTER*6      NAME,  FNAME(3)
      LOGICAL          ERROR
      DATA             MAXNUM   / 3 /
      DATA             FNAME(1),FNAME(2),FNAME(3) / 'G1Z','G2Z' ,'G3Z' /
C
      BLOCK = IABS(NUMBER)
C
C  Test whether or not NUMBER is in range :
C
      IF( BLOCK.GT.MAXNUM ) THEN
         ERROR = .TRUE.
         IF( NUMBER.GT.0 ) WRITE(6,111) BLOCK
 111     FORMAT(/' >>UPDFTN>> Not able to update Function ',I2)
         RETURN
      ENDIF
C
C  If NUMBER is negative then just pass back block name :
C
      NAME = FNAME(BLOCK)
      IF( NUMBER .LT. 0 ) RETURN
C
C  Fix up the GO TO statement to branch to various FORTRAN blocks :
C
      GO TO ( 01, 02, 03 ), BLOCK
C
  01  CALL FTN01 ( T, U, NU, X, DELX, NX, DELY, NY, RP, IP, ERROR )
      GO TO 99
C
  02  CALL FTN02 ( T, U, NU, X, DELX, NX, DELY, NY, RP, IP, ERROR )
      GO TO 99
C
  03  CALL FTN03 ( T, U, NU, X, DELX, NX, DELY, NY, RP, IP, ERROR )
      GO TO 99
C
C  04  CALL FTN04 ( T, U, NU, X, DELX, NX, DELY, NY, RP, IP, ERROR )
C      GO TO 99
C
C  05  CALL FTN05 ( T, U, NU, X, DELX, NX, DELY, NY, RP, IP, ERROR )
C      GO TO 99
C
```

```
C  Convert to implicit form :
C
  99  IF( NX .GT. 0 ) THEN
         DO 998 I = 1, NX
  998       DELX(I) = DELX(I) - XDOT(I)
      ENDIF
      IF( NY .GT. 0 ) THEN
         DO 999 I = 1, NY
  999       DELY(I) = DELY(I) - Y(I)
      ENDIF
      RETURN
      END
```

Microprocessor Emulation Code

System Build has the capability to pass all parameters needed by the microprocessor emulation program. For different simulations it is desirable to change certain parameters for the emulation subroutine. For instance, the wordlength or rounding/truncation specification might be changed from one simulation to the next. Unfortunately, if one parameter is changed, all parameter must be reentered into System Build. The emulation program was originally written with all parameters being passed from System Build but because of the above mentioned limitation, the code was modified so that the difference equation coefficients are coded into the subroutine itself. This alleviates the need to continuously reenter the coefficients. The following parameters are specified by the user and passed to the emulation code from System Build: the rounding/truncation specification, the microprocessor wordlength, the number of bits to the right of the radix point, and the order of the difference equation. These items

are passed in an integer "parameter vector" called IP. In addition, System Build passes the following items to the emulation subroutine in support of the dynamic discrete simulation: the current sample time and the floating point number representing the error signal (i.e. the input to the controller). Other items are passed which are not used. These unused items simply assume their default values. See the definition of variable section of the code for specific variable names. After the emulation subroutine computes the difference equation it passes back the compensation signal to System Build as a floating point number.

It is critical for the emulation subroutine code to be written following certain conventions expected by System Build. For a detailed explanation of these conventions see reference 7 (7:SB 6-3). Pseudocode and an explanation of each variable is given in the code below. Note that a different subroutine is used for each digital controller. This greatly simplifies the interface with System Build. So for the KC-135 longitudinal mode there are three subroutines with identical code except for the difference equation coefficients. The particular version shown below is for G2(z) of the KC-135 longitudinal mode. Note also that double precision arithmetic is used throughout the subroutine as described in Chapter V. The microprocessor emulation code follows:

```
      SUBROUTINE FTN02 ( T, U, NU, X, XDOT, NX, Y, NY,
     >                   RP, IP, ERROR )
C
C-----------------------------------------------------------------------
C|  DESCRIPTION                                                        |
C|    This subroutine interfaces with MATRIX X - SYSTEM BUILD to       |
C|    simulate the finite wordlength fixed point binary                |
C|    arithmetic (addition and multiplication) of a discrete control   |
C|    compensator implemented on a microprocessor.  Currently, the     |
C|    subroutine is capable of simulating only equal order             |
C|    compensators, but this limititation can be removed easily.       |
C|    The highest order denominator coefficient is assumed to be one.  |
C|    The coefficients must be coded in this subroutine and ordered    |
C|    from highest powered coefficient to lowest powered coefficient.  |
C|    The leading denominator coefficient (equal to one) must be       |
C|    entered also.                                                    |
C-----------------------------------------------------------------------
C
C-----------------------------------------------------------------------
C|  PSEUDOCODE                                                         |
C|    - initialize parameters                                          |
C|    - initialize compensator coefficients                            |
C|    - massage compensator coefficients (integer form)                |
C|    - compute overflow values                                        |
C|    - massage current input to compensator (error signal)            |
C|    - compute input portion of difference equation                   |
C|        -- massage multiplies                                        |
C|        -- check for overflow                                        |
C|        -- add terms                                                 |
C|        -- check for overflow                                        |
C|    - compute output portion of difference equation                  |
C|        -- same as input portion except subtract                     |
C|    - shift outputs and inputs                                       |
C|    - compute 'microprocessor' output (floating point number)        |
C-----------------------------------------------------------------------
C
C-----------------------------------------------------------------------
C|  DEFINITION OF VARIABLES                                            |
C|                                                                     |
C|  T - current sample time                                            |
C|  U - input vector (error signal)                                    |
C|  NU - number of inputs (dimension of U: = 1)                        |
C|  X - state vector (not used)                                        |
C|  XDOT - first derivative of state vector (not used)                 |
C|  NX - number of states (dimension of X: = 0)                        |
C|  Y - output vector (compensation signal)                            |
C|  NY - number of outputs (dimension of Y: = 1)                       |
C|  RP - general vector of real values (not used)                      |
C|  IP - general vector of integer parameters                          |
C|  ERROR - logical flag (TRUE means simulation error, not used)       |
C|                                                                     |
C|  ZZA - numerator coefficient vector                                 |
```

```
C|   ZZB - denominator coefficient vector                              |
C|   ZZRT - rounding/truncate value (0 or .5)                          |
C|   ZZSIGN - sign of value to be 'massaged'                           |
C|   ZZL - microprocessor wordlength minus 1                           |
C|   ZZN - numerator order                                             |
C|   ZZP - number of digits to right of radix point                    |
C|   ZZI - generic counter                                             |
C|   ZZOVRH - positive overflow value                                  |
C|   ZZOVRL - negative overflow value                                  |
C|   ZZR - vector of current & past compensator inputs                 |
C|   ZZC - vector of current and past compensator outputs              |
C|                                                                     |
C|     NOTE: All variables unique to this subroutine begin with the    |
C|           letters 'ZZ' to insure uniqueness with MATRIX X           |
C|           variables.  All other variables are initialized in        |
C|           MATRIX X and passed to this subroutine as arguments.      |
C---------------------------------------------------------------------
C
C---------------------------------------------------------------------
C|   SPECIFICATIONS                                                   |
C---------------------------------------------------------------------
C
      IMPLICIT DOUBLE PRECISION (A-H,O-Z)
      DOUBLE PRECISION T, U(1), X(1), XDOT(1), Y(1), RP(1)
      DOUBLE PRECISION ZZA(0:10), ZZB(0:10), ZZRT, ZZSIGN
      DOUBLE PRECISION ZZR(0:10), ZZC(0:10), ZZS, ZZT, ZZOVRH, ZZOVRL
      INTEGER IP(1), ZZL, ZZN, ZZP, ZZI
      LOGICAL ERROR
      COMMON /ZZFTN2/ ZZR, ZZC
C
C---------------------------------------------------------------------
C|   INITIALIZATION OF PARAMETERS                                     |
C---------------------------------------------------------------------
C
    IF ( T .EQ. 0.0D+00 ) THEN
         DO 10 ZZI = 0,ZZN
               ZZR(ZZI) = 0.0D+00
               ZZC(ZZI) = 0.0D+00
 10         CONTINUE
    ENDIF
C
    ZZL = IP(1) - 1
    ZZP = IP(2)
    IF ( IP(3) .EQ. 1 ) THEN
         ZZRT = 0.5D+00
    ELSE
         ZZRT = 0.0D+00
    ENDIF
C
C---------------------------------------------------------------------
C|   INITIALIZATION OF COMPENSATOR COEFFICIENTS                       |
C---------------------------------------------------------------------
```

```
C
      ZZN = 3
C
      ZZA(0) = 13477.2681D+00
      ZZA(1) = 332.7720519D+00
      ZZA(2) = -13144.49605D+00
      ZZA(3) = 0.0D+00
C
      ZZB(0) = 1.0D+00
      ZZB(1) = 1.239327943D+00
      ZZB(2) = -.2396240031D-01
      ZZB(3) = -.3390818422D+00
C
C-----------------------------------------------------------------------
C|   COMPUTE OVERFLOW VALUES                                           |
C-----------------------------------------------------------------------
C
      ZZOVRH = (2.0D+00**ZZL) - 1
      ZZOVRL = -(2.0D+00**ZZL)
C
C-----------------------------------------------------------------------
C|   MASSAGE NUMERATOR COEFFICIENTS (INTEGER FORM)                     |
C-----------------------------------------------------------------------
C
      DO 30 ZZI = 0,ZZN
            IF ( ZZA(ZZI) .LT. 0.0D+00 ) THEN
                 ZZSIGN = -1.0D+00
            ELSE
                 ZZSIGN = 1.0D+00
            ENDIF
            ZZA(ZZI) = DINT( ZZA(ZZI) * (2.0D+00**ZZP) + ZZRT
     +                       * ZZSIGN )
            IF ( ZZA(ZZI) .GT. ZZOVRH )ZZA(ZZI) = ZZOVRH
            IF ( ZZA(ZZI) .LT. ZZOVRL )ZZA(ZZI) = ZZOVRL
   30   CONTINUE
C
C-----------------------------------------------------------------------
C|   MASSAGE DENOMINATOR COEFFICIENTS (INTEGER FORM)                   |
C-----------------------------------------------------------------------
C
      DO 40 ZZI = 0,ZZN
            IF ( ZZB(ZZI) .LT. 0.0D+00 ) THEN
                 ZZSIGN = -1.0D+00
            ELSE
                 ZZSIGN = 1.0D+00
            ENDIF
            ZZB(ZZI) = DINT( ZZB(ZZI) * (2.0D+00**ZZP) + ZZRT
     +                       * ZZSIGN )
            IF ( ZZB(ZZI) .GT. ZZOVRH )ZZB(ZZI) = ZZOVRH
            IF ( ZZB(ZZI) .LT. ZZOVRL )ZZB(ZZI) = ZZOVRL
   40   CONTINUE
C
```

```
C-----------------------------------------------------------------------
C|  MASSAGE CURRENT INPUT                                              |
C-----------------------------------------------------------------------
C
      IF ( U(1) .LT. 0.0D+00 ) THEN
           ZZSIGN = -1.0D+00
      ELSE
           ZZSIGN = 1.0D+00
      ENDIF
      ZZR(0) = DINT( U(1) * (2.0D+00**ZZP) + ZZRT * ZZSIGN )
C
C-----------------------------------------------------------------------
C|  COMPUTE INPUT SEQUENCE                                             |
C-----------------------------------------------------------------------
C
      ZZS = 0.0D+00
      DO 50 ZZI = 0,ZZN
            ZZT = ZZA(ZZI) * ZZR(ZZI)
            IF ( ZZT .LT. 0.0D+00 ) THEN
                 ZZSIGN = -1.0D+00
            ELSE
                 ZZSIGN = 1.0D+00
            ENDIF
            ZZT = DINT( ZZT * (2.0D+00**-ZZP) + ZZRT * ZZSIGN )
            IF ( ZZT .GT. ZZOVRH )ZZT = ZZOVRH
            IF ( ZZT .LT. ZZOVRL )ZZT = ZZOVRL
            ZZS = ZZS + ZZT
            IF ( ZZS .GT. ZZOVRH )ZZS = ZZOVRH
            IF ( ZZS .LT. ZZOVRL )ZZS = ZZOVRL
   50   CONTINUE
C
C-----------------------------------------------------------------------
C|  COMPUTE OUTPUT SEQUENCE                                            |
C-----------------------------------------------------------------------
C
      DO 60 ZZI = 1,ZZN
            ZZT = ZZB(ZZI) * ZZC(ZZI)
            IF ( ZZT .LT. 0.0D+00 ) THEN
                 ZZSIGN = -1.0D+00
            ELSE
                 ZZSIGN = 1.0D+00
            ENDIF
            ZZT = DINT( ZZT * (2.0D+00**-ZZP) + ZZRT * ZZSIGN )
            IF ( ZZT .GT. ZZOVRH )ZZT = ZZOVRH
            IF ( ZZT .LT. ZZOVRL )ZZT = ZZOVRL
            ZZS = ZZS - ZZT
            IF ( ZZS .GT. ZZOVRH )ZZS = ZZOVRH
            IF ( ZZS .LT. ZZOVRL )ZZS = ZZOVRL
   60   CONTINUE
C
```

```
C-------------------------------------------------------------------------
C|  SHIFT PAST INPUTS AND OUTPUTS                                         |
C-------------------------------------------------------------------------
C
      ZZC(0) = ZZS
      DO 70 ZZI = ZZN,1,-1
            ZZC(ZZI) = ZZC(ZZI-1)
            ZZR(ZZI) = ZZR(ZZI-1)
   70   CONTINUE
C
C-------------------------------------------------------------------------
C|  COMPUTE 'MICROPROCESSOR' OUTPUT                                       |
C-------------------------------------------------------------------------
C
      Y(1) = ZZC(0) * (2.0D+00**-ZZP)
      ERROR= .FALSE.
C
      RETURN
C
      END
```

Bibliography

1. Russell, Harvey H. Design of Robust Controllers for a Multiple Input-Multiple Output Control System With Uncertain Parameters Application to the Lateral and Longitudinal Modes of the KC-135 Transport Aircraft. MS Thesis. Air Force Institute of Technology, Wright-Patterson AFB OH, December 1984.

2. Arnold, Phillip B. Flight Control System Reconfiguration Design Using Quantitative Feedback Theory. MS Thesis. Air Force Institute of Technology, Wright-Patterson AFB OH, December 1984.

3. Betzold, Robert W. Multiple Input-Multiple Output Flight Control Design with Highly Uncertain Parameters; Application to the C-135 Aircraft. MS Thesis. Air Force Institute of Technology, Wright-Patterson AFB OH, December 1984.

4. Horowitz, Isaac and T. Kopelman. Multivariable Flight Control Design with Uncertain Parameters. Department of Applied Mathematics, The Weizman Institute of Science, Rehovot, Israel. AFWAL Report-TR-83-3036, September 1982.

5. Horowitz, Isaac and Marcel Sidi. "Synthesis of Feedback Systems with Large Plant Ignorance for Prescribed Time-Domain Tolorances," International Journal of Control, 16 (2): 287-309 (1972).

6. Horowitz, Isaac. "Quantitative Synthesis of Uncertain Multiple Input-Output Feedback Systems," International Journal of Control, 30 (1): 81-106 (1979).

7. Integrated Systems Inc. MATRIXX Users Guide, (Version 5.0). Palto Alto California, January 1985.

8. Phillips, Charles L. and H. Troy Nagle, Jr. Digital Control System Analysis and Design. Englewood Cliffs, N.J.: Prentice-Hall, Inc., 1984.

9. Houpis, Constantine H. and Gary B. Lamont. Digital Control Systems. New York: McGraw-Hill Book Company, 1985.

10. D'Azzo, John J. and Constantine H. Houpis. Linear Control System Analysis and Design, Conventional and Modern (Second Edition). New York: McGraw-Hill Book Company, 1981.

11. Mathlab Group. MACSYMA Reference Manual, (Version 10). Laboratory for Computer Science, Massachusetts Institute of Technology, Cambridge, Massachusetts, January 1983.

12. Katz, P. and J. D. Powell. "Sample Rate Selection for Aircraft Flight Control," AIAA Journal, 13 (8): 975-979 (August 1975).

13. Franklin, Gene F. and J. David Powell. Digital Control of Dynamic Systems. New York: Addison-Wesley Publishing Co., 1980.

14. Larimer, S. J. TOTAL--An Interactive Computer-Aided Design Program for Digital and Continuous Control System Analysis and Synthesis. MS Thesis. Air Force Institute of Technology, Wright-Patterson AFB, OH March 1978.

15. Eckert, Scott B. Development of a Digital Interactive Controller Evaluation System (DICES). MS Thesis. Air Force Institute of Technology, Wright-Patterson AFB, OH December 1985.

16. Follett, Randolph F., Jerrel R. Mitchell, and L. L. Gresham. "A Computer Code for Emulation of Arithmetic Errors Generated by Microprocessor Controllers," Conference of the IEEE Southeastcon (SEACON) 1983. 246-249. IEEE PRESS, New York, 1983.

17. Horowitz, Isaac. "Quantitative Synthesis of Uncertain Multiple Input-Multiple Output Feedback Systems," International Journal of Control, 30(1): 81-106 (1979).

18. Horowitz, Isaac et al. Research in Advanced Flight Control Design. AFFDC-TR-79-3120. Department of Applied Mathematics, The Weizmann Institute of Science, Rehovot, Israel, January 1980.

19. Ashworth, M. J. Feedback Design of Systems with Significant Uncertainty. Chinchester: Research Studies Press, 1982.

20. Horowitz, Isaac and Clayton Loecher. "Design of 3x3 Multivariable Feedback Systems with Large Plant Uncertainty," International Journal of Control, 33(4): 677-699 (1981).

21. Horowitz, Isaac M. Synthesis of Feedback Systems. New York: Academic Press, 1963.

22. Horowitz, Isaac. "Improved Design Technique for Uncertain Multiple Input-Multiple Output Feedback Systems," International Journal of Control, 36(6): 977-988 (1982).

23. Adams, Richard A. Implemnetation and Testing of Numerical Analysis Techniques in Avionics Applications. MS Thesis, EE/79-1. Air Force Institute of Technology, Wright-Patterson AFB OH, March 1979.

24. Coucoules, John S. FORTRAN Subroutine for Microprocessor Emulation. Subroutine written in support of this thesis. Subroutine listing contained in Appendix G. Air Force Institute of Technology, Wright-Patterson AFB OH, December 1985.

Vita

Captain John S. Coucoules was born in Tacoma, Washington on 16 February, 1957. He graduated from the United States Air Force Academy in May 1980 with the degree of Bachelor of Science in Engineering Sciences. From May 1980 until May 1984 he served as an Operations Director and Systems Readiness Officer for the Defense Support Program, Global Positioning System and Vela spacecraft programs at the Air Force Satellite Control Facility, Sunnyvale, California.

His assignment following graduation from the Air Force Institute of Technology is to Detachment 3, Space Division at Buckley Air National Guard Base, Colorado.

UNCLASSIFIED

SECURITY CLASSIFICATION OF THIS PAGE

AD-A164 209

REPORT DOCUMENTATION PAGE

1a. REPORT SECURITY CLASSIFICATION: UNCLASSIFIED	1b. RESTRICTIVE MARKINGS
2a. SECURITY CLASSIFICATION AUTHORITY	3. DISTRIBUTION/AVAILABILITY OF REPORT: Approved for public release; distribution unlimited.
2b. DECLASSIFICATION/DOWNGRADING SCHEDULE	
4. PERFORMING ORGANIZATION REPORT NUMBER(S): AFIT/GE/ENG/85D-10	5. MONITORING ORGANIZATION REPORT NUMBER(S)
6a. NAME OF PERFORMING ORGANIZATION: School of Engineering; 6b. OFFICE SYMBOL (If applicable): AFIT/ENG	7a. NAME OF MONITORING ORGANIZATION
6c. ADDRESS (City, State and ZIP Code): Air Force Institue of Technology, Wright-Patterson AFB, Ohio 45433	7b. ADDRESS (City, State and ZIP Code)
8a. NAME OF FUNDING/SPONSORING ORGANIZATION: Flight Dynamics Lab; 8b. OFFICE SYMBOL (If applicable): AFWAL/FIG	9. PROCUREMENT INSTRUMENT IDENTIFICATION NUMBER
8c. ADDRESS (City, State and ZIP Code): Wright-Patterson AFB, Ohio 45433	10. SOURCE OF FUNDING NOS. — PROGRAM ELEMENT NO. / PROJECT NO. / TASK NO. / WORK UNIT NO.
11. TITLE (Include Security Classification): See Box 19	
12. PERSONAL AUTHOR(S): John S. Coucoules, Capt, USAF	
13a. TYPE OF REPORT: MS Thesis; 13b. TIME COVERED: FROM _____ TO _____; 14. DATE OF REPORT (Yr., Mo., Day): 1985 December; 15. PAGE COUNT: 207	
16. SUPPLEMENTARY NOTATION	

17. COSATI CODES			18. SUBJECT TERMS (Continue on reverse if necessary and identify by block number)
FIELD	GROUP	SUB. GR.	
01	03		Digital Control Systems; Flight Control Systems; Quantitative Feedback Theory; Multivariable Control; Inherent Reconfiguration

19. ABSTRACT (Continue on reverse if necessary and identify by block number)

Title: STUDY OF THE EFFECTS OF DISCRETIZING QUANTITATIVE FEEDBACK THEORY ANALOG CONTROL SYSTEM DESIGNS

Thesis Chairmen: Constantine H. Houpis and Gary B. Lamont

Approved for public release: IAW AFR 190-1.
LYNN E. WOLAVER 16 JAN 86
Dean for Research and Professional Development
Air Force Institute of Technology (AFSC)
Wright-Patterson AFB OH 45433

20. DISTRIBUTION/AVAILABILITY OF ABSTRACT	21. ABSTRACT SECURITY CLASSIFICATION
UNCLASSIFIED/UNLIMITED ☒ SAME AS RPT. ☐ DTIC USERS ☐	UNCLASSIFIED

22a. NAME OF RESPONSIBLE INDIVIDUAL	22b. TELEPHONE NUMBER (Include Area Code)	22c. OFFICE SYMBOL
Constantine H. Houpis, Ph.D. Gary B. Lamont, Ph.D.	513-255-2024	AFIT/EN

DD FORM 1473, 83 APR EDITION OF 1 JAN 73 IS OBSOLETE.

UNCLASSIFIED

SECURITY CLASSIFICATION OF THIS PAGE

This investigation examines the feasibility and a method of extending continuous domain Quantitative Feedback Theory (QFT) flight control system designs to the discrete domain. The results of two previous QFT analog design efforts are modified for a digital implementation. The first design effort is for the KC-135 transport aircraft. Robust analog fixed compensators are designed for three different flight conditions. The second design effort is for the AFTI/F-16 aircraft. In this design, parameter variation is due to both varying flight conditions and different aircraft configurations caused by failed surfaces.

This study is accomplished in two phases. In the first phase only the effects of sampling are included. The compensators are discretized using two transformation techniques after they are modified to counteract the effects of the sampler and zero order hold (ZOH). Simulation results show that the Tustin transformation using a sampling rate of 40 Hz provides good results, as compared to the analog design, for the KC-135 aircraft. For the AFTI/F-16, acceptable results are obtained using the Tustin transformation and a sampling rate of 60 HZ, but only for two out of four flight conditions.

In the second phase both sampling and finite wordlength effects are considered. A computer program is developed to simulate the effects of finite wordlength. It is sufficiently general to allow the specification of rounding or truncation, the controller wordlength and the number of desired binary digits to the right of the radix point. Simulations are conducted using various wordlengths and numbers of digits to the right of the radix point as well as appropriately quantized controller coefficients.

The conclusion drawn from this study is that the Tustin transformation provides good discrete system performance as compared to the continuous QFT design, if the compensator real zeros and poles are located at $S \geq -T/2$. To ensure the same system performance guarantees as provided by QFT in the continuous domain, it is recommended that the QFT design be performed directly in the discrete domain, as opposed to extending analog QFT designs.

END

FILMED

4-85

DTIC